NASA TECHNICAL MEMORANDUM

NASA TM X-72792

NASA TM X-72792

EFFECTS OF UPPER-SURFACE BLOWING AND THRUST VECTORING ON LOW-SPEED AERODYNAMIC CHARACTERISTICS OF A LARGE-SCALE SUPERSONIC TRANSPORT MODEL

By

Paul L. Coe, Jr., H. Clyde McLemore

and

James P. Shivers

NATIONAL AERONAUTICS AND SPACE ADMINISTRATION

LANGLEY RESEARCH CENTER, HAMPTON, VIRGINIA 23665

1 Report No	2. Government Accession No.	3 Recipient's Catalog No.
TM X-72792		

4. Title and Subtitle	5 Report Date
EFFECTS OF UPPER-SURFACE BLOWING AND THRUST VECTORING ON LOW-SPEED AERODYNAMIC CHARACTERISTICS OF A LARGE-SCALE SUPERSONIC TRANSPORT MODEL	November 1975
	6. Performing Organization Code
7 Author(s) Paul L. Coe, Jr., H. Clyde McLemore, and James P. Shivers	8. Performing Organization Report No.
9 Performing Organization Name and Address NASA Langley Research Center Hampton, VA 23665	10. Work Unit No 743-04-12-02
	11. Contract or Grant No
12. Sponsoring Agency Name and Address National Aeronautics and Space Administration Washington, DC 20546	13. Type of Report and Period Covered Technical Memorandum
	14. Sponsoring Agency Code

15. Supplementary Notes

16 Abstract

Tests have been conducted in the Langley full-scale tunnel to determine the low-speed aerodynamic characteristics of a large-scale arrow-wing supersonic transport configured with engines mounted above the wing for upper surface blowing, and conventional lower surface engines with provisions for thrust vectoring, Tests were conducted over an angle of attack range of -10^{0} to 34^{0} and for Reynolds numbers (based on the mean aerodynamic chord) of 5.17×10^{6} and 3.89×10^{6}. A limited number of tests were also conducted for the upper surface engine configuration in the high lift condition for $\beta = 10^{0}$ in order to evaluate lateral directional characteristics, and with the right engine inoperative to evaluate the engine out condition.

17. Key Words (Suggested by Author(s)) (STAR category underlined)	18. Distribution Statement
Advanced Supersonic Transport, Low-Speed Stability and Control, Upper-Surface Blowing	

19. Security Classif. (of this report)	20. Security Classif. (of this page)	21. No. of Pages	22. Price*
Unclassified	Unclassified	78	$4.75

*Available from { For sale by the National Technical Information Service, Springfield, Virginia 22161
STIF/NASA Scientific and Technical Information Facility, P.O. Box 33, College Park, MD 20740

EFFECTS OF UPPER-SURFACE BLOWING AND THRUST VECTORING ON LOW-SPEED AERODYNAMIC CHARACTERISTICS OF A LARGE-SCALE SUPERSONIC TRANSPORT MODEL

By Paul L. Coe, Jr., H. Clyde McLemore

and James P. Shivers

SUMMARY

Tests have been conducted in the Langley full-scale wind-tunnel to determine the effects of thrust vectoring and upper-surface blowing on the low-speed aerodynamic characteristics of a large-scale supersonic transport model.

The results of the investigation showed that the incremental lift provided by thrust vectoring of lower surface engines was limited to the vector component of thrust with no appreciable induced circulation for the particular configuration tested. However, significant additional circulation lift was produced by upper-surface blowing (USB) obtained by deflecting the exhaust of upper-surface mounted engines down onto the wing surface. With either the thrust vectoring or USB concepts, the use of boundary-layer control on the trailing edge flaps was found to improve flap effectiveness for high flap deflections. Low-speed performance considerations indicate that the upper-surface engine arrangement, with 20° elbow deflected exhaust nozzles and trailing-edge BLC, can achieve either 3° climb or 3° approach conditions with angles of attack on the order of 0° and lift coefficients of about 0.74. The tests also showed that the increased lift provided by either the thrust vectoring or USB concept was accompanied by large negative pitching moments.

Both the upper- and lower-surface engine configurations exhibited static longitudinal instability for the aft center-of-gravity location used in the tests, and a marked increase in the instability occurred at angles of attack above 10°. The horizontal tail provided a small increment in static longitudinal stability, and proved to be an effective means of providing pitch control.

The upper surface engine configuration, in the high lift condition, exhibited static directional stability for angles of attack up to $\alpha = 13^{o}$, and positive effective dihedral throughout the angle of attack range. Although the large rolling and yawing moments introduced with one-engine inoperative could not be trimmed with the amount of asymmetric boundary layer control (BLC) used in the investigation; the use of differential flaps in conjunction with asymmetric BLC was found to reduce the magnitude of the engine out rolling moment at low angles of attack. In addition, the use of spoilers was found to be an extremely effective means of providing roll control and also produced favorable yawing moments, but resulted in a large loss of lift.

INTRODUCTION

The National Aeronautics and Space Administration is presently studying the aerodynamic characteristics of advanced supersonic transport concepts which incorporate a highly swept-arrow wing and an aft center-of-gravity location to minimize trim drag at supersonic cruise speeds. Although wind-tunnel tests of such configurations have shown that high levels of aerodynamic efficiency can be obtained at transonic and supersonic speeds (see references 1 and 2), configurations of this type have embodied several design features which result in poor low-speed characteristics. For example, the trailing-edge flaps were relatively ineffective because the conventional lower surface engine arrangement limited the dimensions of the flaps to small spanwise segments located between the engines. The small flap segments, and a relatively long fuselage which limits the ground rotation angle, have resulted in configurations having usable lift coefficients of only about 0.5 for take-off and landing. Because of the relatively low values of lift coefficient, a wing loading about 20 percent less than that required for efficient cruise performance must be used to obtain acceptable take-off and landing speeds. In addition, excessively high pitch attitudes (caused by low values of lift curve slope) and the relatively long fuselage result in long landing gear lengths, and a requirement for deflection of the fuselage forebody for improved visibility during the climb and approach conditions. These configuration features, together with the oversized wing, result in an undesirable increase in operational weight.

A need therefore exists for methods to increase the low-speed lift available for take-off and landing of advanced supersonic transports.

The present investigation was conducted to determine the capability of upper-surface blowing (USB) and thrust-vectoring concepts to improve the low-speed lift characteristics of an advanced arrow-wing supersonic transport model. An exploratory application of the USB concept to an advanced supersonic transport configuration has previously been reported in reference 3 wherein significant additional circulation lift was produced by the concept. The present investigation extended the scope of the previous USB study to include the effects of: (1) boundary-layer control applied to the trailing-edge flap system; (2) deflected engine nozzles for increased lift; and (3) a more representative horizontal tail geometry. The thrust-vectoring concept was studied for a conventional lower-surface engine installation with deflected nozzles. These tests were conducted to determine if additional lift, other than the direct contribution of the component of the thrust force, would be produced by induced circulation arising from the entrainment of flow over the trailing-edge flap system by the engine exhaust.

The tests were conducted in the Langley full-scale tunnel over an angle-of-attack range from about $\alpha = -10^{\circ}$ to $\alpha = 34^{\circ}$, at Reynolds numbers (based on the wing mean aerodynamic chord) of 5.17×10^{6} and 3.89×10^{6}. The configuration variables included leading- and trailing-edge flap deflection, engine nozzle angle, and engine thrust coefficient. Also included in the investigation were a limited number of tests to determine the lateral-directional characteristics of the model and to determine the forces and moments associated with the one-engine inoperative condition.

SYMBOLS

The longitudinal data are referred to the wind system of axes and the lateral-directional data are referred to the body system of axes as illustrated in figure 1. The moment reference center for the tests was located at 53.8-percent of the wing mean aerodynamic chord.

The dimensional quantities herein are given in both the International

System of Units (SI) and the U. S. Customary Units.

b	wing span, m (ft)
B.S.	body station (longitudinal distance from model nose), m (ft)
BLC	boundary layer control
$\bar{c}$	mean aerodynamic chord, 3.368 m (11.05 ft)
C_D	drag coefficient, Drag/qS
C_L	lift coefficient, Lift/qS
C_ℓ	rolling moment coefficient, Rolling moment/qS b
C_m	pitching moment coefficient, Pitching moment/qS $\bar{c}$
C_n	yawing moment coefficient, Yawing moment/qS b
C_Y	side force coefficient, Side force/qS
C_μ	BLC blowing coefficient (thrust produced by BLC/qS)
i_t	horizontal tail incidence, positive leading-edge up, deg
ℓ	tail length, m (ft)
q	free stream dynamic pressure, N/m^2 (lbf/ft^2)
R_N	Reynolds number
S	wing area, 10.232 m^2 (110.14 ft^2)
T/W	thrust to weight ratio
T_C'	thrust coefficient, Thrust/qS
$T_C' = 0$	thrust coefficient corresponding to the condition where the engine exhaust total pressure equals the free stream total pressure
X,Y,Z	body axis coordinates
α	angle of attack, deg
β	angle of sideslip, deg
ε	downwash angle, deg
δ_e	elevator deflection (positive trailing-edge down), deg

δ_{ℓ_e} leading-edge flap deflection (positive downward), deg

δ_f trailing-edge flap deflection (positive trailing-edge down), deg

δ_N exhaust nozzle deflection (positive downward), deg

δ_s spoiler deflection angle, deg

ΔC_L increment in lift coefficient

ΔC_ℓ increment in rolling moment coefficient

ΔC_n increment in yawing moment coefficient

ΔC_Y increment in side force coefficient

Subscripts:

L left

R right

MODEL

The dimensional characteristics of the model are listed in table I and shown in figure 2. Photographs of the model mounted for tests in the Langley full-scale tunnel are presented in figures 3 and 4.

Previous tests with this particular model have been reported in reference 3. For the present tests, the leading- and trailing-edge flaps were modified and the tail configuration was revised.

The wing consisted of an arrow planform with an inboard leading-edge sweep angle of 74°, a midspan sweep angle of 70.5°, and an outboard sweep of 60°. The wing was rigidly constructed to simulate the shape of an elastic wing in 1-g flight at low speeds. The thickness ratio was 3.08 percent and the outboard 27.5 percent semispan had a leading-edge droop of 45° and a trailing-edge droop of 5°. The wing had leading-edge flaps which could be deflected from 0° to 30°.

When configured with lower surface engines (see figure 2(a)) the model was equipped with four engine simulators which consisted of tip driven fans

powered by externally supplied compressed air. The nozzle exhausts could be deflected using either 20^{0}, 30^{0} or 40^{0} elbow segments (see figure 2(b)) and the segmented trailing-edge flap system shown in figure 2(a) could be deflected from 0^{0} to 40^{0}. When configured with upper surface engines (see figure 2(c)), the model was powered by two engine simulators and the nozzle exhaust could be deflected using either 20^{0} tabs or 20^{0} elbow inserts (see figure 2(d)). In the USB configuration, the model incorporated a relatively large-span unsegmented flap which could be deflected from 0^{0} to 40^{0}.

For both the lower and upper surface engine arrangements, blowing slots located forward of the trailing-edge flaps were oriented to provide a sheet of high pressure air over the upper surface of the flap to control flow separation (see figure 2(e)). The inboard and outboard blowing slots were supplied by separate plenums, thus the amount of blowing over the inboard and outboard flaps could be individually varied. The tail configuration used in the present tests was representative of designs under consideration for advanced supersonic transports, and the nose of the fuselage was constructed with a fixed downward deflection to simulate the geometry previously found to be necessary for low-speed operations.

TESTS AND CORRECTIONS

Configuration with Lower Surface Engines

Tests were conducted for the lower surface engine configuration at a Reynolds number (based on the wing mean aerodynamic chord) of 5.17×10^{6} for a range of angle of attack from -10^{0} to 34^{0}. For the tail-off configuration tests were conducted for leading-edge flap deflections of 0^{0} and 30^{0} and a trailing-edge flap deflection of 0^{0}. Tests were also conducted for trailing-edge flap angles of 20^{0}, 30^{0}, 40^{0} and for a $40^{0}/30^{0}/20^{0}$ condition in which the inboard flap angle was 40^{0}, the middle flap angle was 30^{0}, and the outboard flap angle was 20^{0}. These tests were all conducted for nominal values of thrust coefficient of 0.0, 0.1, and 0.2, with and without boundary-layer control applied to the trailing-edge flap.

In addition to tests conducted using straight (undeflected) nozzles, tests were also conducted wherein the engine exhausts were deflected using 20^0, 30^0, and 40^0 elbow segments. Tail-on tests were conducted for a 30^0 nozzle deflection with a $40^0/30^0/20^0$ flap setting with boundary layer control and a thrust coefficient of 0.2. For these tests the horizontal tail was used as an all movable surface with a range of tail incidence angles of -15^0 to $+20^0$.

Configuration with Upper Surface Engines

Tests were conducted for the USB configuration at a Reynolds number of 3.89×10^6 for a leading-edge flap deflection of 30^0. For the tail-off condition, tests were conducted for trailing-edge flap angles of 0^0, 20^0, 30^0, and 40^0 for nominal values of thrust coefficient of 0.0, 0.1, and 0.2, with and without boundary-layer control. In addition to tests conducted using straight (undeflected) nozzles, tests were also conducted for which the engine exhaust was deflected using either 20^0 tabs or 20^0 elbow segments.

Tail-on tests were conducted for the 40^0 trailing-edge flap deflection with boundary-layer control, a thrust coefficient of 0.2, and 20^0 elbow exhaust nozzles. During these tests the horizontal tail was used as an all-movable tail with elevator having a range of tail incidence/elevator deflection angles of $-15^0/-30^0$ to $+20^0/+40^0$; (corresponding to 15^0 leading-edge down/30^0 trailing-edge up, and 20^0 leading-edge up/40^0 trailing-edge down, respectively).

In addition to the foregoing tests, a limited number of tests were conducted for the USB configuration (1) at $\beta = 10^0$ to evaluate lateral-directional characteristics; and (2) with the right engine inoperative to evaluate the engine-out condition.

Corrections

The test data have been corrected for air-flow angularity, buoyancy, and for strut tares. Wall corrections were found by the theory of reference 4 to be negligible and were not applied.

OUTLINE OF RESULTS AND DISCUSSION

In accordance with the primary objective of the investigation, emphasis is herein placed on the effects of boundary-layer control, USB, and vectored thrust on the longitudinal aerodynamic characteristics of the model and the bulk of data pertain to this subject. The results of a limited number of tests to determine lateral-directional characteristics and the problems associated with engine-out operation for the USB configuration are presented in a later section of the paper. An outline of the presentation of results is given in the following table.

I. RESULTS AND DISCUSSION OF LONGITUDINAL CHARACTERISTICS

Leading-edge flap deflection.- The longitudinal aerodynamic characteristics of the basic wing-body combination ($\delta_{\ell_e} = 0^o$) and the wing-body combination with leading-edge flaps deflected 30^o, are presented in figure 5. The data shown are for the condition of zero trailing-edge flap deflection and $T_C' = 0$. For the aft reference center-of-gravity location used in the tests, the wing-body combination was statically unstable. For the basic wing-body combination ($\delta_{\ell_e} = 0^o$) the data of figure 5 show that the level of instability increased gradually with increasing angle of attack up to about $\alpha = 10^o$; and for angles of attack greater than 10^o the data show a marked increase in the level of instability. Figure 5 also shows that deflection of the leading-edge flap to 30^o had no effect on the longitudinal characteristics below $\alpha = 10^o$. However, for higher angles of attack the leading-edge flap deflection was effective in both reducing the magnitude of the instability, and in delaying the angle of attack at which the abrupt increase in instability occurred. The leading-edge flap deflection of 30^o resulted in relatively small reduction in both lift and drag at angles of attack above 10^o.

Observation of tufts on the upper surface of the wing indicated that the abrupt increase in instability near $\alpha = 10^o$ was associated with the stalling of the outboard wing tips, and with the formation of leading-edge vortex

sheets above the wing surface. Apparently, deflecting the leading-edge flap was effective in reducing the instability associated with the vortex flow, but it was found to have no effect on the stall of the outboard wing tips. Although other values of leading-edge flap deflection were not investigated in this study, results presented in reference 5 indicate that increasing the leading-edge flap deflection beyond 30° may provide additional reductions in the instability associated with the leading-edge vortices, but would also result in a reduction in lift. As a result of the beneficial effect obtained by deflecting the leading-edge flaps through 30°, this value of deflection was used in all subsequent tests.

Trailing-edge flap deflection.- Figure 6 shows the results obtained for the model with lower surface engines at $T_C' = 0$, for various trailing-edge flap deflections with the tail off. The data of figure 6(a) show that deflecting the trailing-edge flaps from 0° to 20° provided a substantial increment in lift and pitching moment throughout the angle of attack range tested; and that increasing the deflection of the flaps to 30° provided only a small additional increment in lift. The results obtained for a flap deflection of 40° and a flap setting of $40^{\circ}/30^{\circ}/20^{\circ}$ (inboard flaps 40°, middle flaps 30°, outboard flaps 20°) are compared to the results obtained for the 30° flap deflection in figure 6(b). These data show that both the 40° flap deflection and the $40^{\circ}/30^{\circ}/20^{\circ}$ flap setting resulted in longitudinal characteristics which were essentially the same as those obtained for the 30° flap deflection.

Presented in figure 7 are the results of flow visualization studies for the 30°, 40°, and $40^{\circ}/30^{\circ}/20^{\circ}$ flap deflections. From these photographs it can be seen that the reduction in flap effectiveness for the higher flap deflections may be attributed to flow separation on the deflected flap segments. Figure 7 also indicates the separated flow on the outboard wing tips which, as previously mentioned, is partially responsible for the marked increase in the instability of the wing-body combination at angles of attack greater than 10°.

Trailing-edge flap deflection with boundary-layer control.- Figures 8, 9 and 10 show the results obtained for the wing-body combination with lower surface engines at $T_C' = 0$, for various trailing-edge flap deflections with boundary-layer control. The data of figure 8 show that for a given flap

deflection, the addition of boundary-layer control (C_μ = 0.02) increased lift by an approximately constant increment over the angle of attack range tested. Since this increment in lift is obtained by increasing the flap effectiveness, and since the flap hinge line is aft of the moment reference center, the increased lift is accompanied by a negative increment in pitching moment, as would be expected. It is interesting to note that for the $\delta_f = 40^o$ condition (figure 8(c)) doubling the pressure in the outboard boundary-layer control plenum (C_μ = 0.025) produced no improvement over the aerodynamic characteristics obtained for $C_\mu = 0.02$.

Presented in figure 9 are the results of flow visualization studies conducted to determine the effect of boundary-layer control on the flow over the trailing-edge flap system. From these photographs it can be seen that the application of boundary-layer control was extremely effective in producing flow attachment over the inboard deflected flap segments; however, the outboard flaps appear to experience some separation when the angle of attack was increased above $\alpha = 0^o$.

The data of figure 10 summarize the trailing-edge flap effectiveness, for the wing-body combination with lower surface engines at $T_C' = 0$, with boundary-layer control applied. These data are similar to those discussed for tests without boundary layer control (see figure 6) in that deflecting the trailing-edge flap from 0^o to 20^o provided a substantial increment in lift throughout the angle of attack range tested; and that increasing the deflection to 30^o provided a smaller additional increment in lift. The results obtained for the previously discussed 40^o flap deflection and $40^o/30^o/20^o$ flap setting are presented in figure 10(b), and the data show very small changes in the longitudinal characteristics when compared to the data obtained for the 30^o flap deflection.

Effect of thrust coefficient.- The effects of thrust coefficient on the longitudinal characteristics of the wing-body combination, with lower-surface engines and undeflected ($\delta_N = 0^o$) nozzles, are presented in figure 11 for a flap deflection of 30^o. An analysis of these data indicates that, with or without boundary-layer control applied to the trailing-edge flap system, the increment in lift due to thrust is simply the vector component of the thrust

force given by the expression:

$$\Delta C_L = T_C' \sin \alpha \qquad (1)$$

Thus, the conventional lower surface engine arrangement produced no additional circulatory lift due to thrust for $\delta_N = 0^o$. The data obtained for other trailing edge flap deflections show similar results and therefore are not presented.

Effect of thrust with deflected exhaust nozzles.- Figure 12 shows the effects of thrust with lower surface engines using the 30^o deflected exhaust nozzles. The data are presented for flap deflections of 30^o and 40^o, with and without boundary layer control applied to the trailing edge flap system. Analysis of the data again indicates that the increment in lift due to thrust is simply the vector component of the thrust force which for this condition is:

$$\Delta C_L = T_C' \sin (\alpha + \delta_N) \qquad (2)$$

Therefore, (as in the undeflected condition) the lower surface engine with deflected nozzles produced no additional circulatory lift. This result may have been expected based on a consideration of the location of the nozzle exits relative to the trailing-edge flap for this particular configuration. In this case, the nozzle was evidently too far aft to produce any beneficial jet-flap effect. It should be pointed out, however, that other supersonic transport configurations which have the lower surface engines located farther forward may derive more beneficial effects from thrust vectoring.

Tail-Off Results for Upper-Surface Engines

Trailing-edge flap deflection.- Figure 13 shows the results obtained for the wing-body combination with upper-surface engines and $T_C' = 0$, for various trailing-edge flap deflections without boundary-layer control. These data are similar to those obtained for the lower surface engine arrangement (see figure 6) in that deflecting the trailing-edge flaps from 0^o to 20^o provided a substantial increment in lift; increasing the flap deflection to 30^o provided

small additional lift, and the 40^{o} flap deflection produced aerodynamic characteristics which were virtually identical to those obtained for the 30^{o} flap deflection.

It should be noted that the trailing-edge flap effectiveness was slightly higher for the upper surface engines than for the lower surface engines. This result would be expected because of the increased flap area associated with the upper surface engine configuration (see figure 2).

Trailing-edge flap deflection with boundary-layer control.- Figures 14 and 15 show the results obtained for the wing-body combination for $T_C' = 0$, for various trailing-edge flap deflections with boundary-layer control. It should be noted that the blowing coefficient per length of span, over the inboard flap segments, is the same for both the upper and lower surface engine configurations. However, preliminary observations indicated that the blowing over the outboard flap segments was insufficient to provide flow attachment over the outboard flap segments, and therefore the pressure in the outboard boundary-layer control plenums was doubled. The increased flap span obtained by mounting the engines on the upper surface resulted in a total boundary layer control blowing coefficient of 0.04 for these tests. It should be noted that no attempt was made during the course of the investigation to determine the minimum value of C_μ required for flow attachment over the inboard flap segments. It is therefore possible that reduced levels of boundary-layer control may be as effective as those tested herein.

Figure 14 shows that boundary-layer control was successful in providing flap effectiveness for the highest flap deflection tested ($\delta_f = 40^{o}$) at low angles of attack; and by comparison of figures 13 and 14 it is seen that boundary-layer control also provides substantial increments in both lift and pitching moments, for a given flap deflection, at low angles of attack. However, as the angle of attack increases the effects of boundary layer control are seen to be reduced.

Figure 15 shows the results of flow visualization studies for the wing-body combination with upper surface engines at zero thrust. Figure 15(a) shows that without boundary-layer control the flaps are partially stalled when deflected to 20^{o}, and are completely stalled when deflected to either 30^{o} or 40^{o}.

Figure 15(b) presents results obtained when boundary-layer control was applied to the 30^{o} and the 40^{o} flap systems. From these photographs it is seen that, as in the case for the lower surface engines, boundary-layer control was extremely effective in providing flow attachment over the inboard flap segment; however, the outboard flap segment appeared to be experiencing some separation when the angle of attack was increased above $\alpha = 0^{o}$. These results are in agreement with the measured aerodynamic data presented in figures 13 and 14. Although the cause for the stall of the outboard flap segments is unknown, the inward direction of the flow over these segments suggests that the problem may be partly associated with the relatively high sweep of the outboard flap hinge line.

Effect of thrust and engine exhaust deflection.- Results presented in reference 3 show that only modest increments in circulatory lift can be obtained using upper surface engines exhausting straight back over the wing. However, reference 3 also indicates that significant increases in lift may be obtained when the exhaust is deflected down onto the wing surface. In the present study, a straight nozzle, a straight nozzle with a 20^{o} tab deflector (similar to that used in reference 3), and a 20^{o} elbow arrangement (see figure 2(d)) were used to deflect the exhaust down onto the upper surface of the wing. It should be noted that the elbow arrangement required a modified exit, as shown in figure 2(d)), in order for the 20^{o} deflection to be accomplished. This in turn required the use of higher exhaust velocities in order to obtain the desired levels of thrust.

Presented in figure 16 is a comparison of the longitudinal characteristics obtained for each of the above mentioned exhaust nozzle arrangements at values of T_C' of 0.1 and 0.2. These data are for trailing-edge flap deflections of 20^{o}, 30^{o}, and 40^{o} and for values of C_μ of 0 and 0.04. The results for each flap deflection are similar and show that for each condition the 20^{o} elbow exhaust nozzle produced higher values of lift than did the straight nozzle, or the 20^{o} tab deflector. It should be noted that other values of elbow exhaust nozzle deflection were not tested. It is therefore possible that reduced elbow deflections may be as effective as those tested herein.

Figure 17 compares the results of flow visualization studies conducted for the model with undeflected exhaust nozzles and 20^{o} elbow exhaust nozzles. The photographs presented are for conditions corresponding to $\alpha = 10^{o}$, $T_C' = 0.2$, $\delta_f = 40^{o}$, and $C_\mu = 0$. It can be seen that the flow over the trailing-edge flap system is separated for the undeflected nozzles; however, for the 20^{o} nozzles the flow over the inboard flap segments is seen to be attached. Thus the deflected nozzles are effective in aiding the trailing-edge flaps to turn the jet exhaust and thereby provide an increase in circulation lift. It should be noted that the jet exhaust had only small effects on the outboard flap segments, indicating that by repositioning the engines, or perhaps by using a four engine configuration, even higher lift coefficients may be obtained. The results obtained for other flap deflections show similar flow conditions and are not presented.

Figure 18 shows the effect of thrust on the static longitudinal aerodynamic characteristics of the wing-body combination with upper-surface engines and straight nozzles, for various flap deflections. These data show that for the unpowered configuration, a marked break in the lift curve occurred at an angle of attack of approximately 20^{o}. The data show that thrust produced some additional circulation lift at positive angles of attack and a significant increase in the angle of attack at which the lift curve break occurred.

The effect of thrust on the static longitudinal aerodynamic characteristics of the wing-body combination with upper surface engines and 20^{o} elbow exhaust nozzles is shown in figure 19. These data show that for a given trailing-edge flap deflection, with or without boundary-layer control, very significant increments in both lift and pitching moment were obtained when thrust was applied.

Comparison of Lift and Pitching Moment Characteristics For Lower- and Upper-Surface Engines

Figure 20 summarizes the lift and pitching moment characteristics obtained for both the lower- and upper-surface engine configurations at $\alpha = 0^{o}$ and $T_C' = 0.2$. The data are presented as a function of trailing-edge flap deflection for the various arrangements considered. Figure 20(a) shows that for the lower

surface engine arrangement the highest value of lift coefficient obtained at $\alpha = 0^0$ was $C_L = 0.62$ for a 40^0 trailing-edge flap deflection with boundary-layer control (BLC) and $\delta_N = 30^0$. The data presented in figure 20(b) show that at zero angle of attack a lift coefficient of $C_L = 0.87$ was obtained using the upper surface engine arrangement, with 20^0 elbow exhaust nozzles and 40^0 flaps with BLC. The lift produced by the upper surface engine configuration at low-speeds was well in excess of the value for which the wing under investigation was initially sized.

These data also illustrate the previously mentioned beneficial effects of boundary-layer control. In particular, analysis of the data indicates that increments in lift coefficient of about $\Delta C_L = 0.1$ may be obtained from the boundary-layer control used with the lower surface engine configuration at $\alpha = 0^0$ and $\delta_f = 40^0$. The data also show that the use of BLC for the upper surface engine configuration with straight nozzles provided an increment in lift of about $\Delta C_L = 0.27$ at $\alpha = 0^0$ and with a flap deflection of 40^0. In the USB arrangement with deflected nozzles, BLC provided an increment in lift coefficient of about $\Delta C_L = 0.09$ for $\alpha = 0^0$ and $\delta_f = 40^0$.

Figure 20 also shows that the increment in lift obtained by thrust vectoring of the lower-surface engines, and the increased lift obtained by deflecting the exhaust of the upper surface mounted engines down onto the wing surface, was accompanied by large negative pitching moments.

Horizontal Tail Effectiveness

Lower surface engine arrangement.- Presented in figures 21 and 22 are the longitudinal data for the tail-on configuration with lower surface engines. The configuration included 30^0 deflected leading-edge flaps, a $40^0/30^0/20^0$ trailing-edge flap setting with boundary-layer control, and 30^0 deflected nozzles operating at a thrust coefficient of 0.2. Figure 21 compares data obtained with the tail off to data obtained with the tail on at zero tail incidence and zero elevator deflection. These data show that for angles of attack below about 13^0 the horizontal tail provides a small contribution to static longitudinal stability and a positive increment in pitching moment resulting from a negative lift force acting on the tail surface. These results

indicate the presence of a strong downwash field acting at the horizontal tail location and high values of the downwash factor $\frac{\partial \varepsilon}{\partial \alpha}$. At angles of attack greater than 13° the horizontal tail provided a somewhat greater contribution to longitudinal stability, indicating a reduction in the downwash factor $\frac{\partial \varepsilon}{\partial \alpha}$; however, the presence of the strong downwash field is still apparent. For example, at approximately 20° angle of attack the horizontal tail is seen to produce no increment in either lift or pitching moment indicating that the tail is at an effective angle of attack of 0°.

Figure 22 shows that the use of the horizontal tail as an all-movable surface provided a relatively constant value of control effectiveness throughout the angle of attack range; the only exception being $i_t = 20^{\circ}$ for which the data of figure 22(b) snow tail stall at the higher angles of attack.

Upper surface engine arrangement.- Figures 23 and 24 present the static longitudinal data for the tail-on configuration with upper surface engines. The configuration had 30° deflected leading-edge flaps, a 40° trailing-edge flap deflection with boundary-layer control, and 20° elbow exhaust nozzles operating at a thrust coefficient of 0.2. Figure 23 compares the data obtained for the tail-off and tail-on conditions at zero elevator deflection. These data indicate trends similar to those for the lower surface engine arrangement, in that for angles of attack less than approximately 13°, the horizontal tail provides a slightly favorable contribution to static longitudinal stability, and increased stabilizing effect at angles of attack above 13°.

The elevator effectiveness for the upper surface engine arrangement was investigated using a two segment, all movable horizontal tail. This two segment surface was used in order to introduce camber, and thereby increase tail lift. The results for positive and negative tail deflections presented in figure 24 show that this tail configuration was more effective in providing pitch control than was the lower-surface engine configuration with the all-movable single-segment horizontal tail.

It should be noted that for both the upper- and lower-surface engine arrangements operating in the high lift condition, the horizontal tail was an effective means of providing pitch control, but did not provide a capability for longitudinal trim for angles of attack less than 15°. This result is

directly related to the large negative pitching moments, exhibited by the wing body combination at low angles of attack (see figure 20). Similar results are presented in reference 3, and a brief consideration of possible methods for providing pitch trim will be discussed in a subsequent section of this report.

Performance Considerations

As previously discussed, the upper surface engine configuration with 20^{0} elbow exhaust nozzles is an effective means of providing increased values of lift, as compared with the lower surface engine configuration. In order to establish the relative performance of these configurations during the landing and take-off phases of flight, a 3^{0} approach and a 3^{0} climb condition have been analyzed. It was assumed that a 40^{0} flap deflection with boundary-layer control was used for the 3^{0} approach condition; and a 30^{0} flap deflection with boundary-layer control was used for the 3^{0} climb condition. The data presented in this section correspond to that obtained for the untrimmed, tail-off configurations. This assumes (as will be discussed in a subsequent section) that pitch trim can be provided without penalizing the values of lift obtainable for these conditions.

Figures 25 and 26 compare the lift-drag polars for the lower surface engine configuration with 30^{0} deflected nozzles, to the lift drag polars for the upper surface engine configuration with straight (undeflected) nozzles and with 20^{0} elbow exhaust nozzles. Figure 25 presents the polars for the 3^{0} approach condition. From these data the lift coefficients and the values of T/W for the 3^{0} climb condition can be obtained. The angle of attack is determined for these conditions from the corresponding longitudinal data. The results obtained are presented in table II(a) for each of these configurations at a thrust coefficient of 0.1 and 0.2. From table II(a) it is seen that the upper surface engine configuration with the 20^{0} elbow exhaust nozzles provides the lowest approach angle of attack for a given thrust coefficient. In addition, it is seen that this configuration can perform the 3^{0} approach at a thrust coefficient of $T_C' = 0.1$, an angle of attack of approximately -1.5^{0}; and a lift coefficient of 0.72.

Presented in figure 26 are the polars for the assumed 3^0 climb condition, and the results obtained from analysis of these polars are presented in table II(b). From table II(b) it is seen that the upper surface engine configuration with the 20^0 elbow exhaust nozzles provides the lowest climb angle of attack for a given thrust coefficient. In particular, this configuration could achieve a climb angle of attack of 1.5^0 at a lift coefficient of 0.74 and a thrust coefficient of 0.2, which corresponds to a thrust to weight ratio of 0.27. Presented in table II(c) are the results obtained assuming a 20^0 flap deflection for the 3^0 climb condition. The results are similar to those for the 30^0 flap except that the angle of attack is higher for each configuration.

The important point obtained from the foregoing results is the fact that the upper surface engine arrangement with 20^0 elbow exhaust nozzles will permit operation at relatively low angles of attack during the landing and take-off phases of flight. Lower angles of attack would allow reduced landing gear length and would also eliminate the requirement for deflection of the fuselage nose. Elimination of these features could result in a significant weight reduction. In addition, it should be noted that the lift coefficient obtained for the climb and approach condition is about $C_L = .74$. This value is in considerable excess of the value $C_L = .5$ for which the wing was initially sized. Thus, the wing area may be reduced, which would result in an additional weight savings, and would reduce the magnitude of the pitching moments associated with flap deflection. Thus, smaller aerodynamic surfaces would be required for pitch trim. It should also be noted that the reduced wing size would result in less drag and therefore less required thrust. This may provide increased cruise efficiency through the use of smaller engines.

Pitch Trim Considerations

One of the problems associated with the use of the upper surface blowing concept is that the lift loads induced on the flap produce large negative pitching moments (see figure 20). The significance of the problem is illustrated by the horizontal tail effectiveness data, shown in figures 23 and 24, which indicates that the 7-percent conventional tail arrangement tested could not provide trim capability at low angles of attack. As discussed in the performance section, significant weight savings may be obtained with the USB

concept provided that a method of obtaining pitch trim, which does not penalize the lift capability of the configuration at low angles of attack, is developed. Therefore, a brief consideration of the relative merits of several methods of providing pitch trim is included. For purposes of discussion it is assumed that the position of the center of gravity and horizontal tail remain fixed.

Horizontal tail modifications.- The non-dimensional horizontal tail length ($\ell/\bar{c}$) for the present configuration was approximately 1.0; therefore any modification to the horizontal tail designed to increase the amount of negative tail lift, and therefore provide a nose-up pitching moment for trim, will obviously result in an undesirable one-to-one reduction in net lift. For example a tail providing a negative lift coefficient of 0.16 would provide pitch trim; however, it would also result in a reduction of the net C_L of 0.16.

Fixed canard.- One possible means of providing pitch trim and increased lift is through the use of a fixed canard located forward of the center of gravity. However, this arrangement has the undesirable effect of introducing an additional destabilizing contribution to C_{m_α}.

Free-floating canard.- An alternate approach to the fixed canard is an arrangement in which the canard is allowed to float freely about a hinge line. In such an arrangement the canard could provide pitch trim without the destabilizing effect associated with the fixed canard. However, experience with such arrangements has shown that they are prone to flutter and gust response problems.

Geared canard.- Another attractive canard arrangement is one in which the canard is geared such that its incidence angle is reduced as the airplane angle of attack is increased. Such an arrangement results in a beneficial contribution to lift, a nose-up moment for trim, and a means of providing artificial stability. A qualitative analysis of the benefits of such an arrangement is presented in reference 3. That analysis shows that a relatively small geared canard, used in conjunction with a conventional aft tail, may be an effective means for achieving low-speed longitudinal stability and trim. Such an arrangement might be required to be retractable for flight at high speeds, and therefore a weight penalty may be introduced by the system. However, it may allow

the full benefits of the upper surface blowing concept to be realized.

It is recognized that alternate approaches to the stability and trim problems are available, and a comprehensive study is required in order to resolve the trade-offs and advantages of the various systems.

RESULTS AND DISCUSSION OF LATERAL-DIRECTIONAL CHARACTERISTICS

During the present investigation a limited number of tests were conducted in order to determine the static lateral-directional characteristics of the model and to determine the problems associated with the loss of an engine. Inasmuch as the upper surface engine configuration appeared to exhibit superior longitudinal characteristics, the tests were restricted tc that configuration. In particular, these tests were conducted for the high lift condition, corresponding to a flap deflection of 40° and a 20° deflection of the exhaust nozzles.

Effect of Sideslip

The variation of the lateral-directional coefficients C_Y, C_n, and C_ℓ with angle of attack, for a sideslip angle of $\beta = 10^{\circ}$, are presented in figure 27. The data show that, without thrust, the model exhibited static directional stability for angles of attack up to approximately 13°, and positive effective dihedral throughout the angle of attack range tested. The data also show that thrust tends to increase the directional stability and delay the angle of attack at which the directional instability occurs. Although detailed studies of the flow field at the vertical tail location were not conducted, it is conceivable that the engine exhaust may impinge on the vertical tail, thereby enhancing its effectiveness. It should also be noted that both thrust and boundary-layer control had marked effects on the effective dihedral.

Effect of Spoiler Deflection

Figure 28 presents the increments of force and moment coefficients produced by deflecting a spoiler located directly ahead of the right inboard flap segments (see figure 2(e) for geometric details) with the engines operating

at $T_C' = 0.2$. The data show that the spoiler provided a large amount of roll control and favorable yawing moments over the angle of attack range tested. However, the longitudinal data presented in figure 28(b) show that the spoiler deflection also resulted in an extremely large loss of lift. It should be noted that the data presented are for a spoiler deflection of 70°; and that reduced spoiler deflection angles, or a reduction in spoiler span, may still provide adequate roll control with a reduced lift penalty.

Engine-out Characteristics

The problems associated with the loss of an engine are particularly severe for configurations dependent upon propulsive lift. In order to establish the severity of the problems (and to investigate possible means for alleviating these problems), tests were conducted in which the right engine was inoperative. It should be noted that in all of the engine-out tests asymmetric boundary-layer control was applied. For example, with the right engine inoperative, boundary layer control was applied to the right trailing-edge flap system only.

The data of figure 29 show the increment of force and moment coefficient produced for the right engine-out condition. The data show that with the right engine inoperative very large out-of-trim rolling and yawing moments occurred and that the application of asymmetric boundary-layer control was insufficient to provide lateral-directional trim. It is interesting to note that the increment in yawing moment produced by the loss of the engine was essentially constant over the angle of attack range; while the increment in rolling moment increased with increasing angle of attack. Although flow visualization photographs are not available for these conditions, observation of the surface tufts showed that the increase in the out-of-trim rolling moment with increasing angle of attack could be attributed to a progressive increase in flow separation, over the portion of the wing located behind the inoperative engine and inboard of the outboard vertical fin. Figure 29(b) shows that in addition to lateral-directional trim problems, the loss of an engine also resulted in a marked reduction in lift.

Since the amount of asymmetric boundary-layer control used in the investigation proved to be insufficient for providing lateral-directional trim for the right-engine inoperative condition, additional tests were conducted using differential flap settings in conjunction with asymmetric boundary-layer control. For these tests the left flap deflection was reduced from 40° to 30°, and the results are presented in figure 30. Comparison of figures 30(a) and 29(a) shows that differential flap deflection in conjunction with asymmetric boundary layer control reduced the magnitude of the out-of-trim rolling moments for angles of attack from -5° to about 10°; however, the moments provided were insufficient for trim. In addition, at higher angles of attack the magnitudes of the out-of-trim rolling moments were about the same as those for the symmetric flap condition. Comparison of figures 30(a) and 29(a) also shows that the differential flap deflection resulted in significantly higher values of out-of-trim yawing moments throughout the angle of attack range. Since rudder effectiveness was not investigated, it is not known whether directional trim could be provided by rudder deflection.

Comparison of figures 30(b) and 29(b) shows that as expected, the differential flap setting resulted in a slightly larger lift loss than that produced by symmetric flap deflection.

The foregoing considerations illustrate the severity of the engine-out problem for the present upper surface engine configuration. Although spoiler deflection may provide the required lateral trim, the lift loss associated with spoiler deflection would be undesirable.

In addition, it should be pointed out that the engine-out data presented are for a two-engine arrangement, and that a four-engine configuration may provide more acceptable engine-out characteristics.

SUMMARY OF RESULTS

The results of wind-tunnel tests to determine the effects of upper surface blowing and thrust vectoring on the low speed aerodynamic characteristics of a large-scale supersonic transport model may be summarized as follows:

1. The incremental lift provided by thrust vectoring of lower-surface engines was limited to the vector component of thrust with no appreciable induced circulation for the particular configuration tested.

2. Significant additional circulatory lift was produced by upper-surface blowing obtained by deflecting the exhaust of upper-surface mounted engines down onto the wing surface.

3. With either the thrust vectoring or USB concepts, the use of boundary-layer control on the trailing-edge flaps was found to improve flap effectiveness for high flap deflections.

4. The increased lift provided by either thrust vectoring or upper surface blowing was accompanied by large negative pitching moments.

5. Both the upper- and lower-surface engine configurations exhibited static longitudinal instability for the aft center of gravity used in the tests, and a marked increase in the instability occurred at angles of attack above 10^0.

6. The horizontal tail provided a small increment in static longitudinal stability for the configuration with either engine arrangement and proved to be an effective means of providing pitch control.

7. Low-speed performance considerations indicate that the upper surface engine arrangement, with 20^0 elbow deflected exhaust nozzles and trailing-edge BLC, could achieve either 3^0 climb or 3^0 approach conditions with angles of attack on the order of $\alpha = 0^0$ and lift coefficients of about $C_L = 0.74$.

8. The upper surface engine configuration, in the high lift condition, exhibited static directional stability for angles of attack up to 13^0, and positive effective dihedral throughout the angle of attack range.

9. The large rolling and yawing moments introduced with one-engine inoperative for the USB configuration could not be trimmed with the amount of asymmetric boundary layer control (BLC) used in the investigation. However, the use of differential flaps in conjunction with asymmetric BLC was found to significantly reduce the magnitude of the engine-out rolling moment at low angles of attack.

10. Spoiler deflection for the USB configuration was found to be an extremely effective means of providing roll control and also produced favorable yawing moments, but resulted in a large loss of lift.

REFERENCES

1. Morris, Odell A.; and Fournier, Roger H.: Aerodynamic Characteristics at Mach Numbers 2.30, 2.60 and 2.96 of a Supersonic Transport Model Having A Fixed, Warped Wing. NASA TM X-1115, 1965.

2. Morris, Odell A.; and Patterson, James C., Jr.: Transonic Aerodynamic Characteristics of a Supersonic Transport Model With a Fixed, Warped Wing Having 74° Sweep. NASA TM X-1167, 1965.

3. Shivers, James P.; McLemore, H. Clyde; and Coe, Paul L., Jr.: Low-Speed Wind Tunnel Investigation of a Large-Scale Advanced Arrow Wing Supersonic Transport Configuration With Engines Mounted Above the Wing for Upper Surface Blowing. NASA TM X-72761.

4. Heyson, Harry H.: Use of Superposition in Digital Computers to Obtain Wind-Tunnel Interference Factors for Arbitrary Configuration, With Particular Reference to V/STOL Models. NASA TR R-302, 1969.

5. McLemore, H. Clyde; and Parlett, Lysle P.: Low-Speed Wind-Tunnel Tests of a 1/10-Scale Model of a Blended-Arrow Advanced Supersonic Transport. NASA TM X-72671, 1975.

National Aeronautics and Space Administration
Langley Research Center, Hampton, Va.

November 3, 1975

TABLE I

DIMENSIONAL CHARACTERISTICS OF MODEL

Wing:		
Area, M^2 (ft^2)	10.232	(110.14)
Span, M (ft)	4.199	(13.778)
Aspect Ratio	1.72	
Root Chord, M (ft)	5.589	(18.337)
Tip Chord, M (ft)	0.538	(1.764)
Mean Aerodynamic Chord, M (ft)	3.368	(11.05)
L. E. Sweep (B. S. 1.275 (4.184)), deg	74.00	
L. E. Sweep (B. S. 4.758 (15.609)), deg	70.50	
L. E. Sweep (B. W. 6.238 (20.615)), deg	60.00	
Vertical Tail:		
Area, M^2 (ft^2)	0.101	(1.09)
Span, M (ft)	0.393	(1.291)
Root Chord, M (ft)	0.711	(2.333)
Tip Chord, M (ft)	0.163	(0.534)
L. E. Sweep, deg	59.0	
Vertical Fin (Two):		
Area, M^2 (ft^2)	0.415	(4.472)
Span, M (ft)	0.328	(1.075)
Root Chord, M (ft)	1.109	(3.638)
Tip Chord, M (ft)	0.158	(0.518)
L. E. Sweep, deg	73.40	
Horizontal Tail:		
Area, M^2 (ft^2)	0.739	(7.963)
Span, M (ft)	1.015	(3.33)
Aspect Ratio	1.39	
Root Chord, M (ft)	1.200	(3.937)
Tip Chord, M (ft)	0.258	(0.845)
L. E. Sweep, deg	43.00	
Dihedral, deg	-15.00	

TABLE II

SUMMARY OF RESULTS FOR APPROACH AND CLIMB PERFORMANCE

(a) 3^{o} approach with 40^{o} flap deflection and boundary-layer control

Configuration	T_C'	C_L	α, deg	T/W
Lower surface engines with 30^{o} deflected nozzles	0.1	0.63	3.0	0.16
	0.2	0.90	8.5	0.22
Upper surface engines with straight nozzles	0.1	0.70	2.0	0.14
	0.2	0.88	7.2	0.24
Upper surface engines with 20^{o} elbow exhaust nozzles	0.1	0.72	-1.5	0.14
	0.2	0.90	2.0	0.22

(b) 3^{o} climb with 30^{o} flap deflection and boundary-layer control

Configuration	T_C'	C_L	α, deg	T/W
Lower surface engines with 30^{o} deflected nozzles	0.1	0.45	-0.8	0.22
	0.2	0.70	5.2	0.29
Upper surface engines with straight nozzles	0.1	0.51	-0.8	0.19
	0.2	0.72	5.5	0.28
Upper surface engines with 20^{o} elbow exhaust nozzles	0.1	0.45	-3.7	0.22
	0.2	0.74	1.5	0.27

TABLE II (Concluded)

(c) 3^{o} climb with 20^{o} flap deflection and boundary-layer control

Configuration	T_C'	C_L	α, deg	T/W
Lower surface engines with 20^{o} deflected nozzles	0.1	0.5	4	0.20
	0.2	0.7	8	0.29
Upper surface engines with straight nozzles	0.1	0.5	2	0.2
	0.2	0.68	8	0.29
Upper surface with 20^{o} elbow nozzles	0.1	0.5	0	0.20
	0.2	0.75	6	0.27

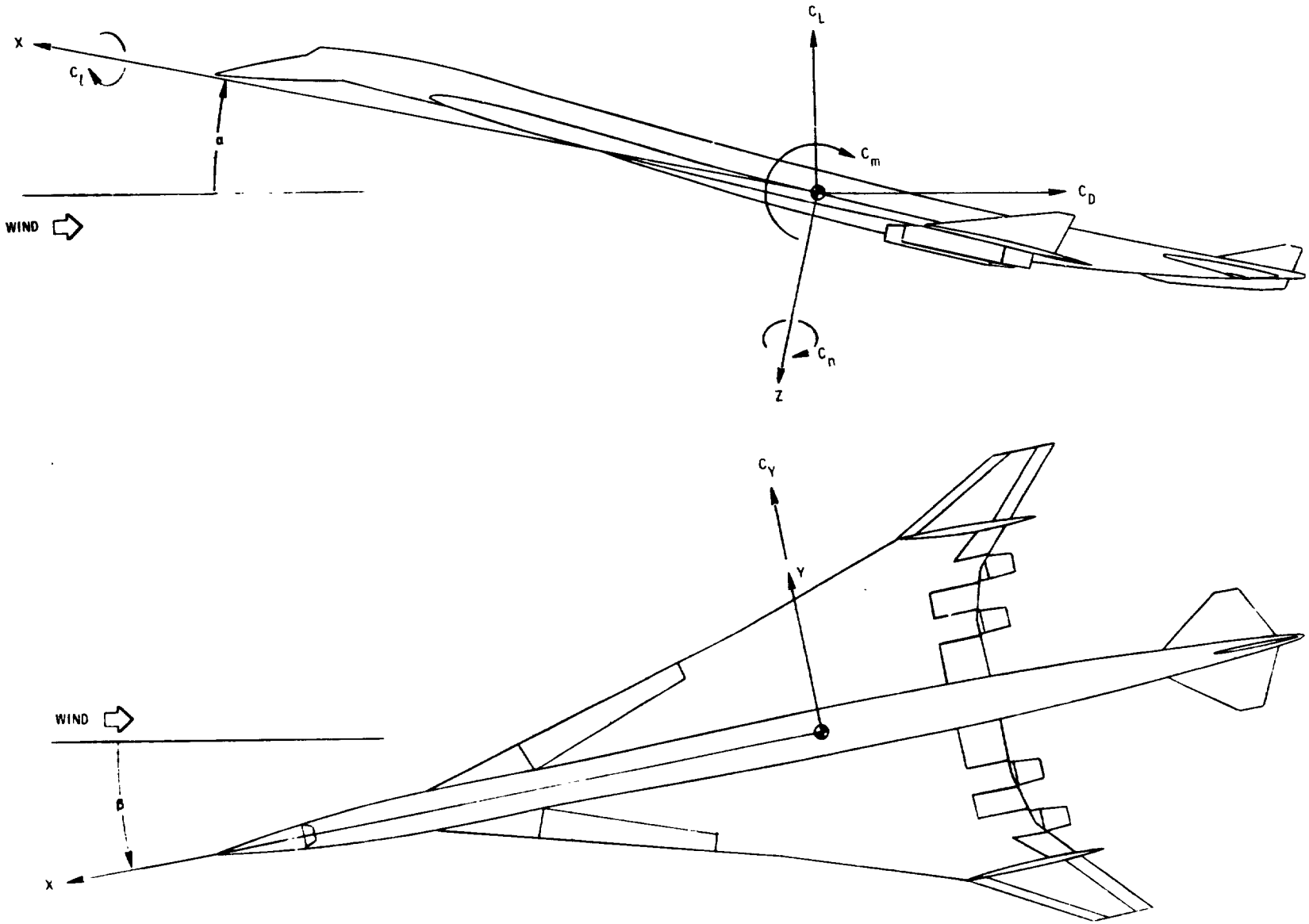

Figure 1. - The body system of axes.

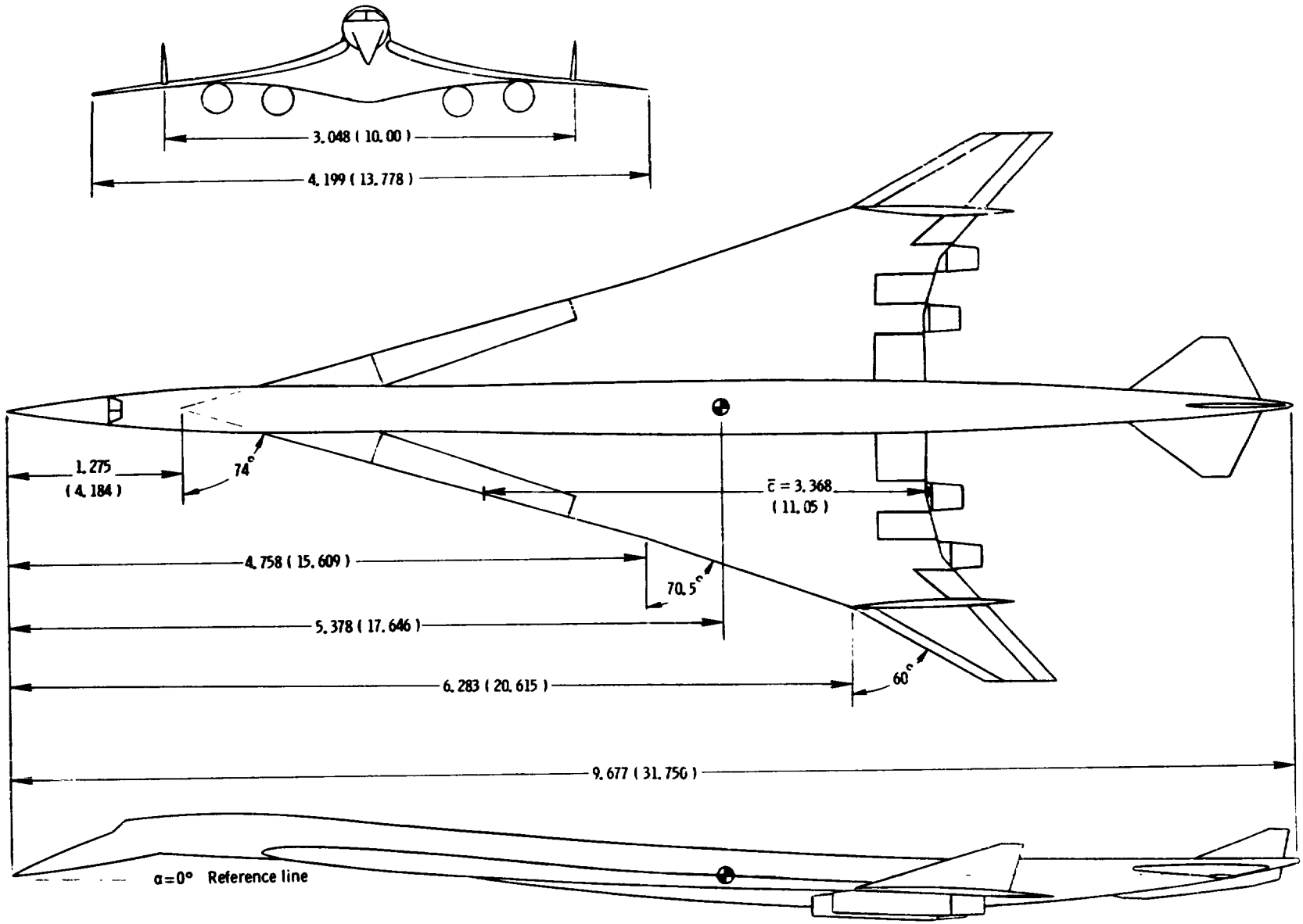

(a) Three-view sketch of model with lower surface engines. Dimensions are given in meters and parenthetically in feet.

Figure 2. - Dimensional characteristics.

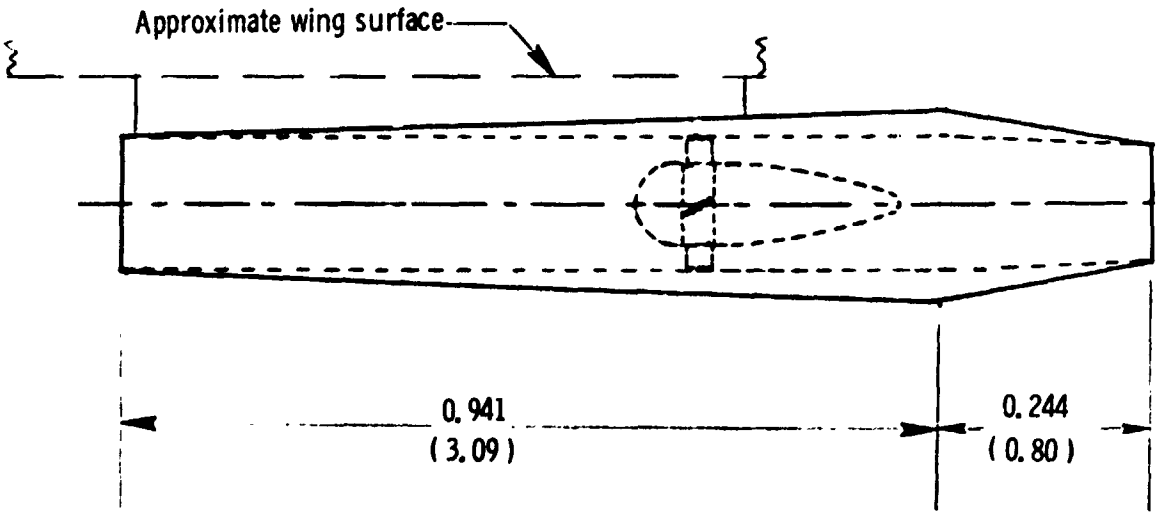

Engine with undeflected exhaust nozzle

Fan dia. = 0.140 (0.458)

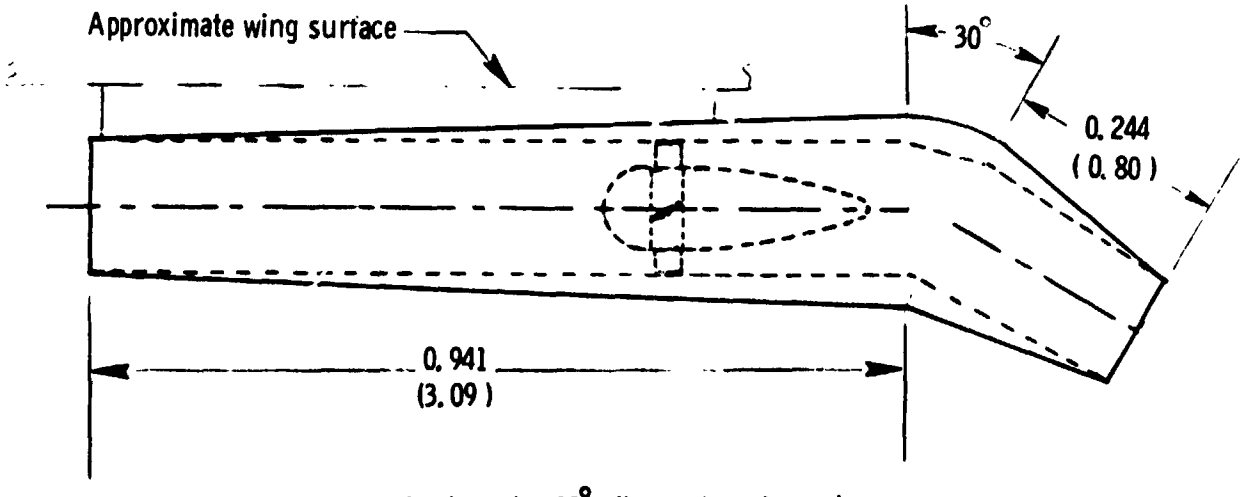

Engine with 30° elbow exhaust nozzle

(b) Lower surface engine with compressed air driven fan.

Dimensions are given in meters and parenthetically in feet.

Figure 2. - Continued.

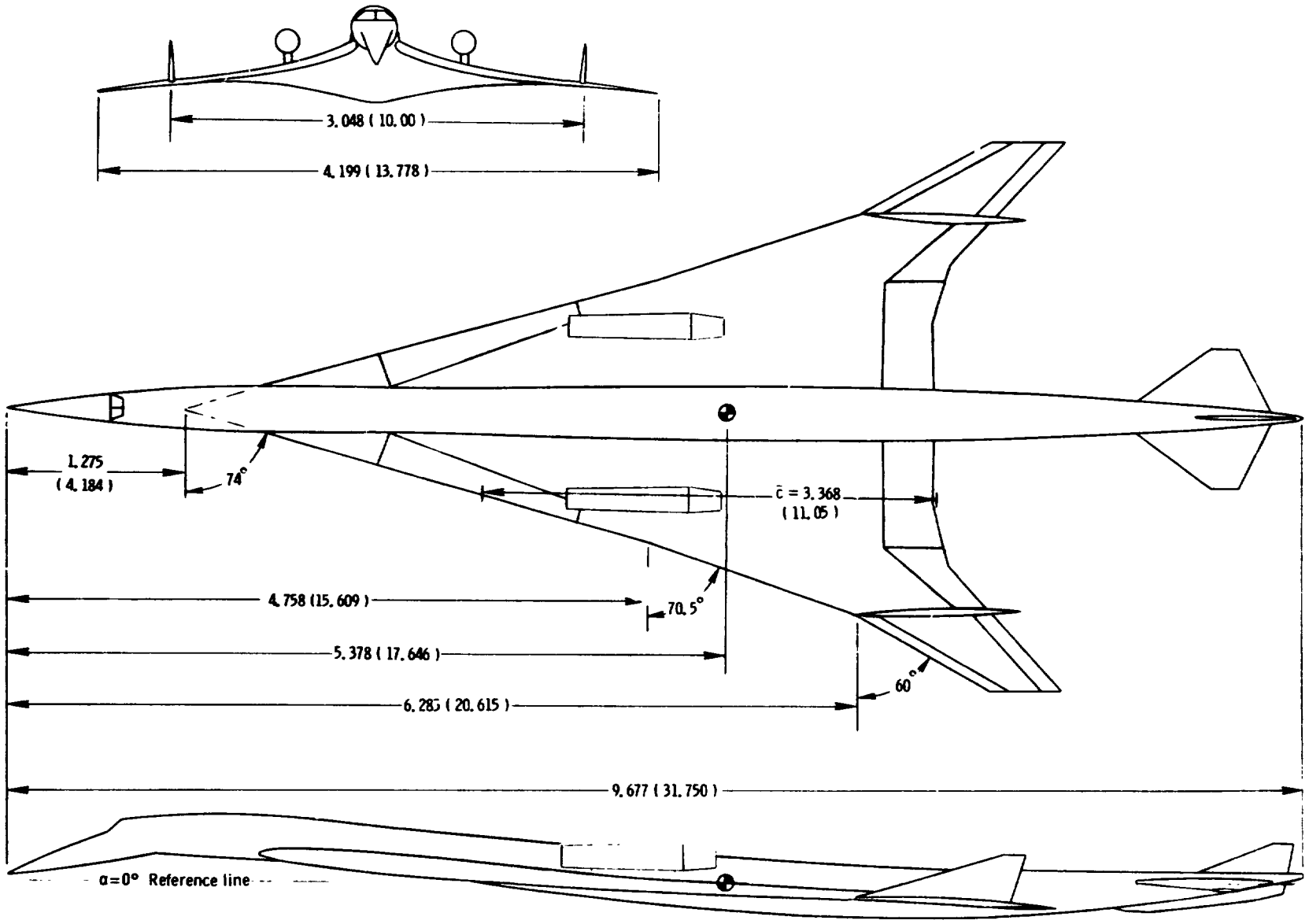

(c) Three-view sketch of model with upper surface engines. Dimensions are given in meters and parenthetically in feet.

Figure 2. - Continued.

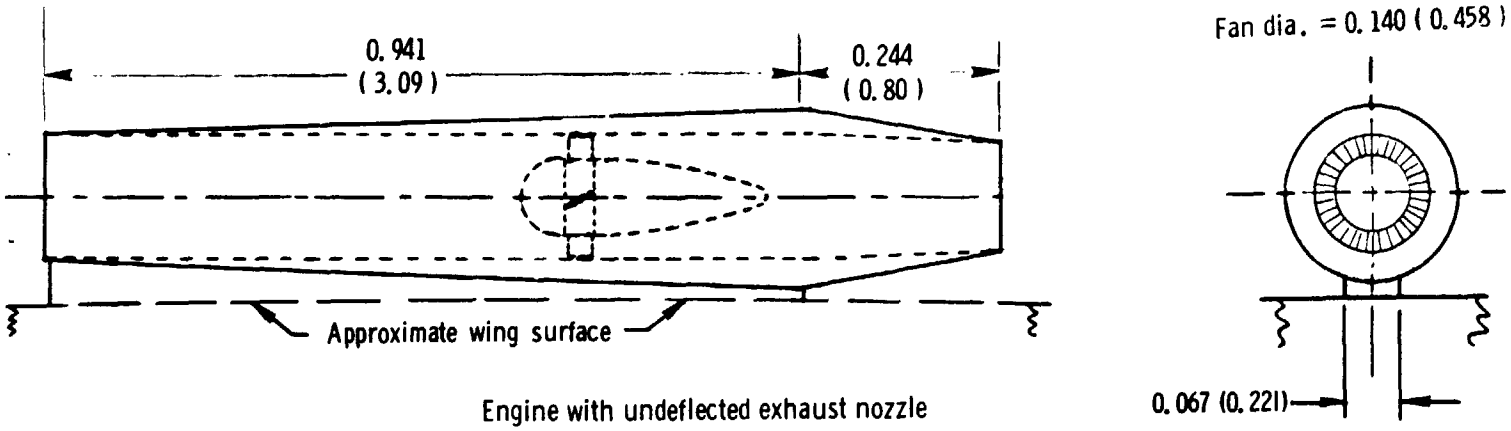

Engine with undeflected exhaust nozzle

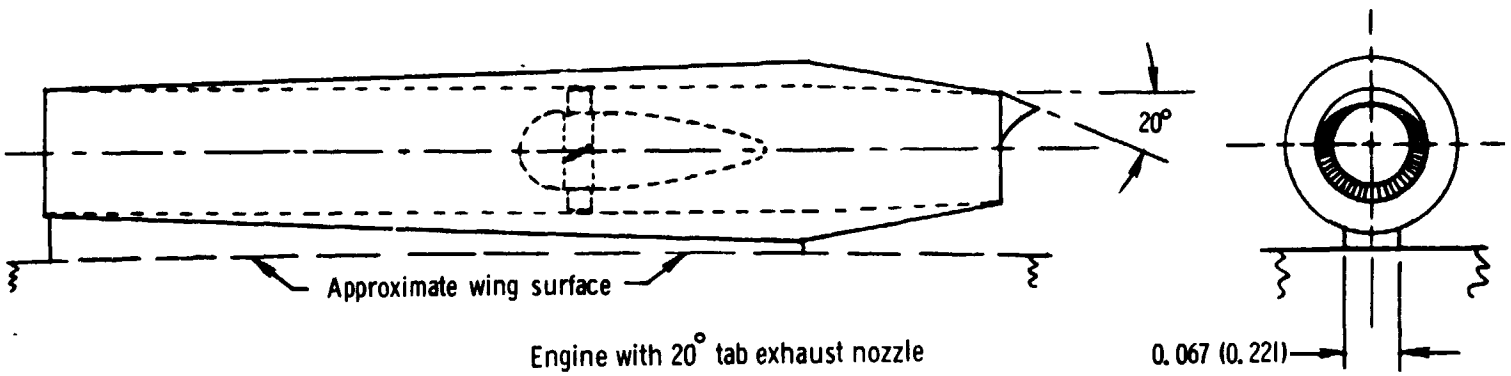

Engine with 20° tab exhaust nozzle

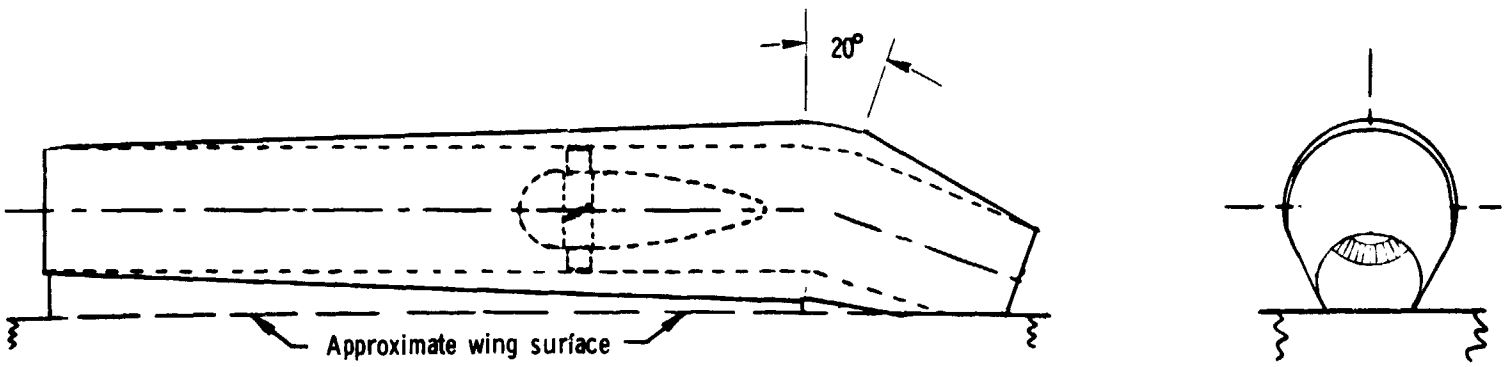

Engine with 20° elbow exhaust nozzle

(d) Upper surface engine with compressed air driven fan.
Dimensions are given in meters and parenthetically in feet.

Figure 2. - Continued.

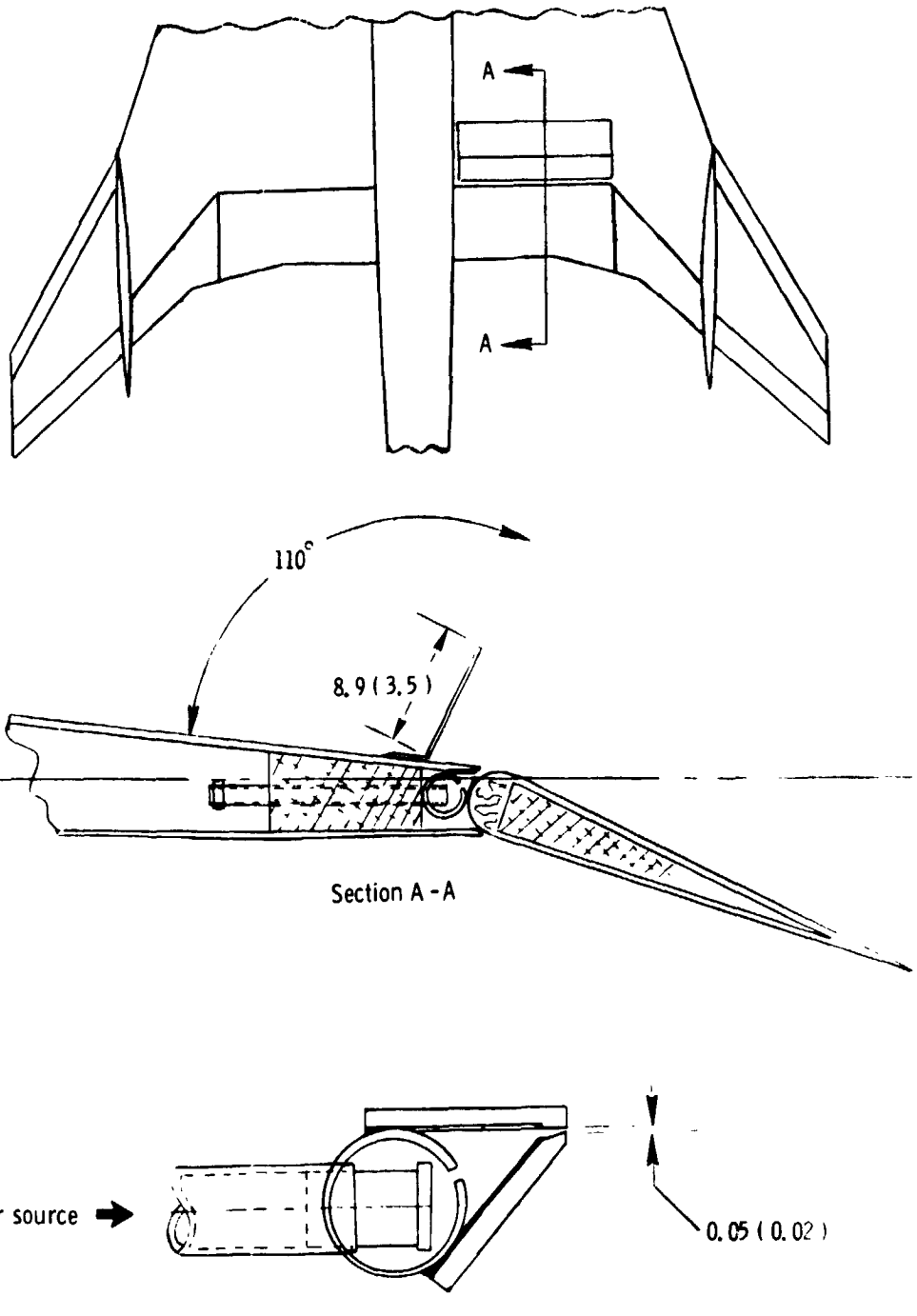

(e) Sketch of flap boundary layer control and spoiler.

Dimensions are given in centimeters and parenthetically in inches.

Figure 2. - Concluded.

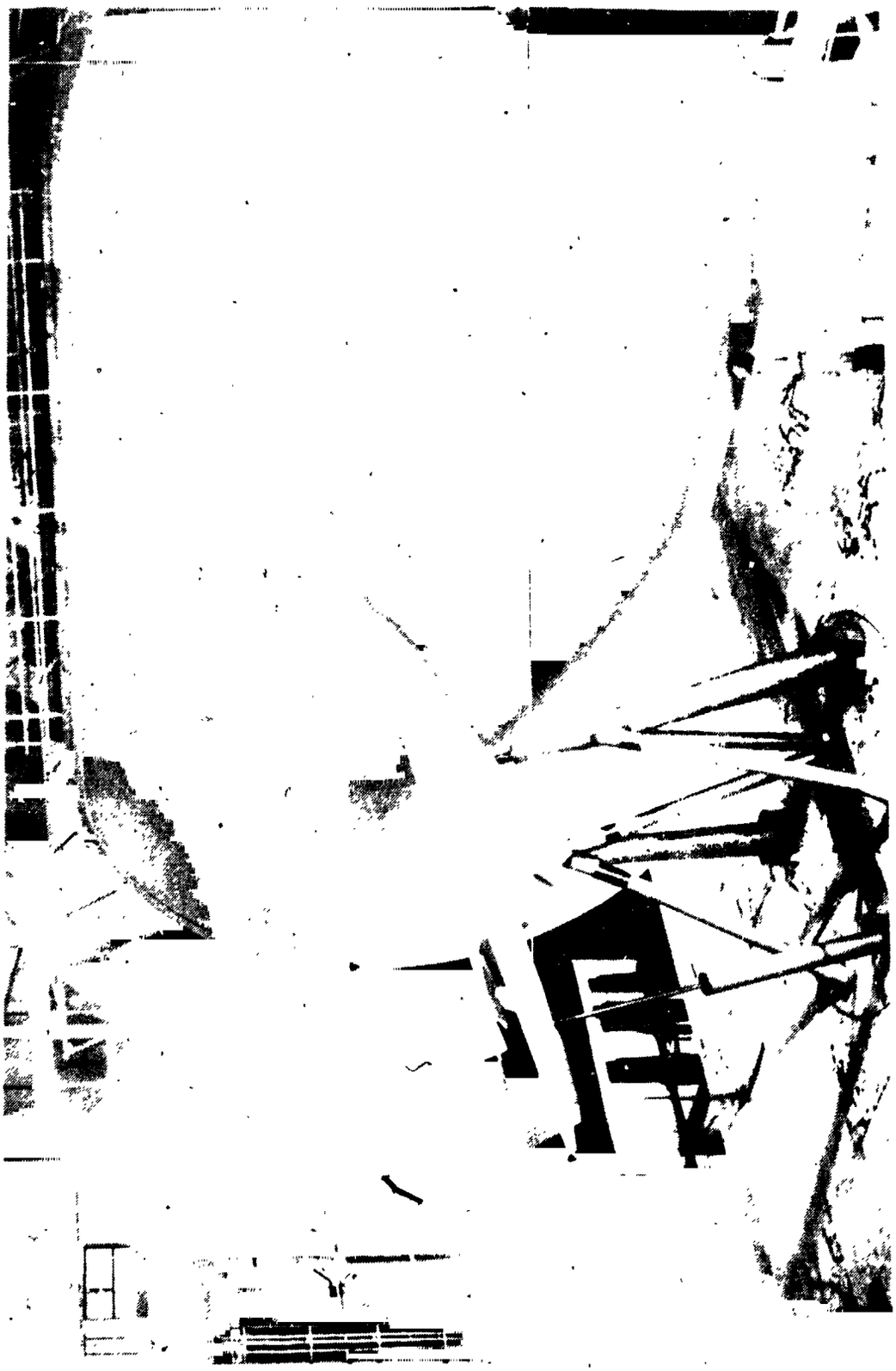

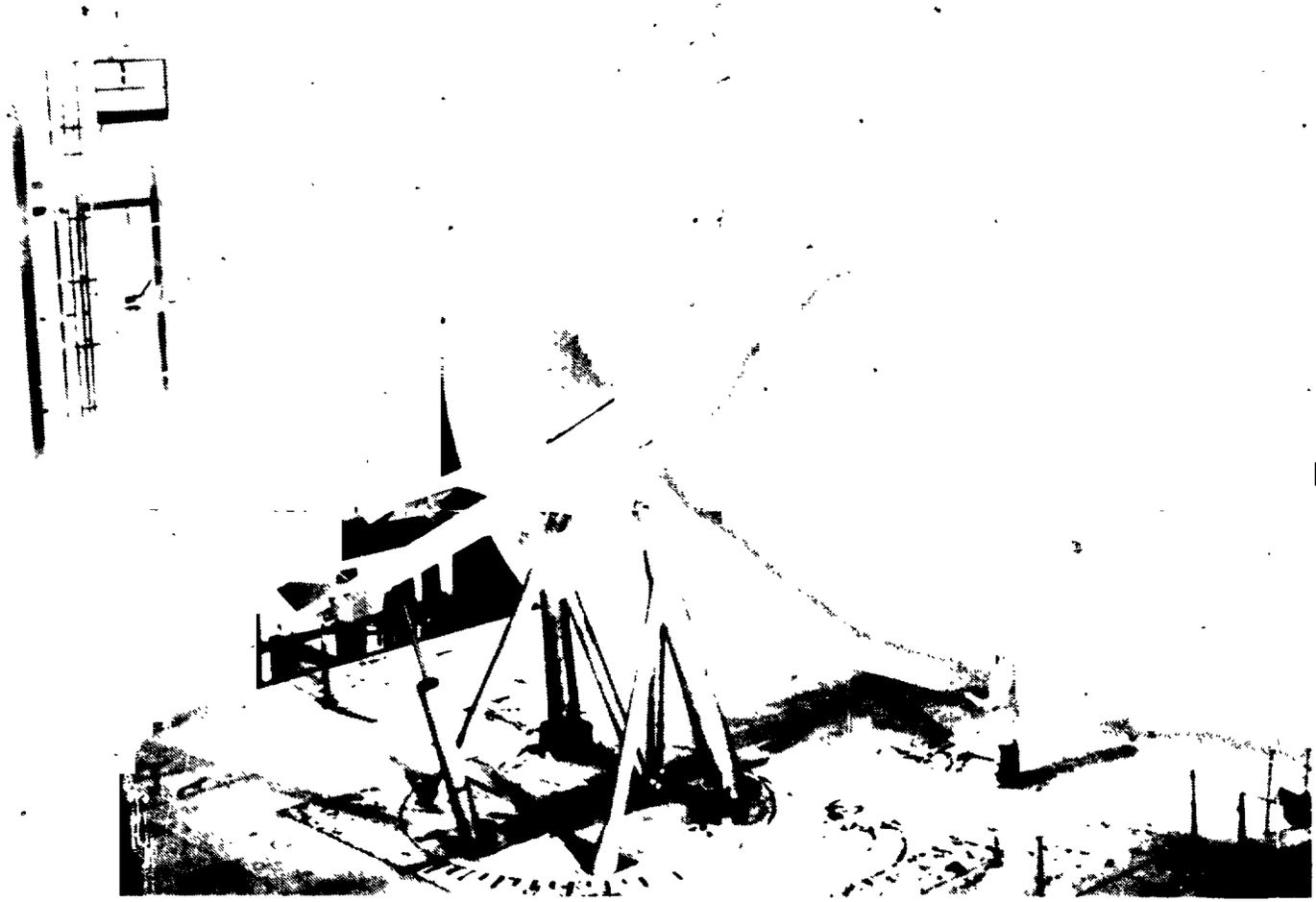

Figure 4. -Three-quarter rear view of the model with upper surface [illegible] mounted for tests in the Langley full-scale tunnel.

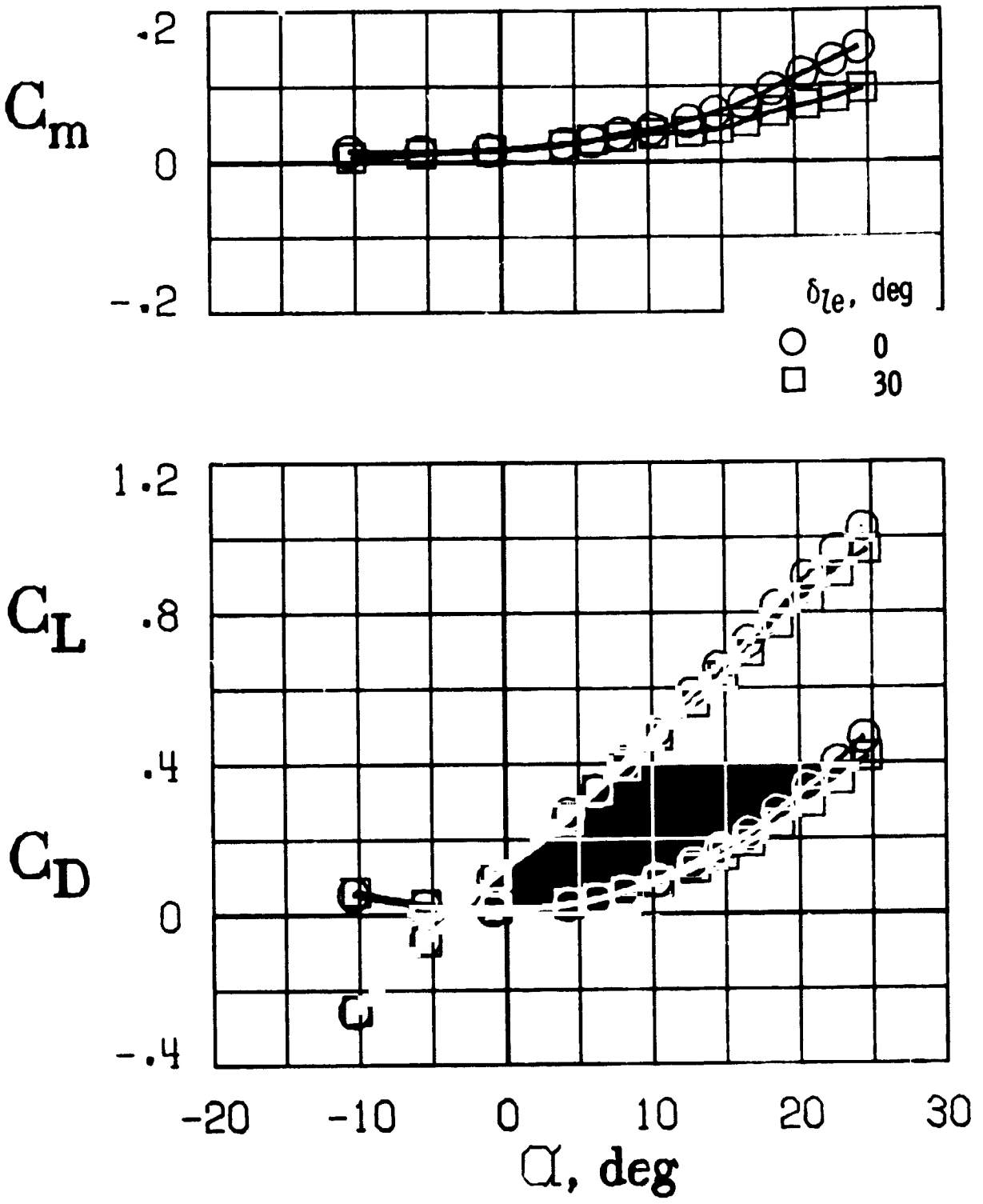

Figure 5. - Effect of leading-edge flap deflection on longitudinal characteristics of the model with lower surface engines. Tail off, $T_C' = 0$, $\delta_f = 0°$.

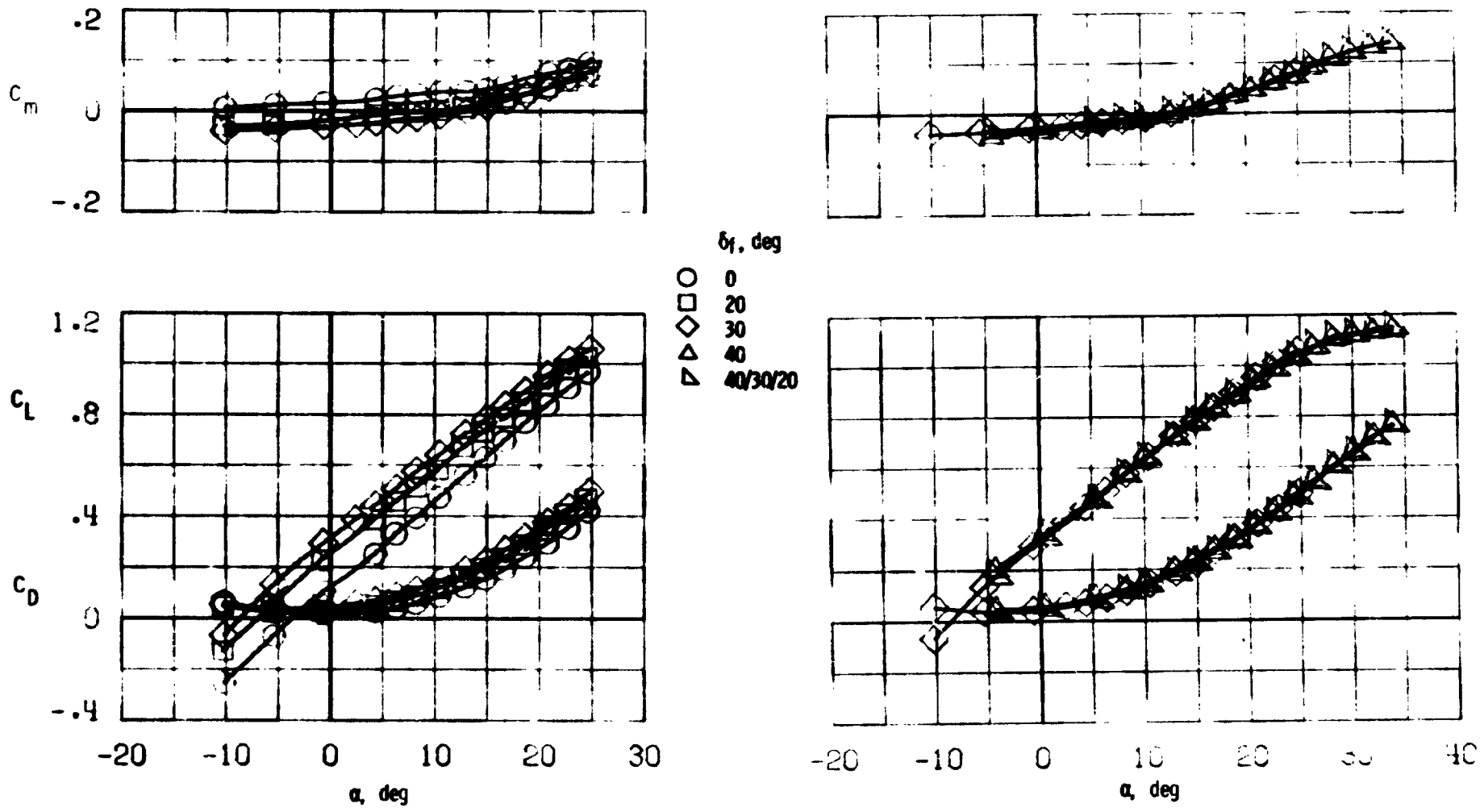

(a) $\delta_f = 0°, 20°, 30°$.

(b) $\delta_f = 30°, 40°, 40°/30°/20°$.

Figure 6. - Effect of trailing-edge flap deflection for the model with lower surface engines. Tail off, $T_c' = 0$, $C_\mu = 0$.

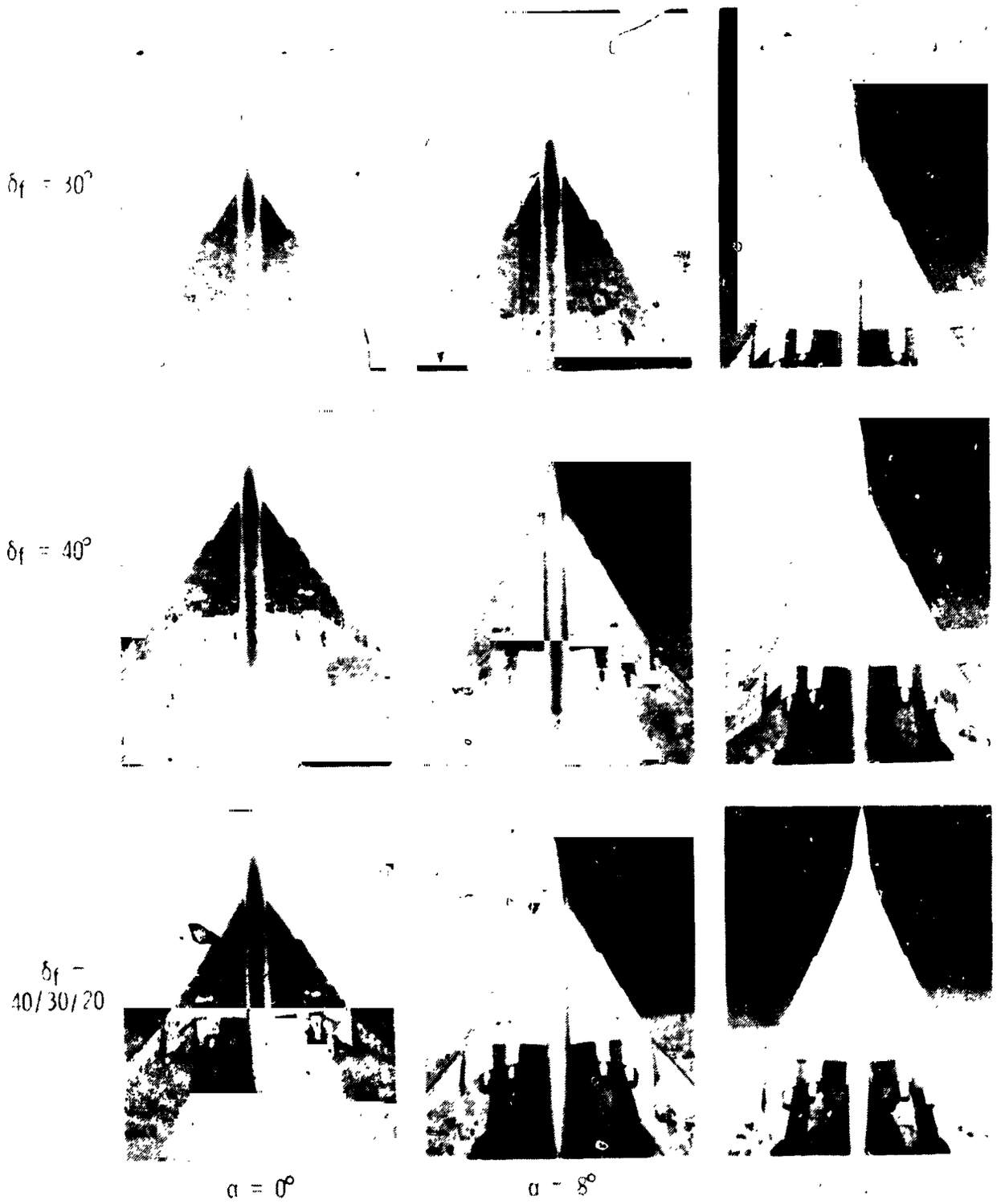

Figure 7. - Flow-visualization of flow over trailing-edge flap with [illegible] control. (Lower surface engine.)

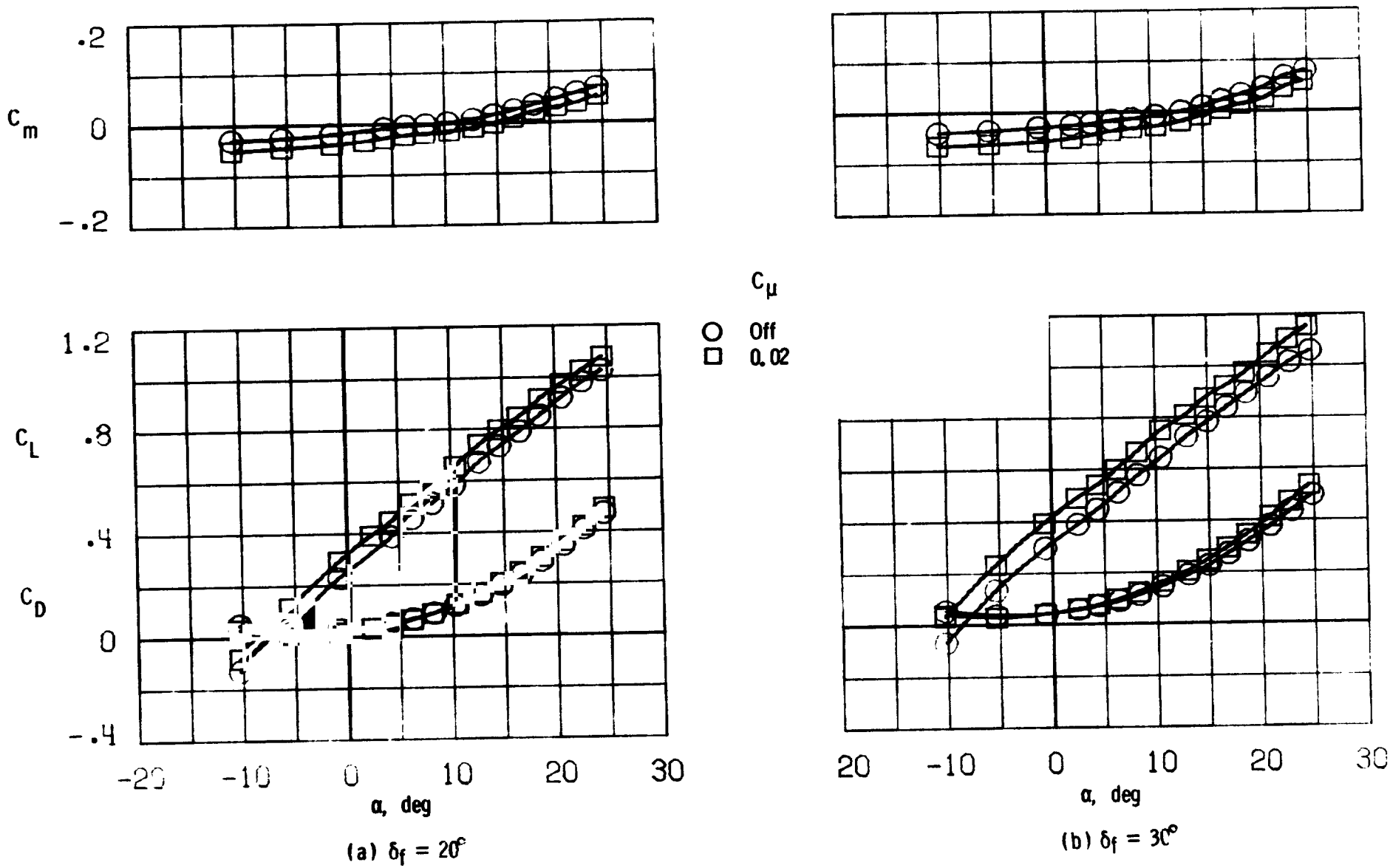

Figure 8. - Effect of boundary-layer control on trailing-edge flaps. Wing-body combination with lower surface engines. $T_C' = 0$.

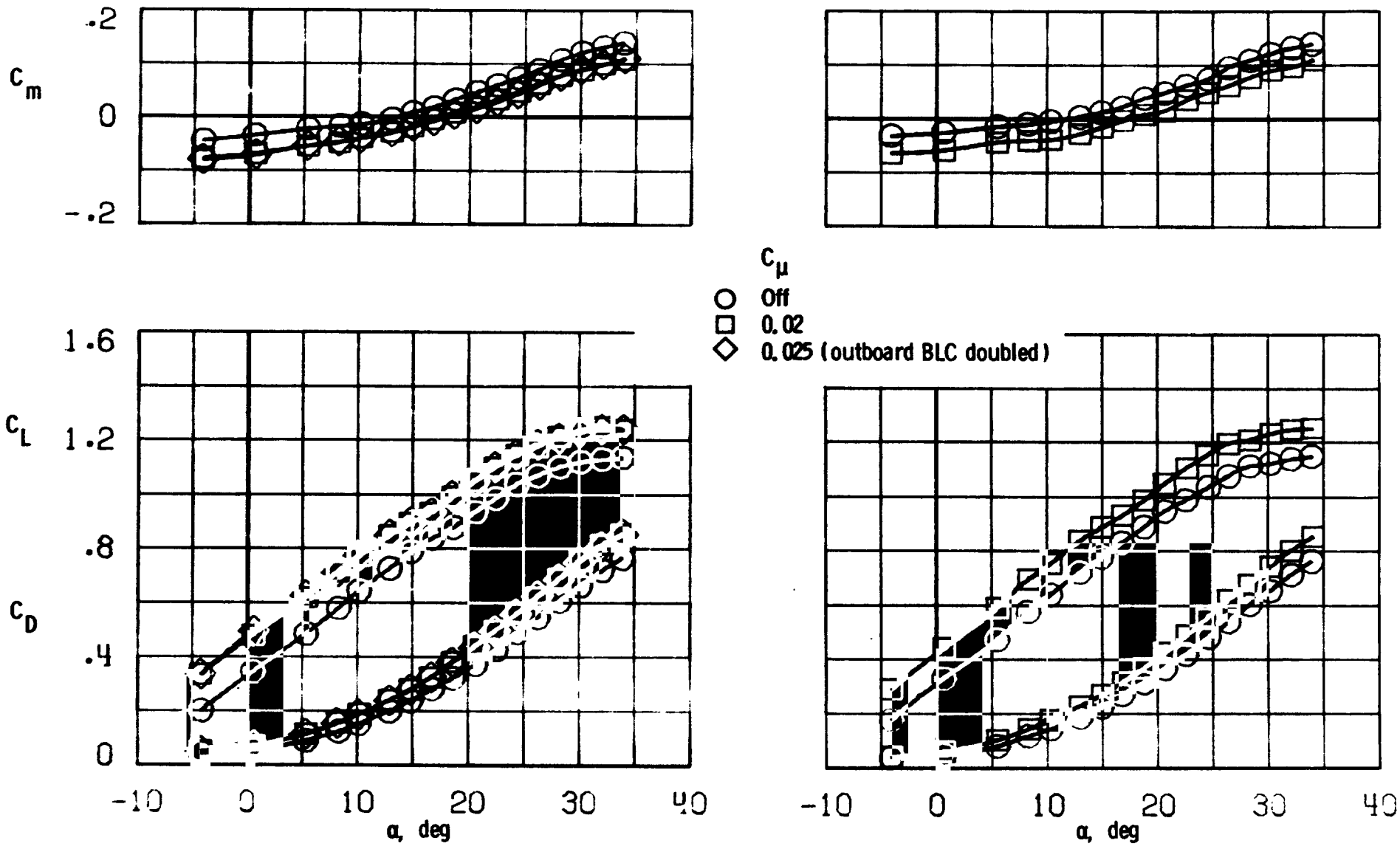

(c) $\delta_f = 40°$

(d) $\delta_f = 40°/30°/20°$

Figure 8. - Concluded.

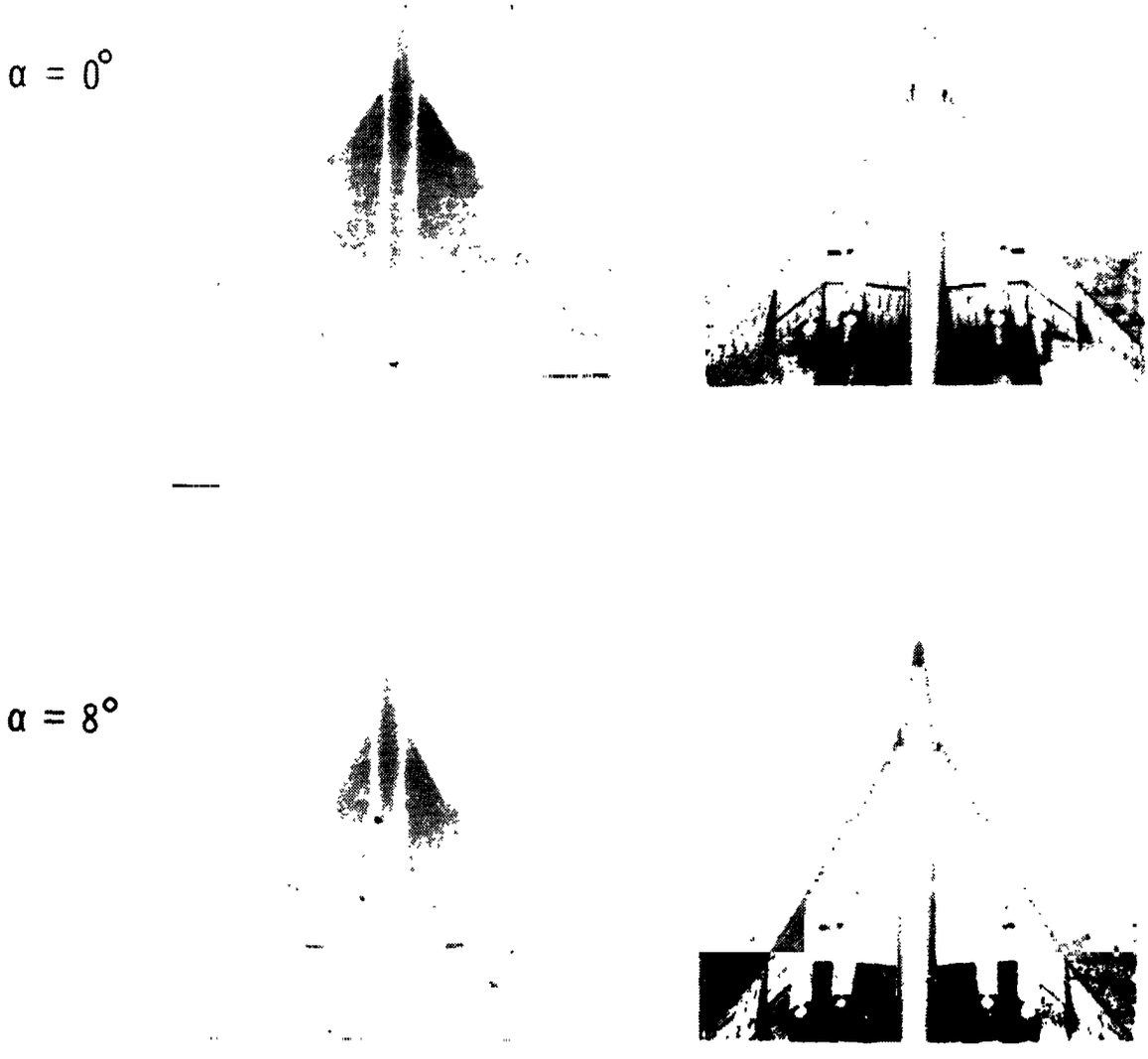

(a) $\delta_f = 30°$

Figure 9. - Effect of boundary-layer control on flow over trailing-edge flaps. (Lower surface engines)

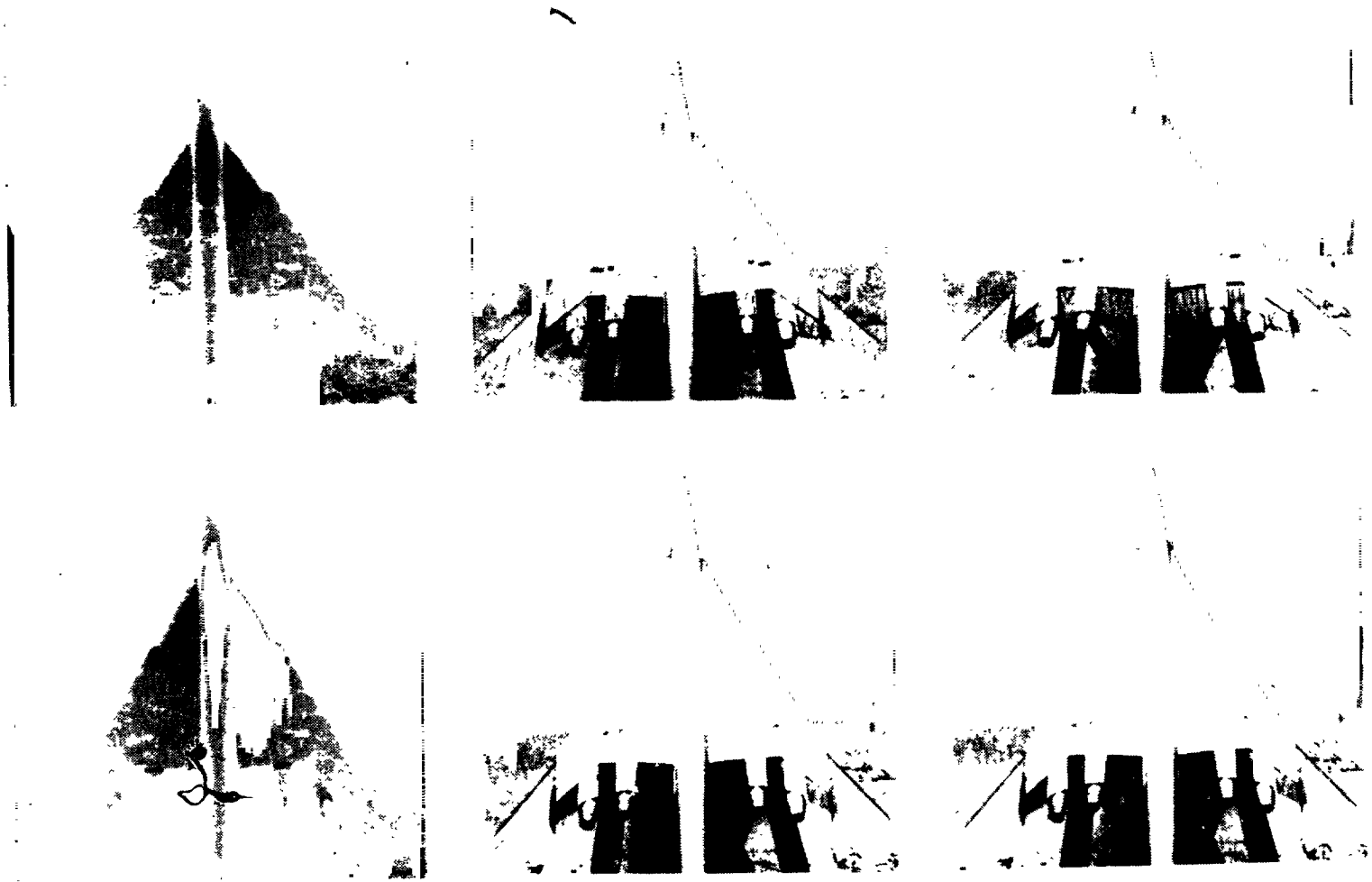

(b) $\delta_f = 40^\circ$

Figure 9. - Continued.

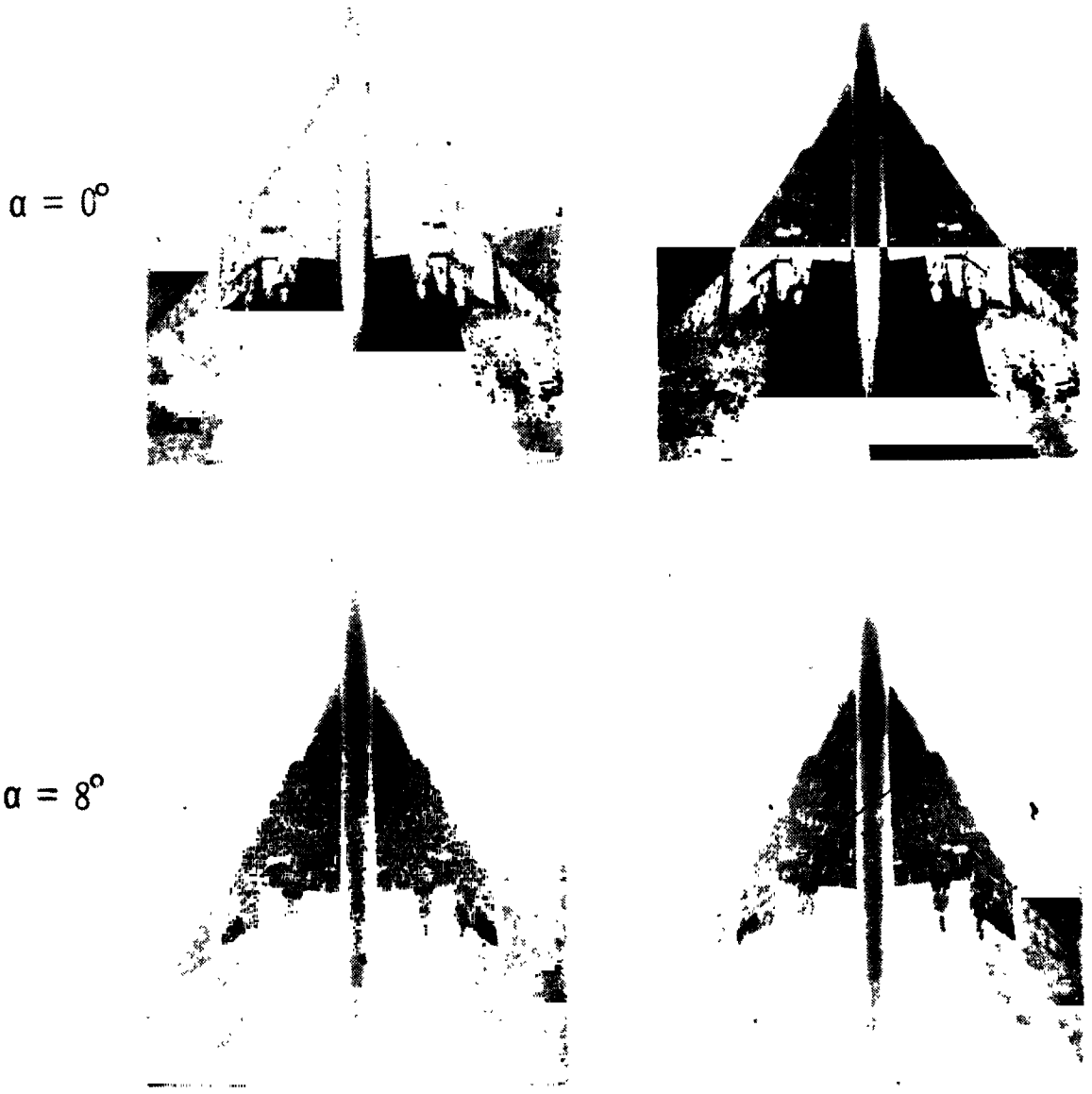

(c) δ_f = 40°/30°/20°

Figure 9. - Concluded.

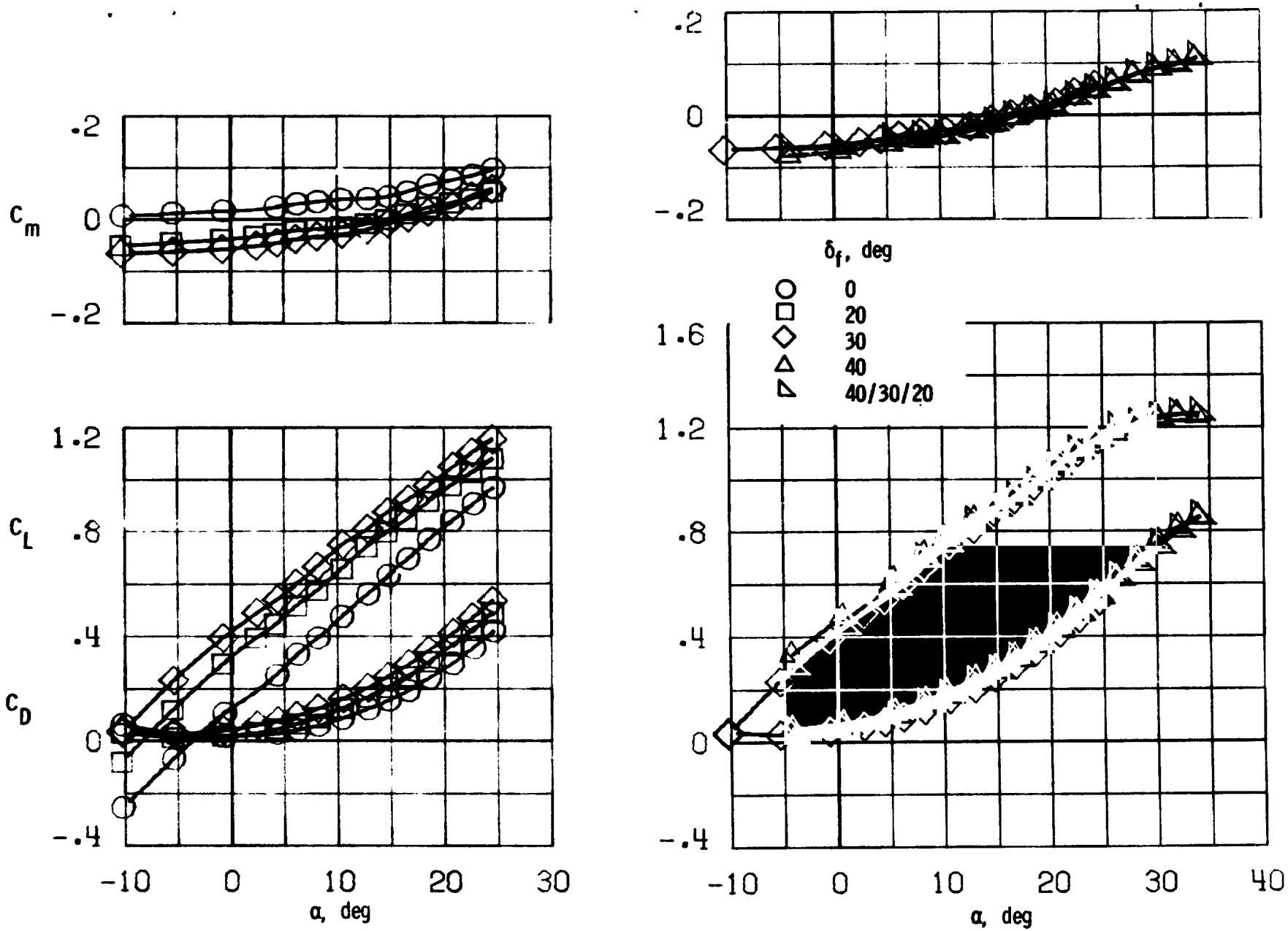

(a) $\delta_f = 0°, 20°, 30°$.

(b) $\delta_f = 30°, 40°, 40°/30°/20°$

Figure 10. - Trailing-edge flap effectiveness with boundary-layer control. Wing-body combination with lower surface engines. $T_C' = 0$, $C_\mu = 0.02$.

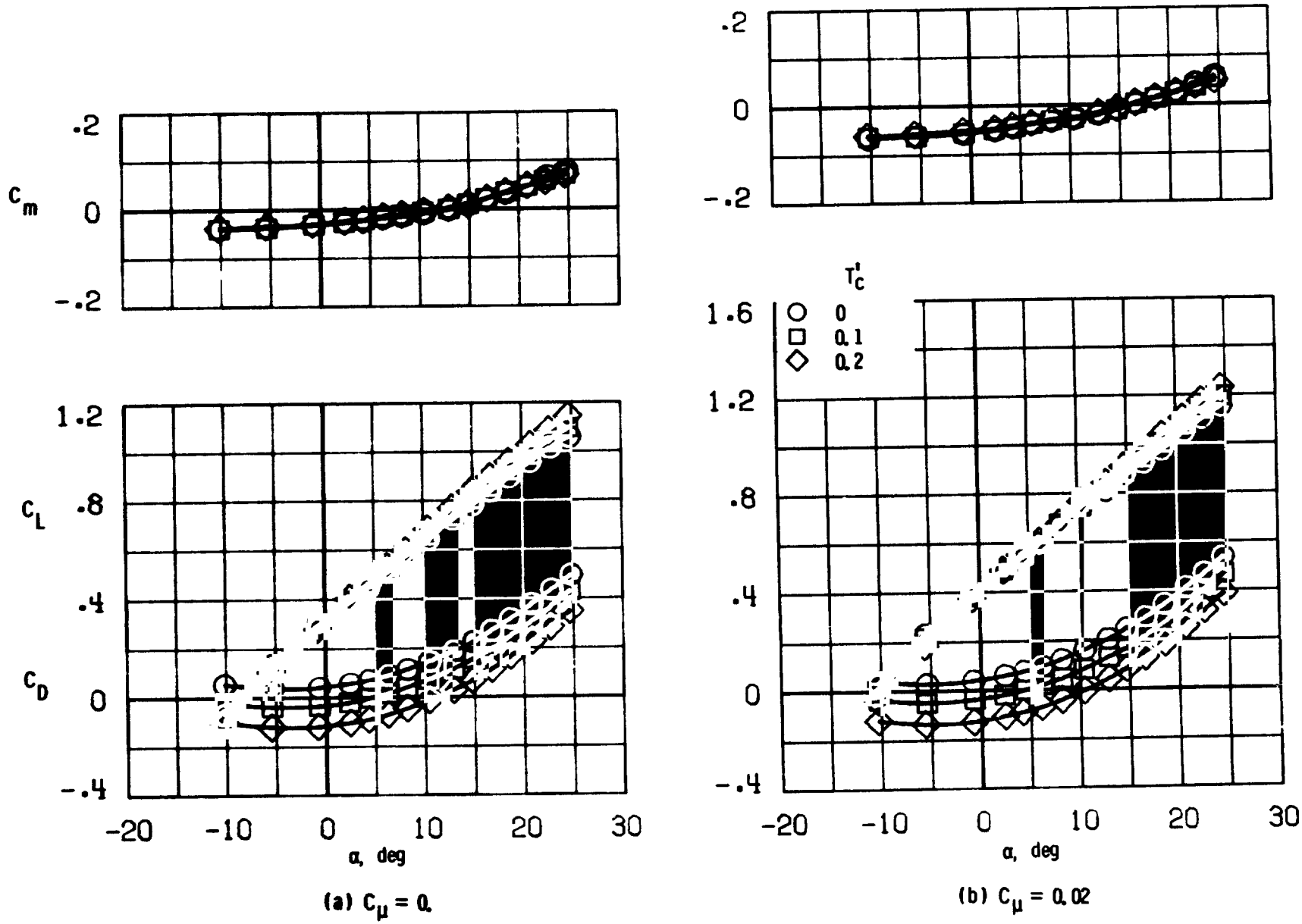

Figure 11. - Effect of thrust on longitudinal aerodynamic characteristics. Wing-body combination with lower surface engines. $\delta_f = 30°$, $\delta_N = 0°$.

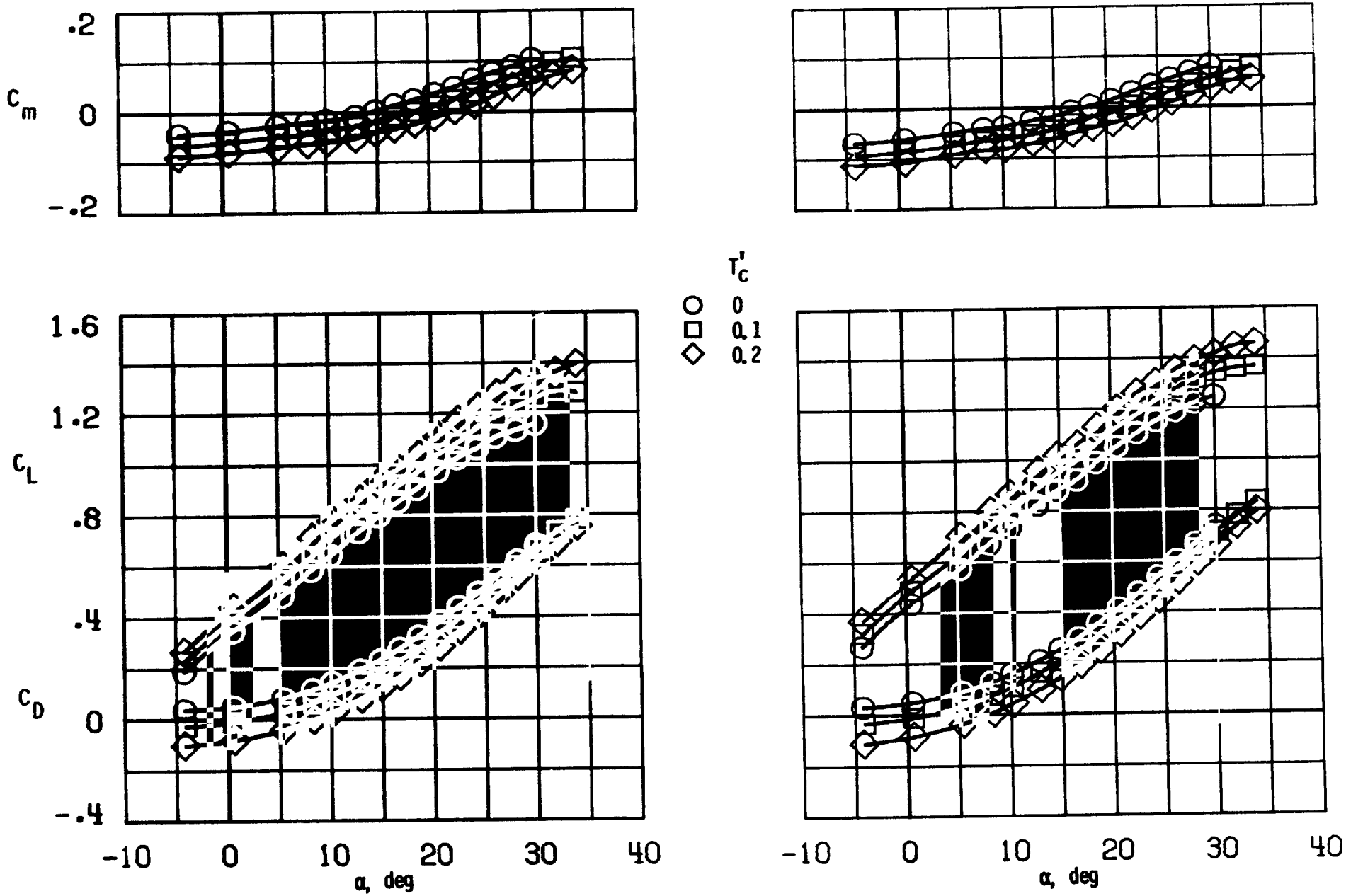

Figure 12. - Effect of thrust on longitudinal aerodynamic characteristics. Wing-body combination with lower surface engines and 30° deflected exhaust nozzles.

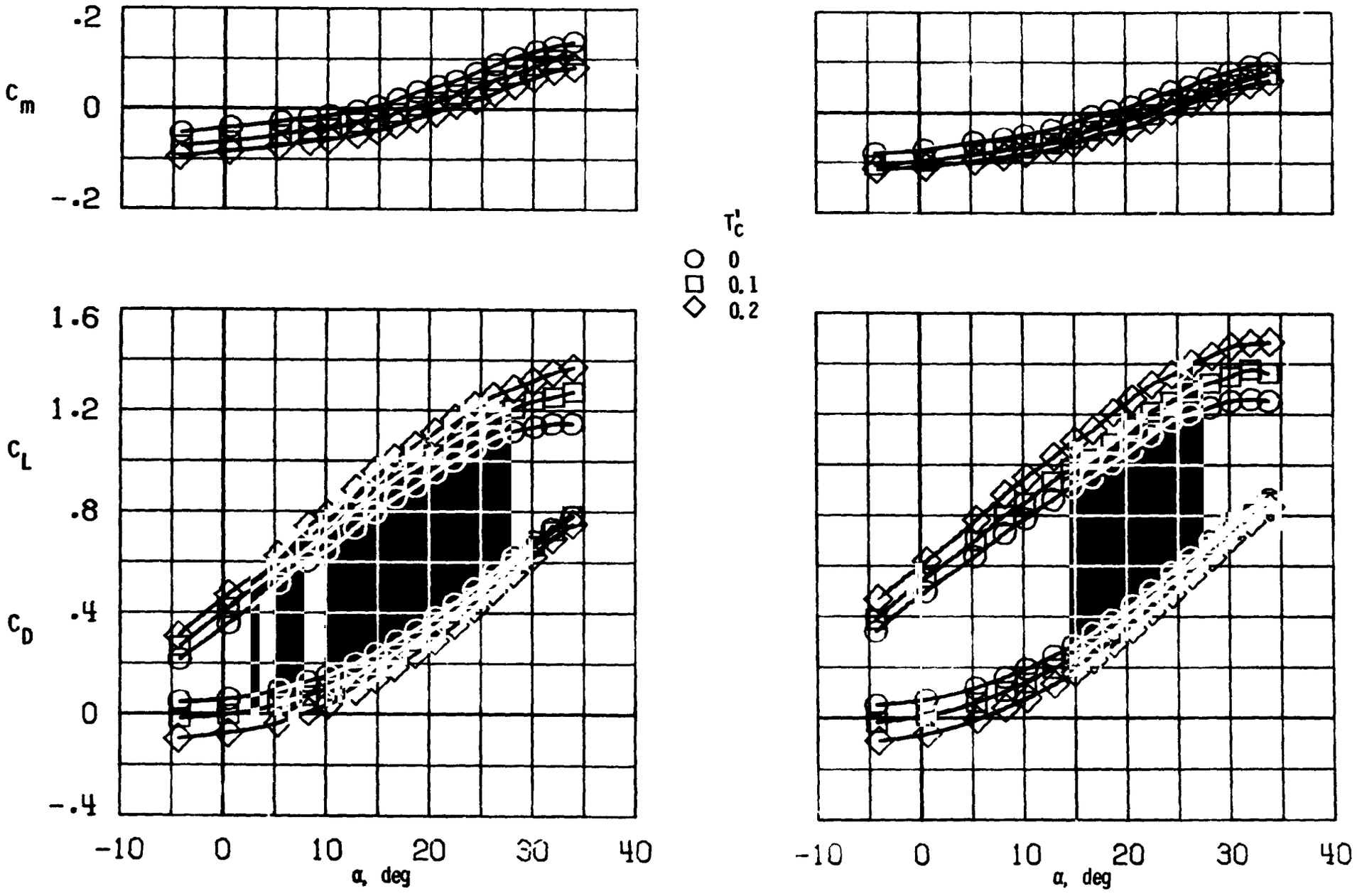

(c) $\delta_f = 40°$, $C_\mu = 0$.

(d) $\delta_f = 40°$, $C_\mu = 0.02$

Figure 12. - Concluded.

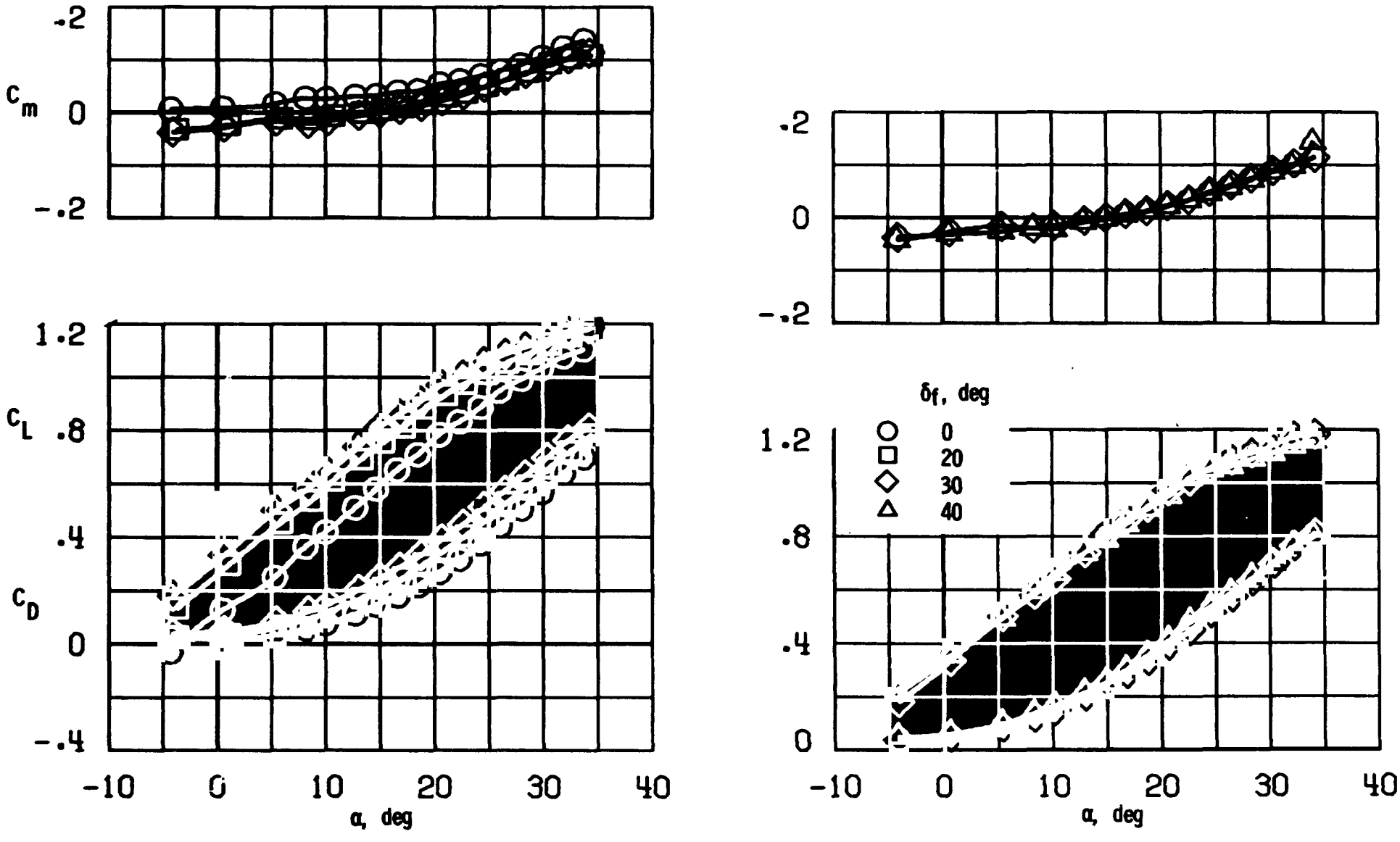

(a) $\delta_f = 0°, 20°, 30°$.

(b) $\delta_f = 30°, 40°$.

Figure 13. - Trailing-edge flap effectiveness for the wing-body combination with upper surface engines. $T_C' = 0$, $C_\mu = 0$.

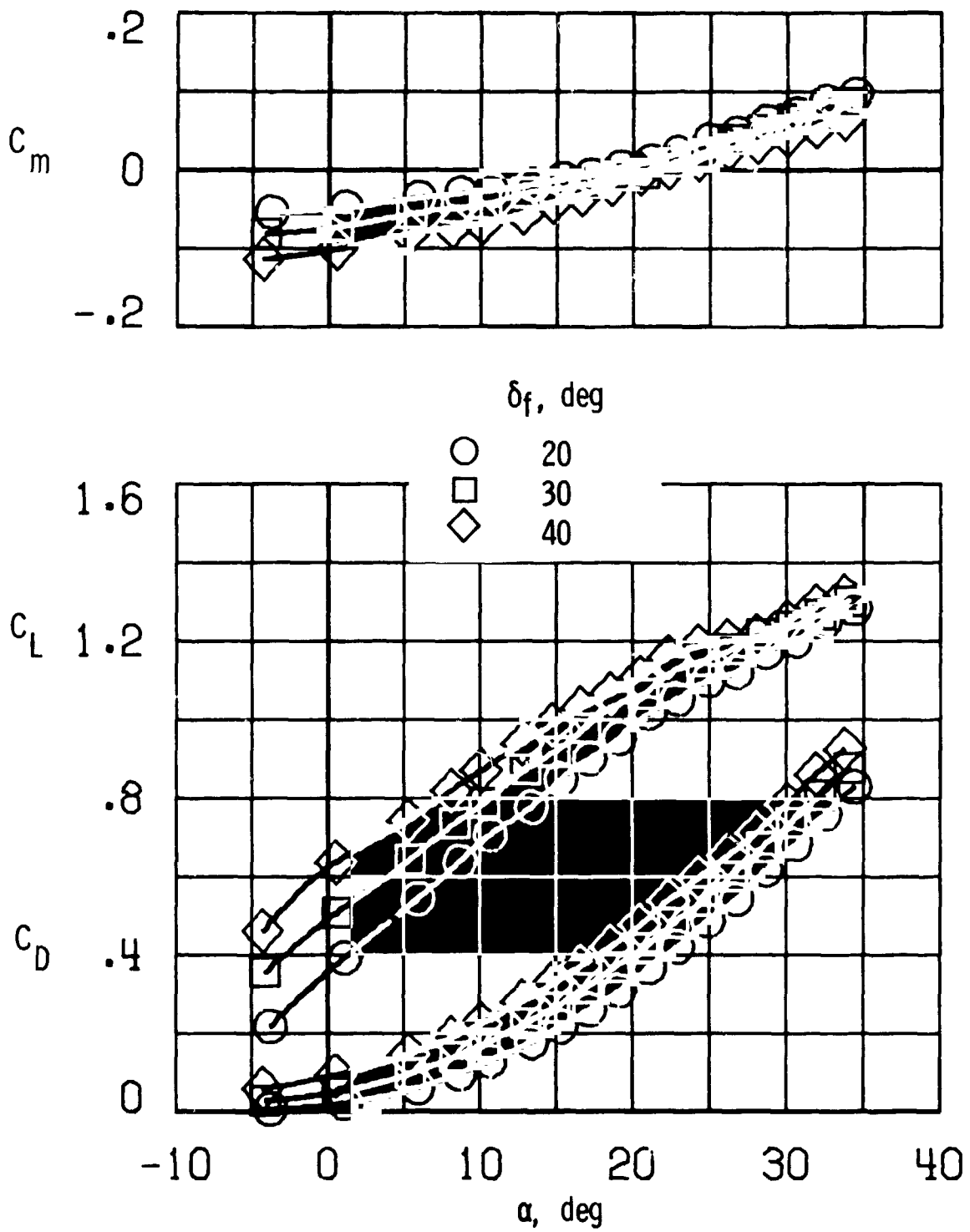

Figure 14. - Trailing-edge flap effectiveness with boundary layer control. Wing-body combination with upper surface engines. $T_c' = 0$, $C_\mu = 0.04$.

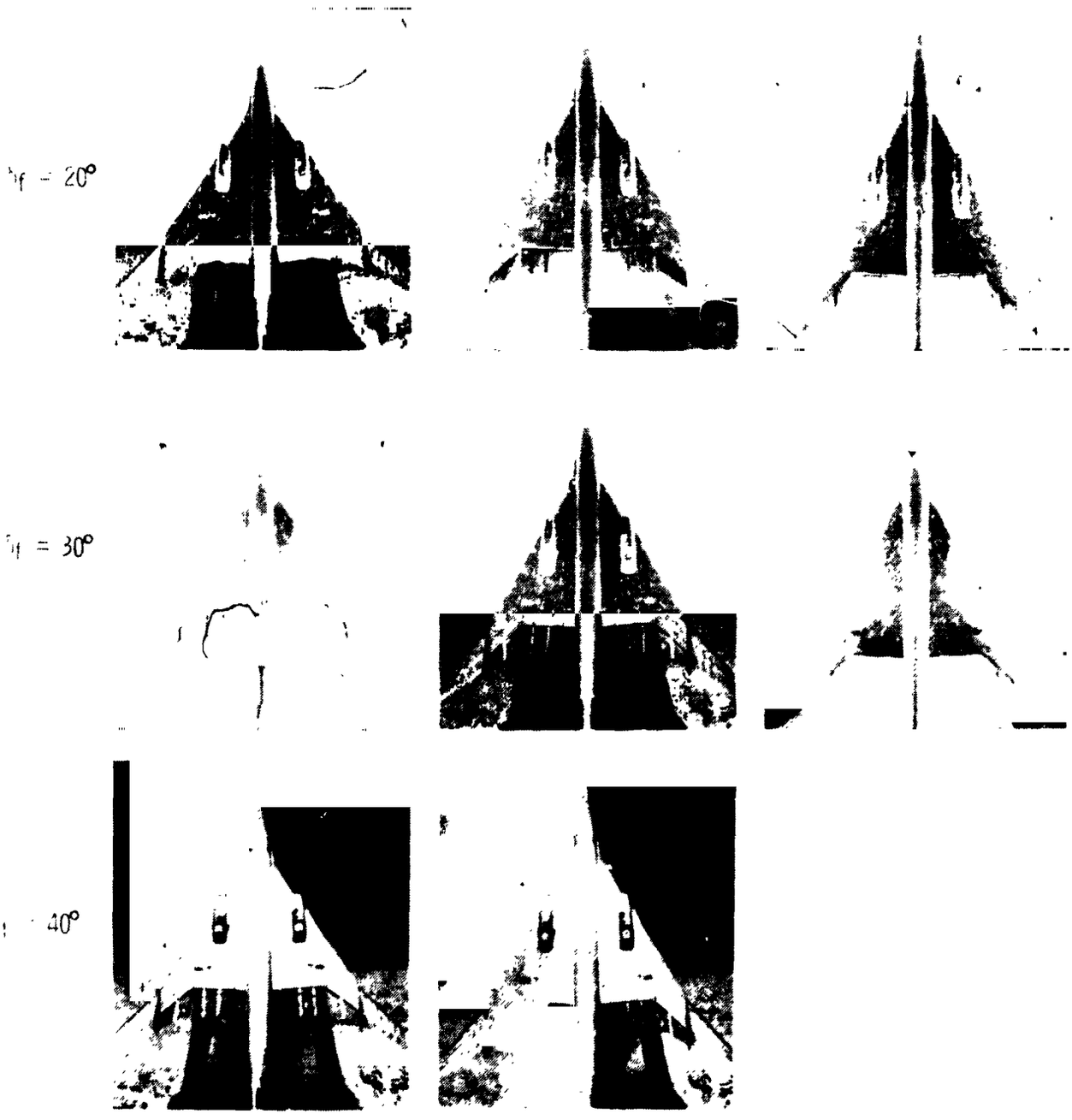

(a) $C_\mu = 0$.

Figure 15. - Flow-visualization of flow over trailing-edge flaps. (upper surface engines, $T_c' = 0$.)

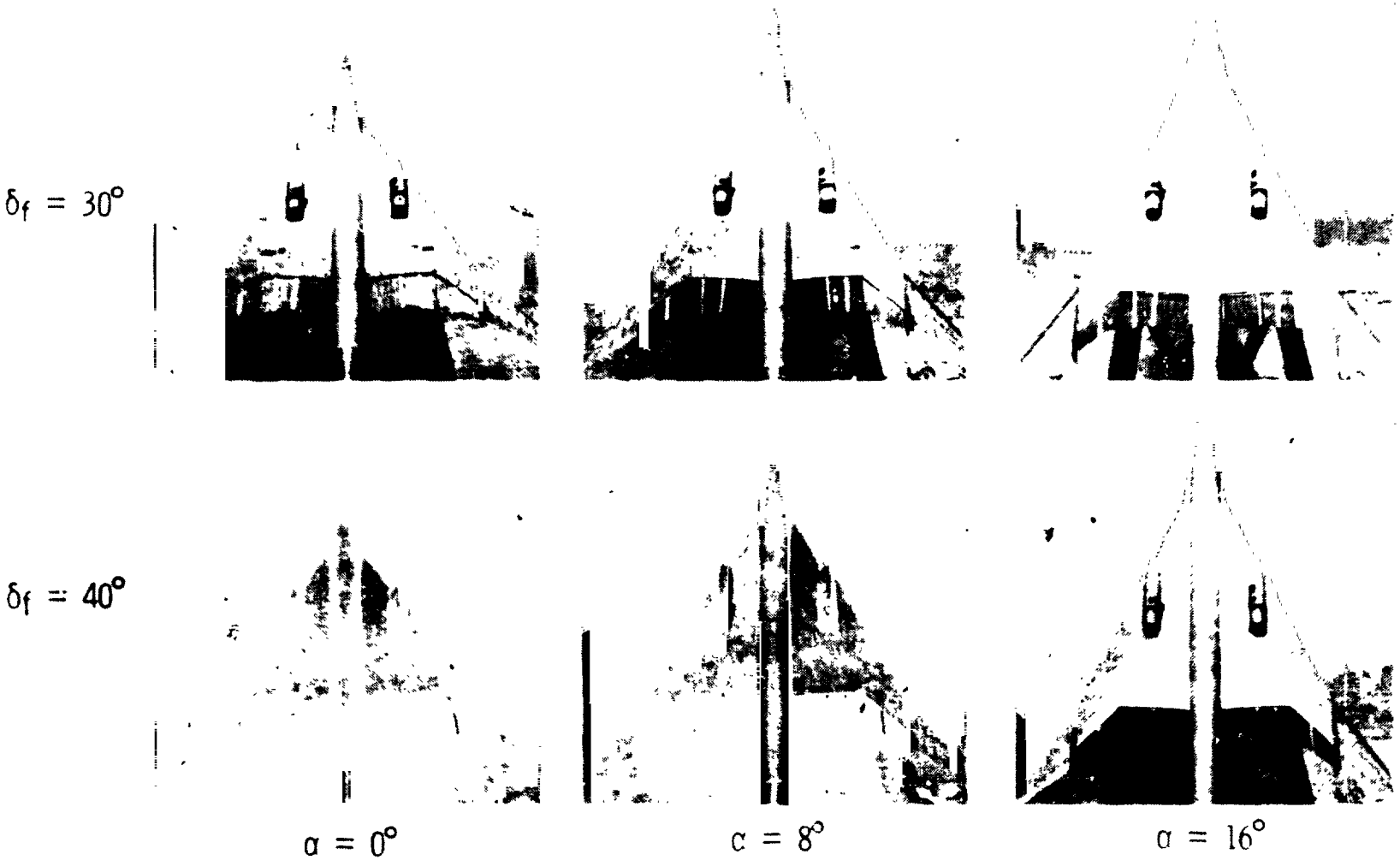

(b) C_μ = 0 04

Figure 15. - Concluded

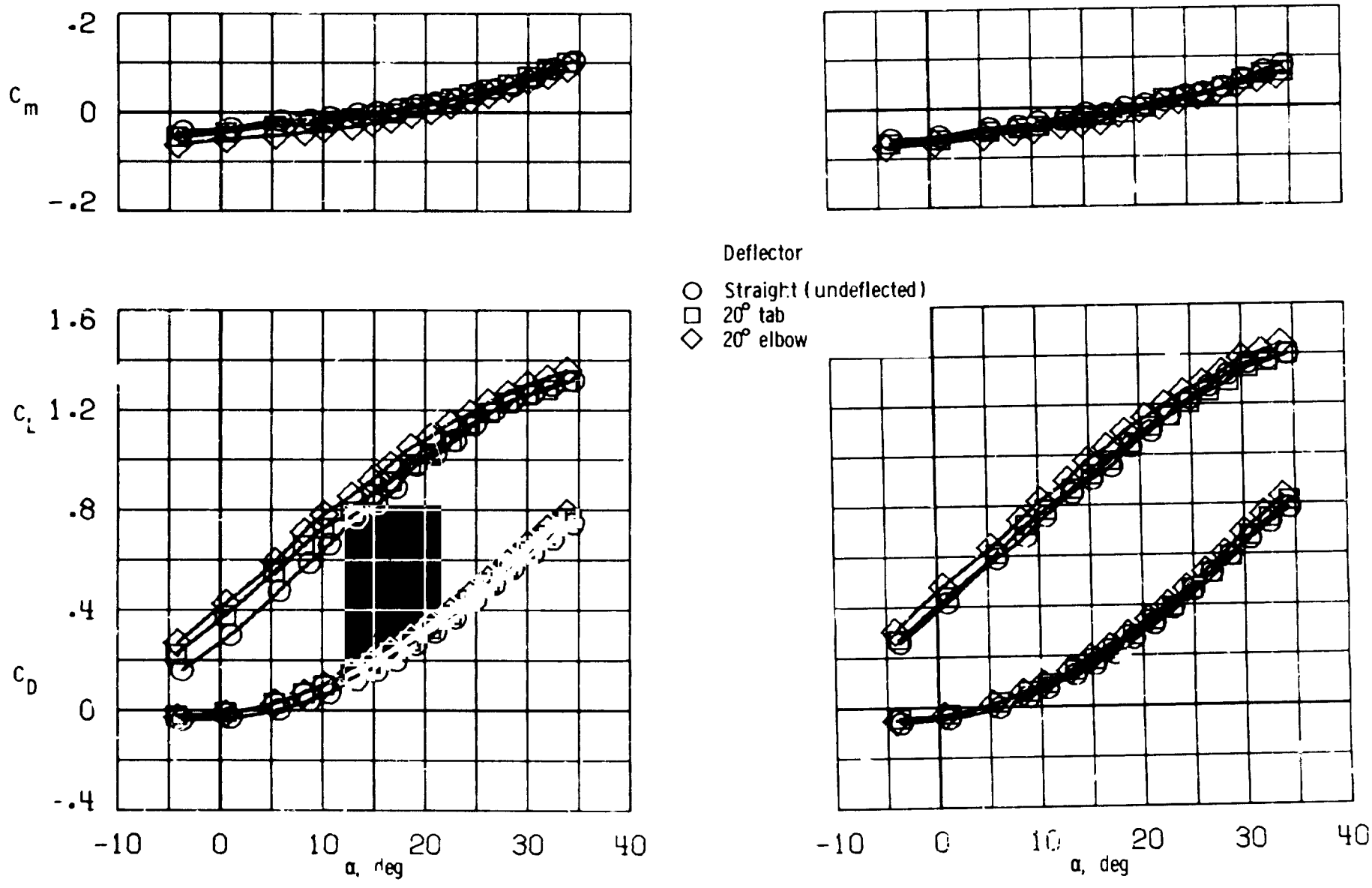

(a) $T_C' = 0.1$, $\delta_f = 20°$, $C_\mu = 0$.

(b) $T_C' = 0.1$, $\delta_f = 20°$, $C_\mu = 0.04$.

Figure 16. - Comparison of the longitudinal aerodynamic characteristics obtained with different engine exhaust deflection devices. Wing - body combination with upper surface engines.

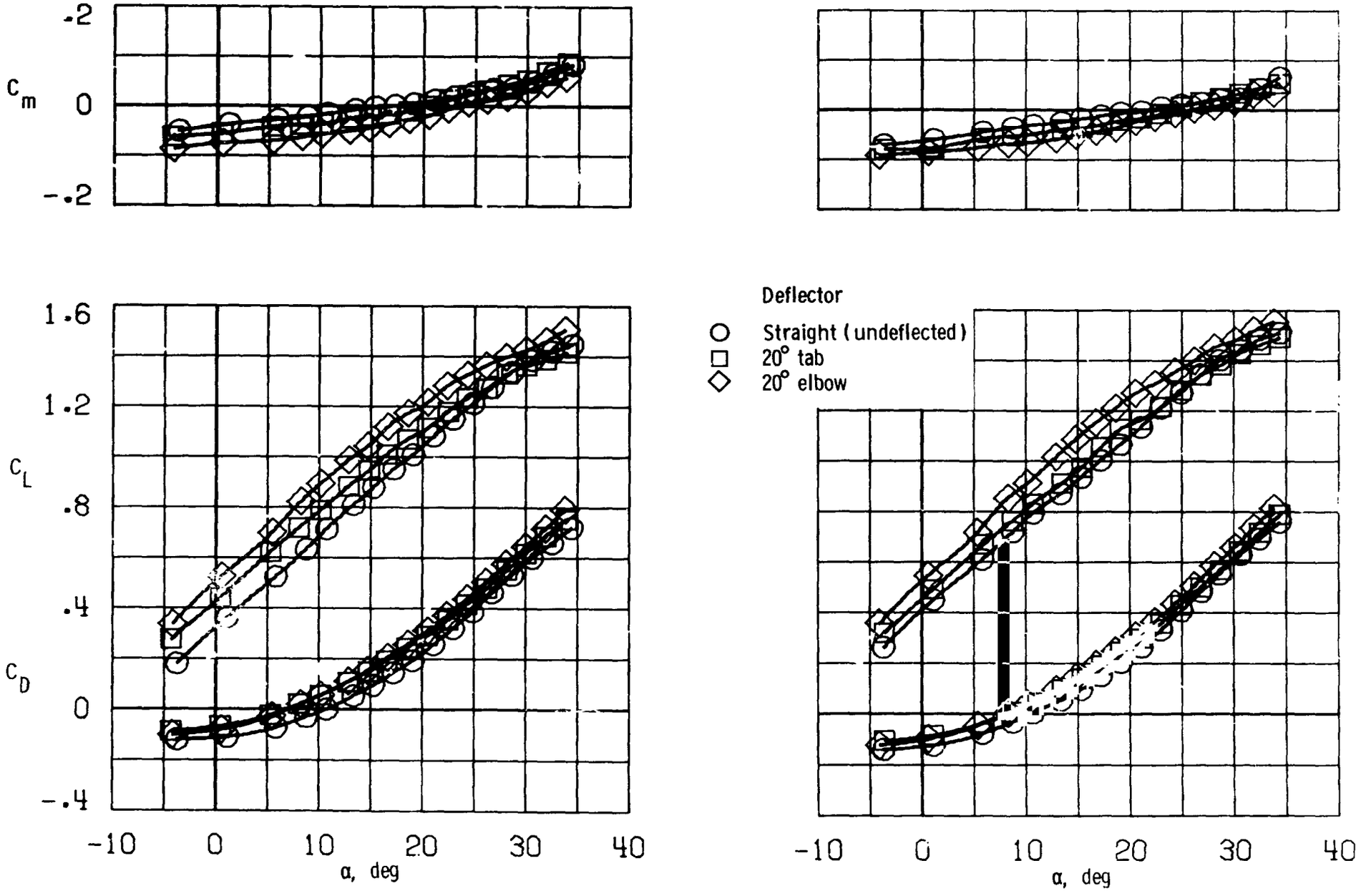

(c) $T_c' = 0.2$, $\delta_f = 20°$, $C_\mu = 0$.

(d) $T_c' = 0.2$, $\delta_f = 20°$, $C_\mu = 0.04$.

Figure 16. - Continued.

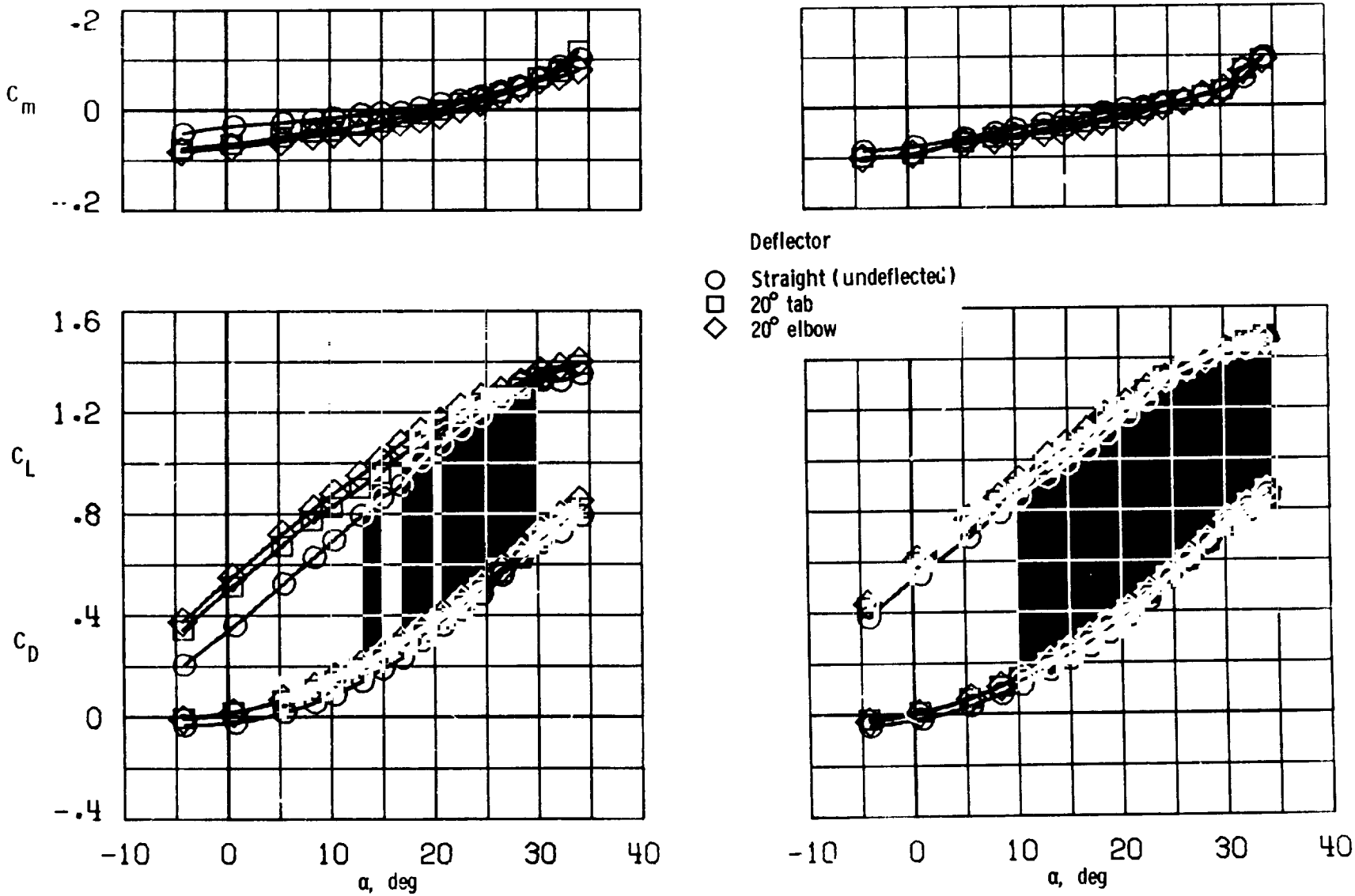

(e) $T_c' = 0.1$, $\delta_f = 30°$, $C_\mu = 0$.

(f) $T_c' = 0.1$, $\delta_f = 30°$, $C_\mu = 0.04$.

Figure 16. - Continued.

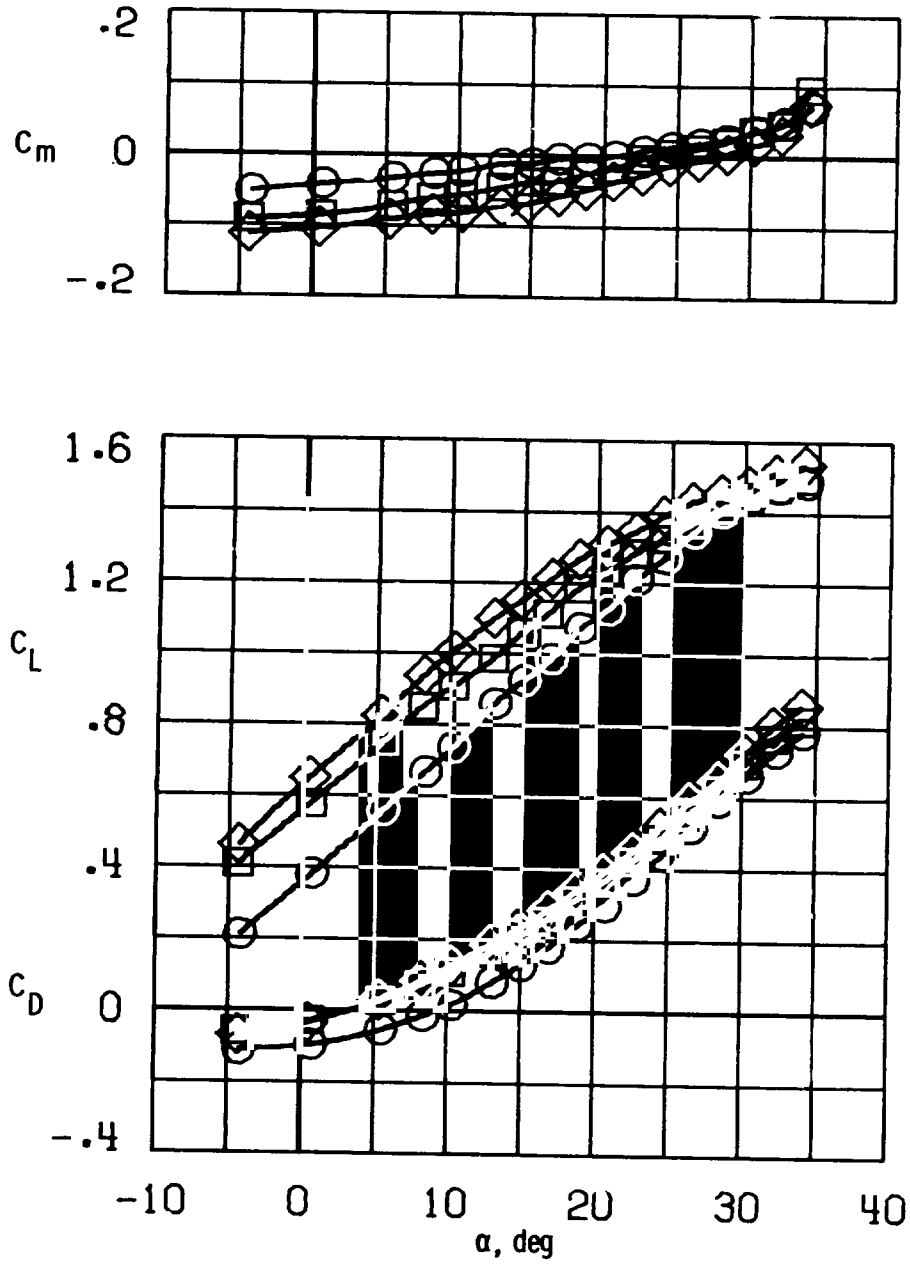

(g) $T_c' = 0.2$, $\delta_f = 30°$, $C_\mu = 0$.

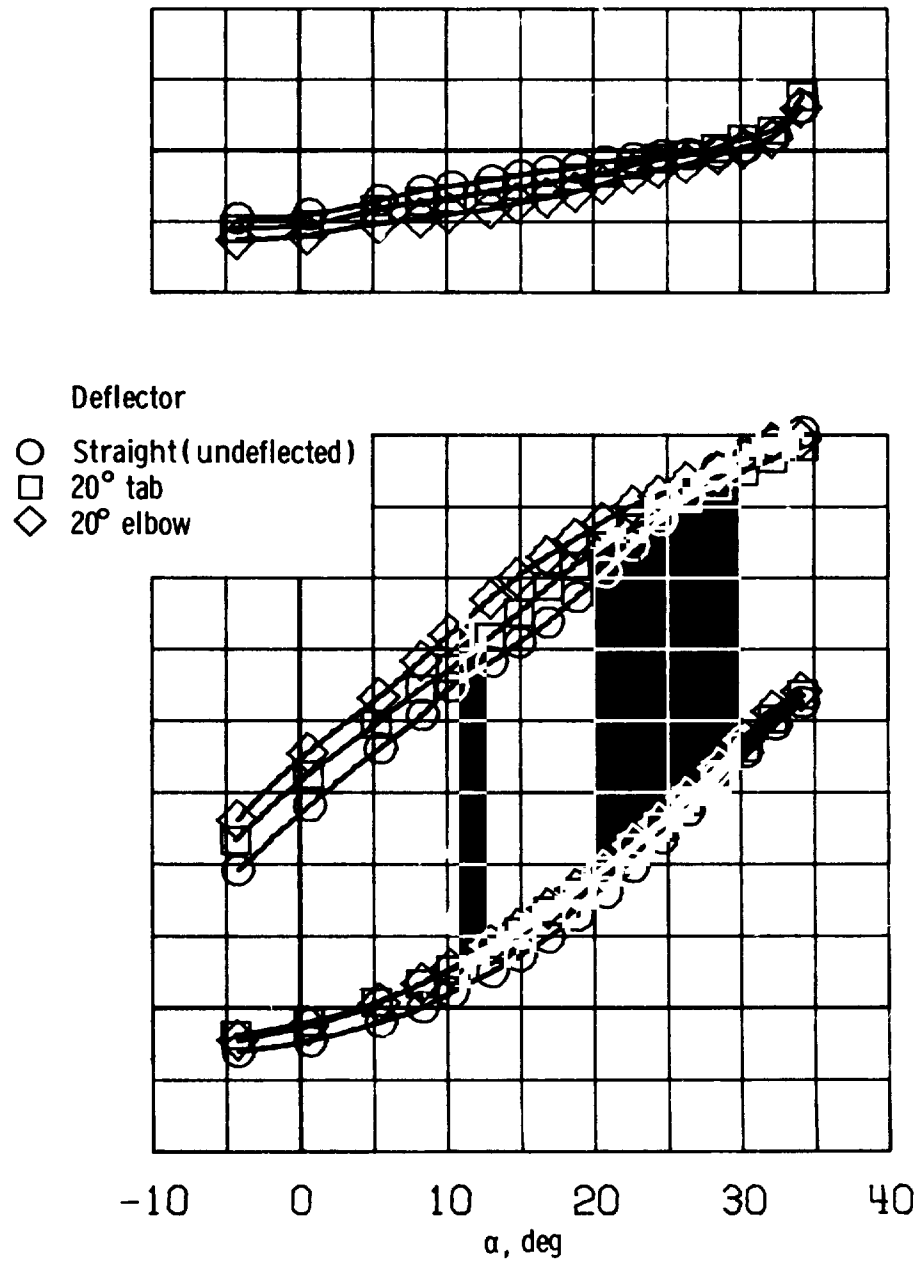

(h) $T_c' = 0.2$, $\delta_f = 30°$, $C_\mu = 0.04$.

Figure 16. - Continued.

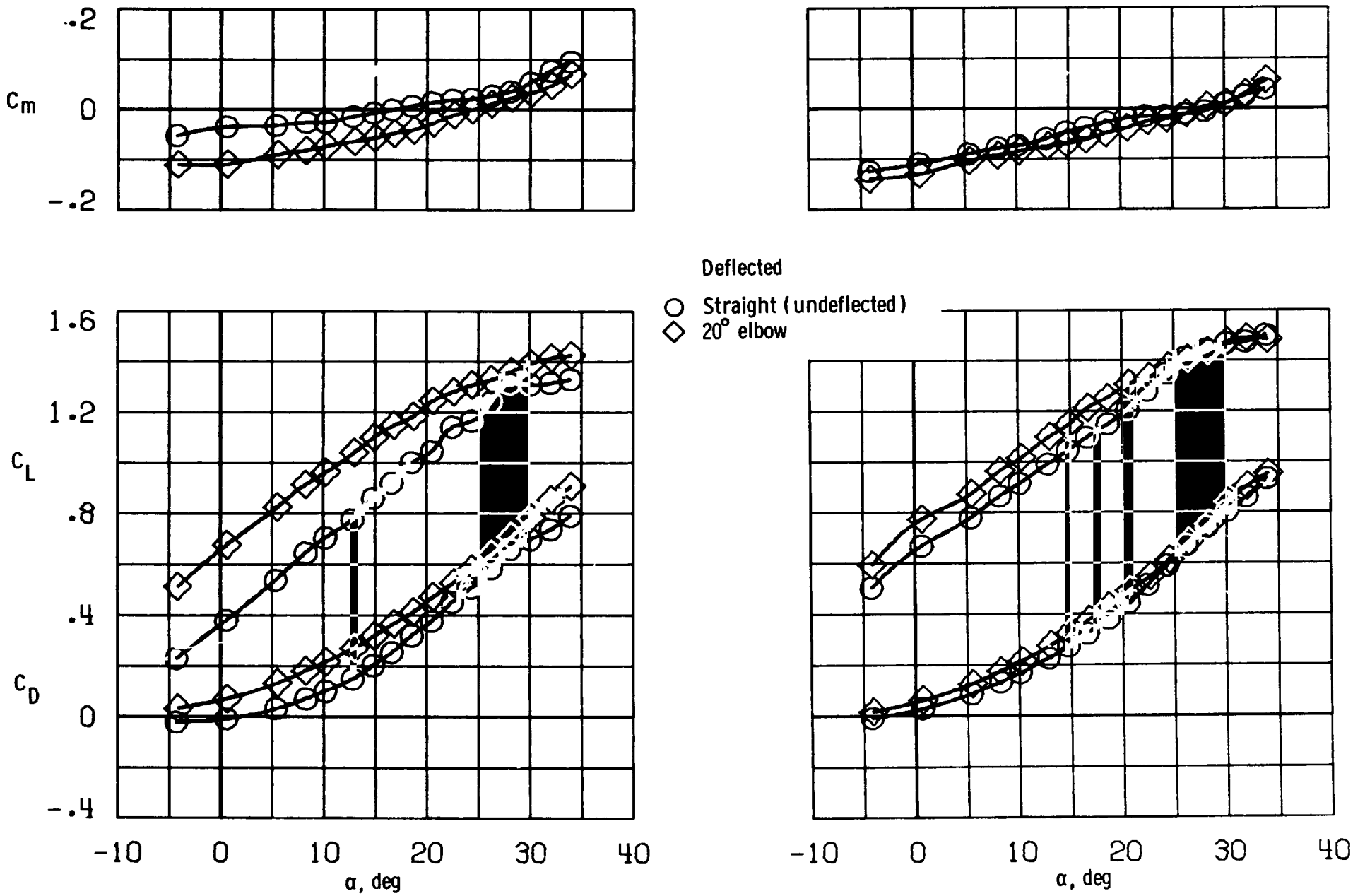

(i) $T_c' = 0.1$, $\delta_f = 40°$, $C_\mu = 0$.

(j) $T_c' = 0.1$, $\delta_f = 40°$, $C_\mu = 0.04$.

Figure 16. - Continued.

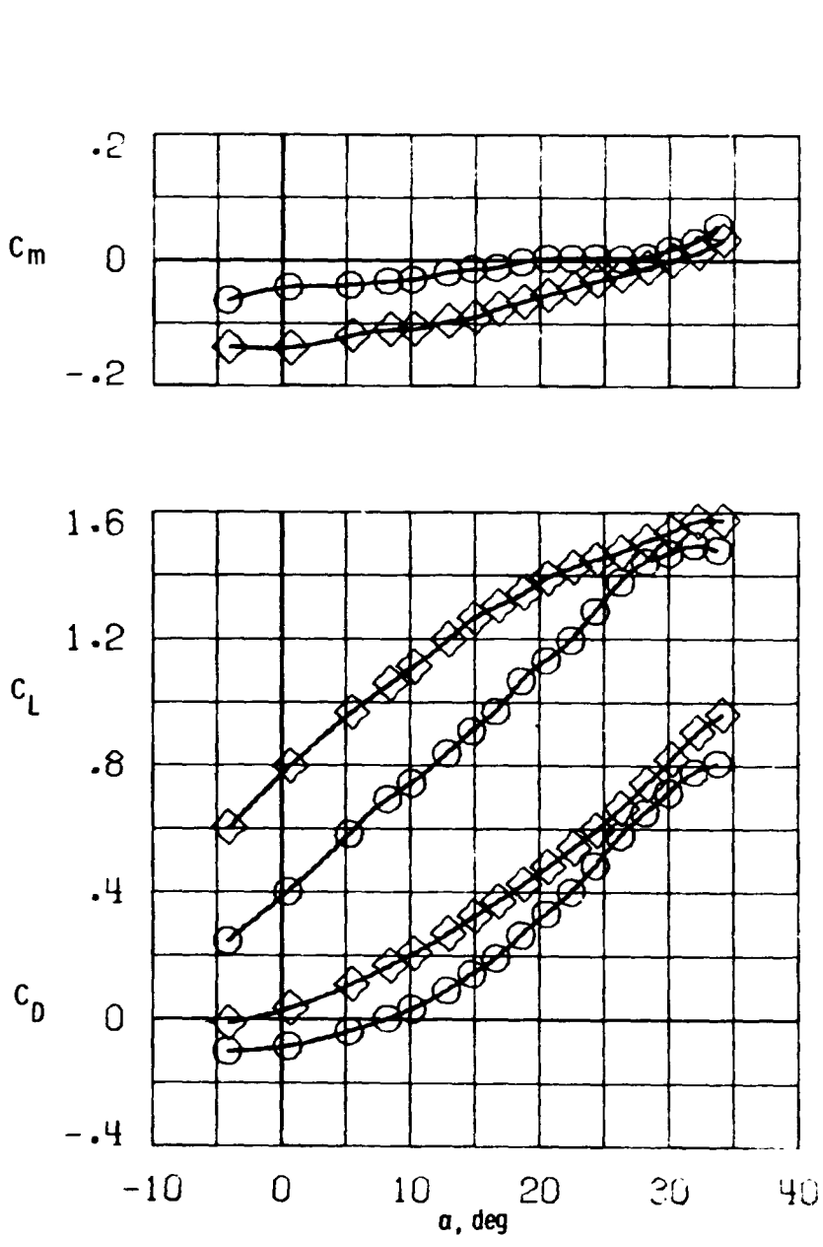

(k) $T_c' = 0.2$, $\delta_f = 40°$, $C_\mu = 0$.

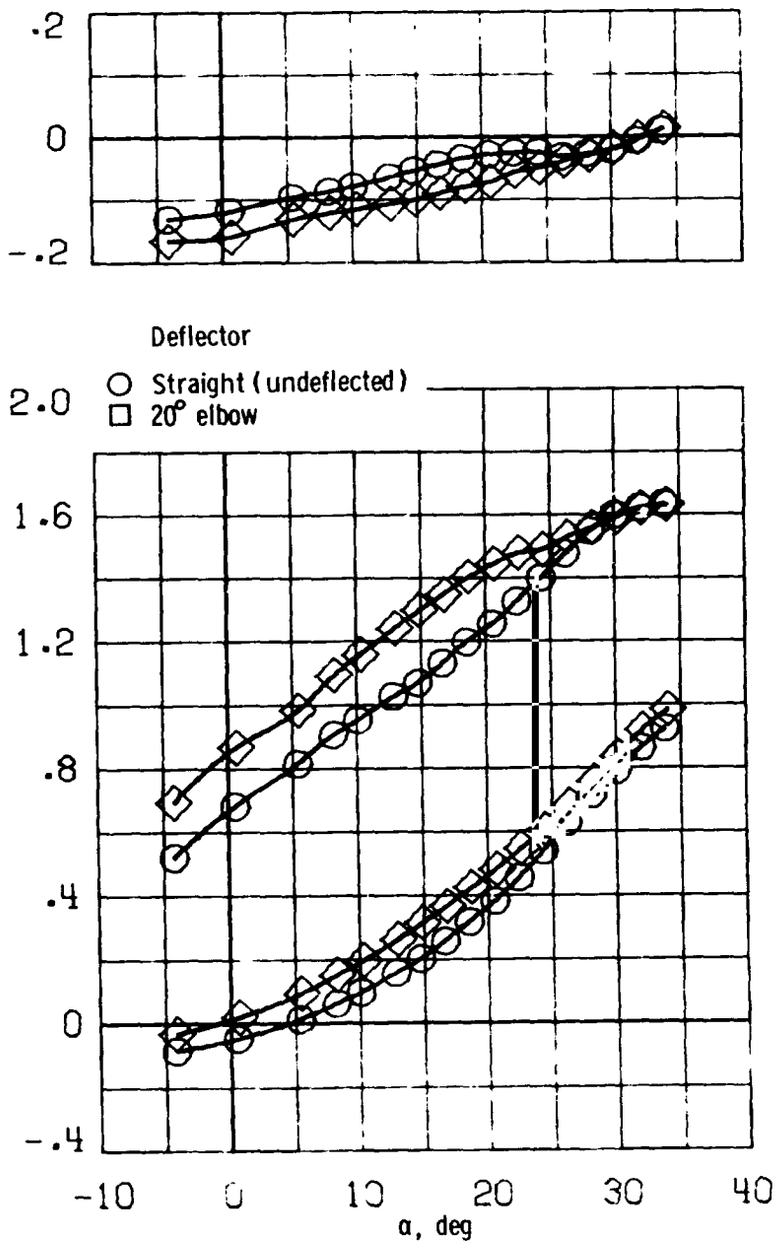

(l) $T_c' = 0.2$, $\delta_f = 40°$, $C_\mu = 0.04$.

Figure 16. - Concluded.

$\delta_N = 0°$ $\delta_N = 20°$

Figure 17. - Flow visualization for upper surface engine configuration with straight and 20° elbow exhaust nozzles ($\delta_f = 40°$, $C_\mu = 0.$, $T_c' = 0.2$, $\alpha = 10°$)

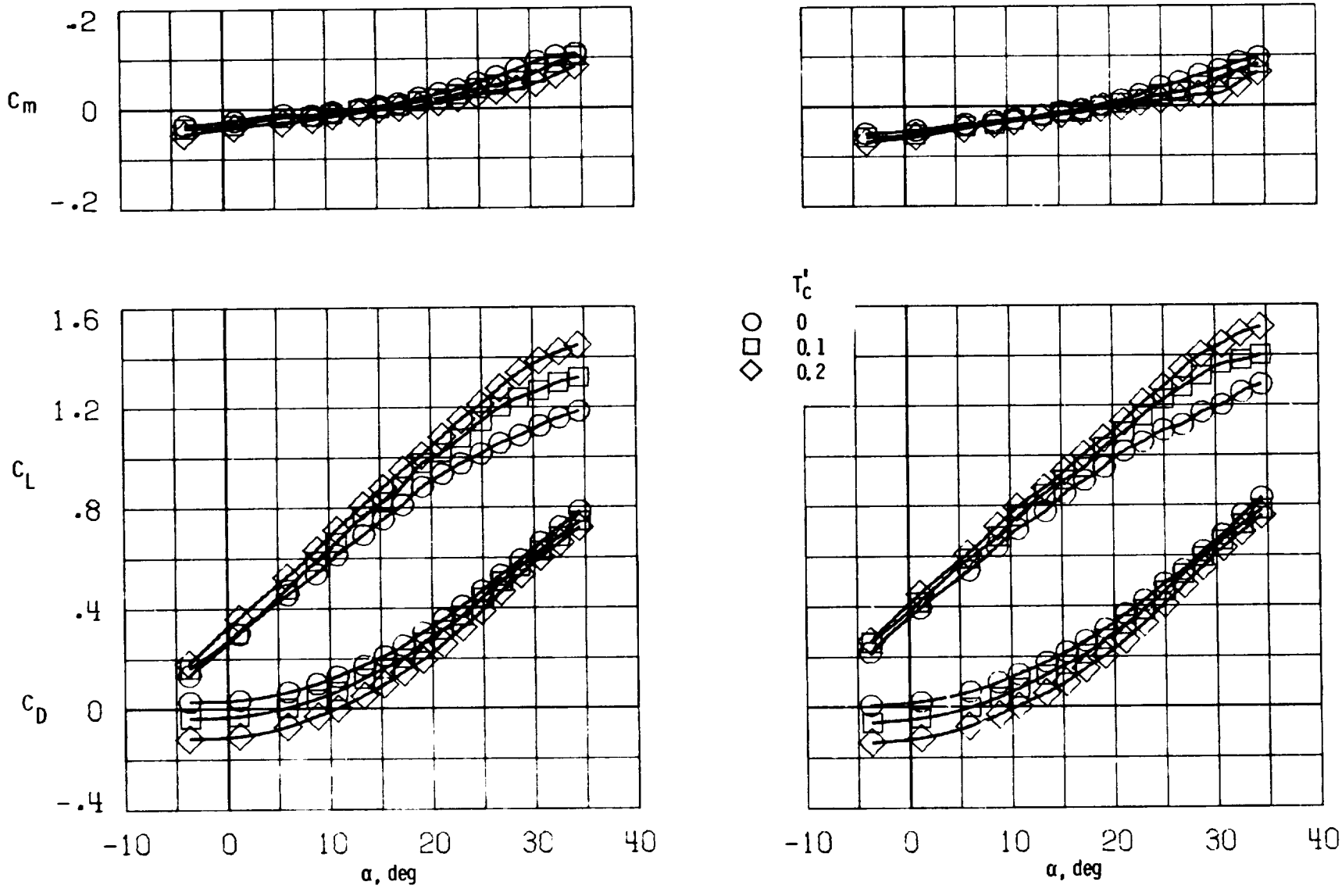

(a) $\delta_f = 20°$, $C_\mu = 0.$

(b) $\delta_f = 20°$, $C_\mu = 0.04$

Figure 18. - Effect of thrust on longitudinal aerodynamic characteristics. Wing-body combination with upper surface engines and straight exhaust nozzles.

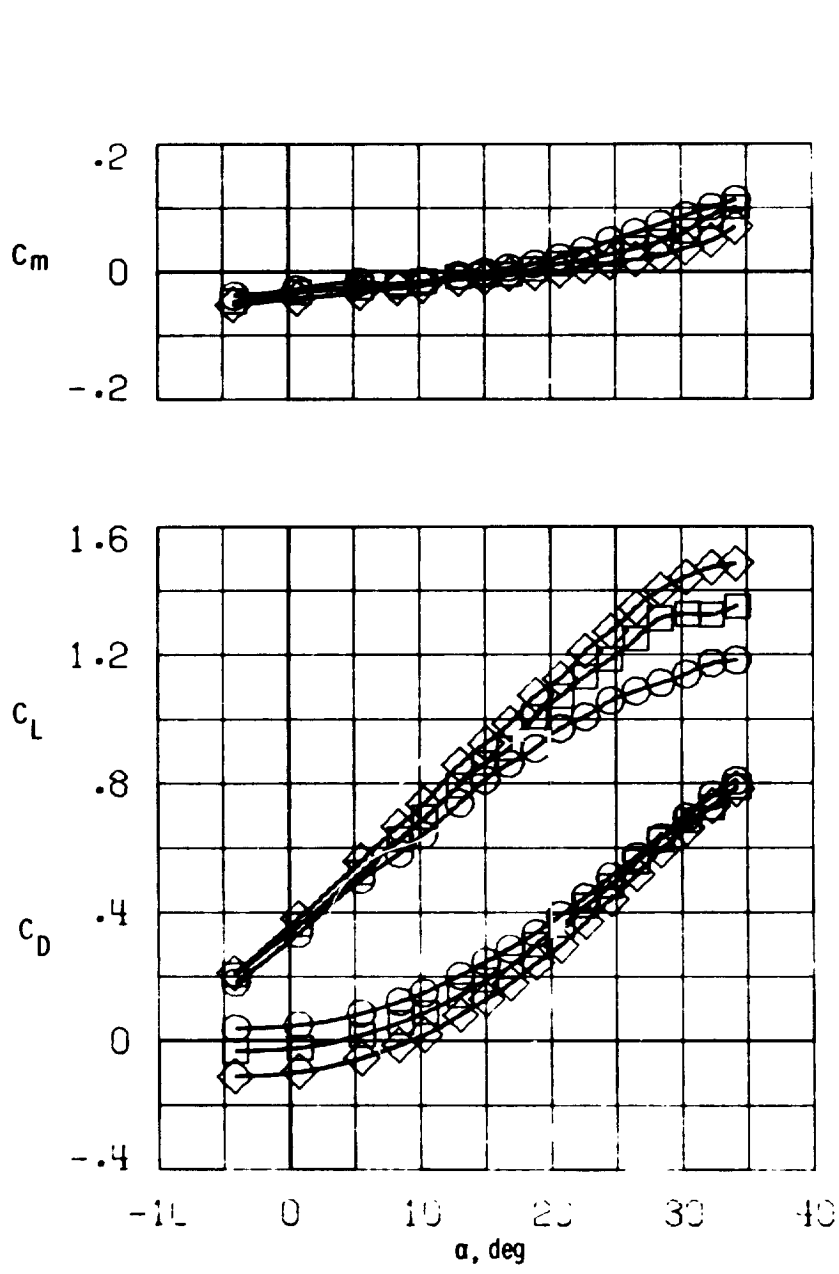

(c) $\delta_f = 30°$, $C_\mu = 0$.

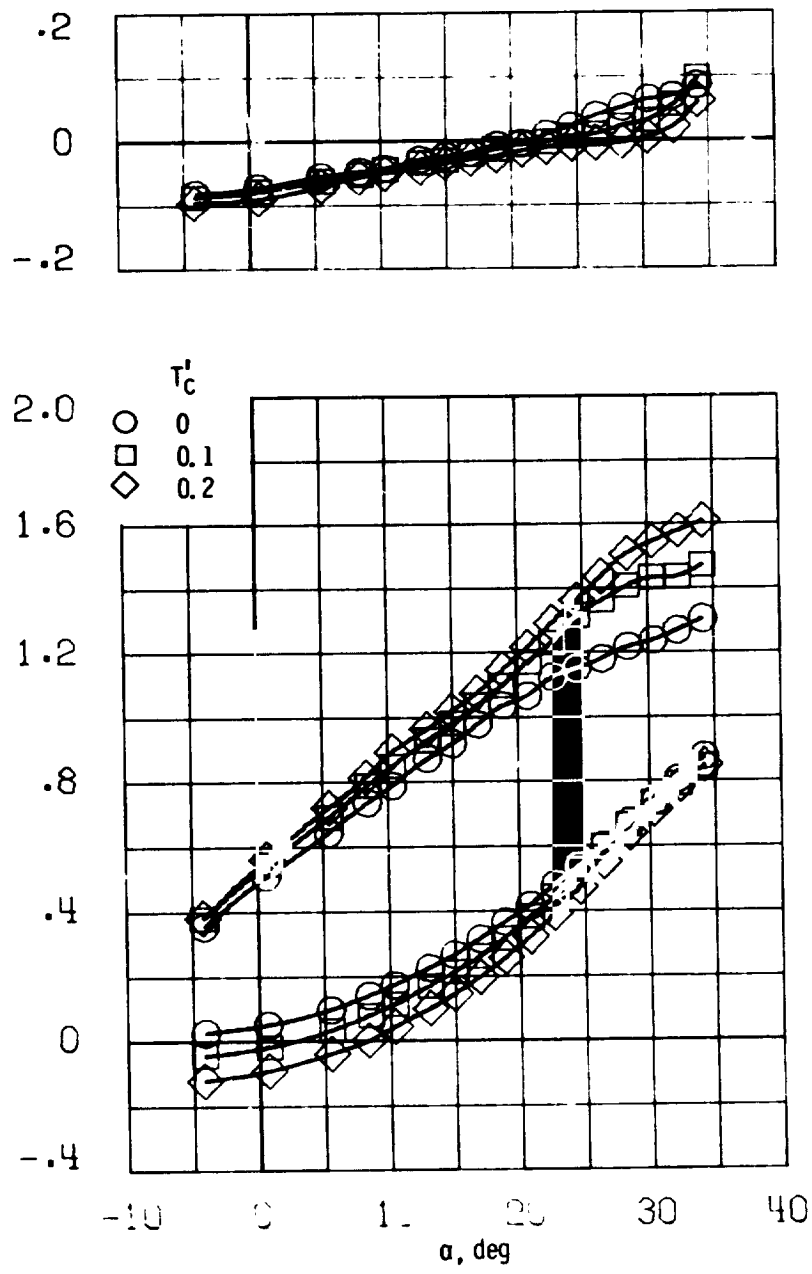

(d) $\delta_f = 30°$, $C_\mu = 0.04$.

Figure 18. - Continued.

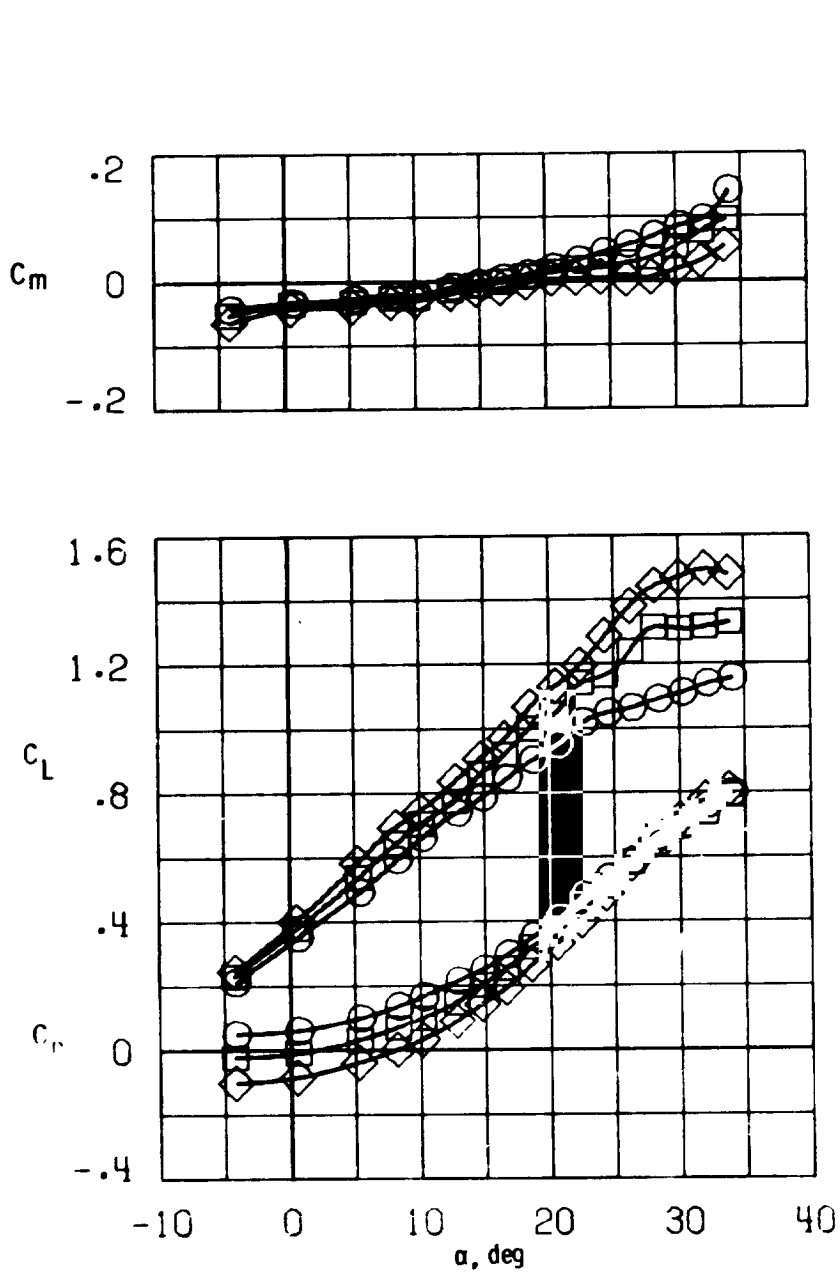

(e) $\delta_f = 40°$, $C_\mu = 0.$

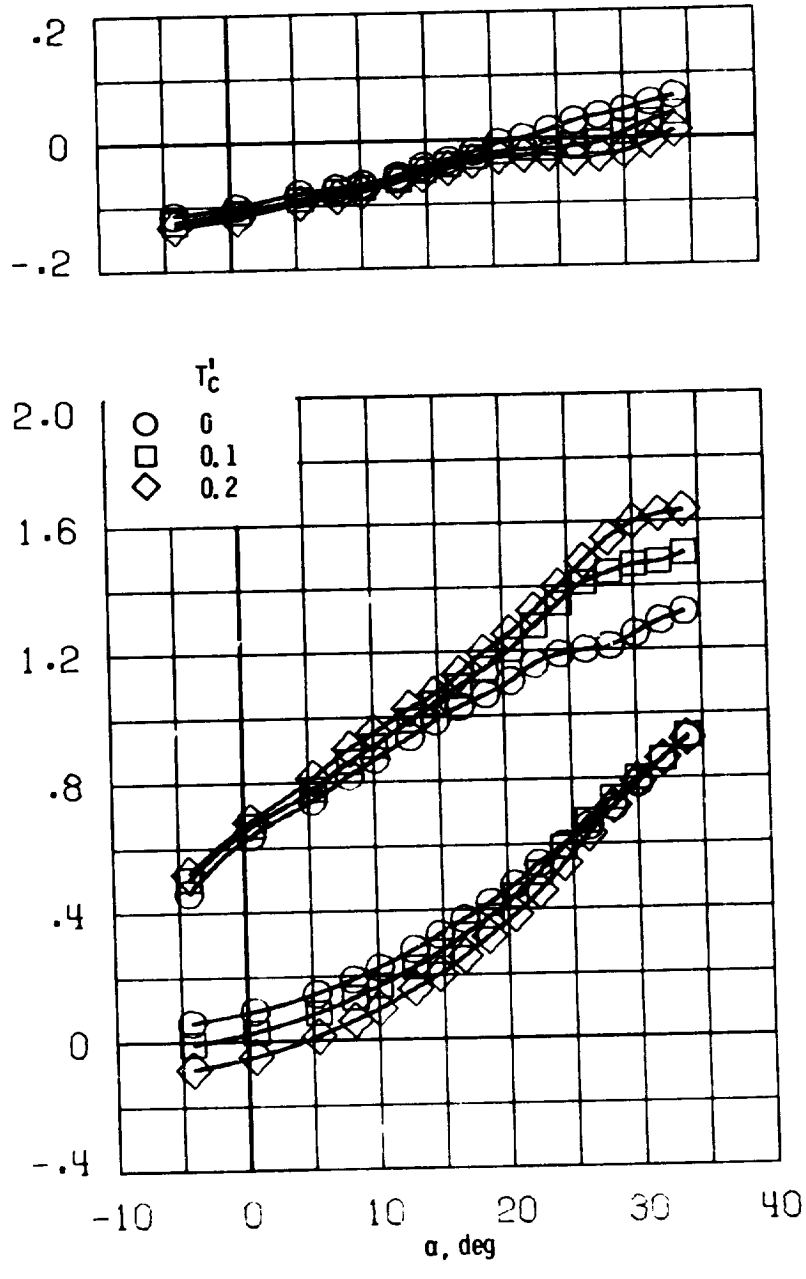

(f) $\delta_f = 40°$, $C_\mu = 0.04.$

Figure 18. - Concluded.

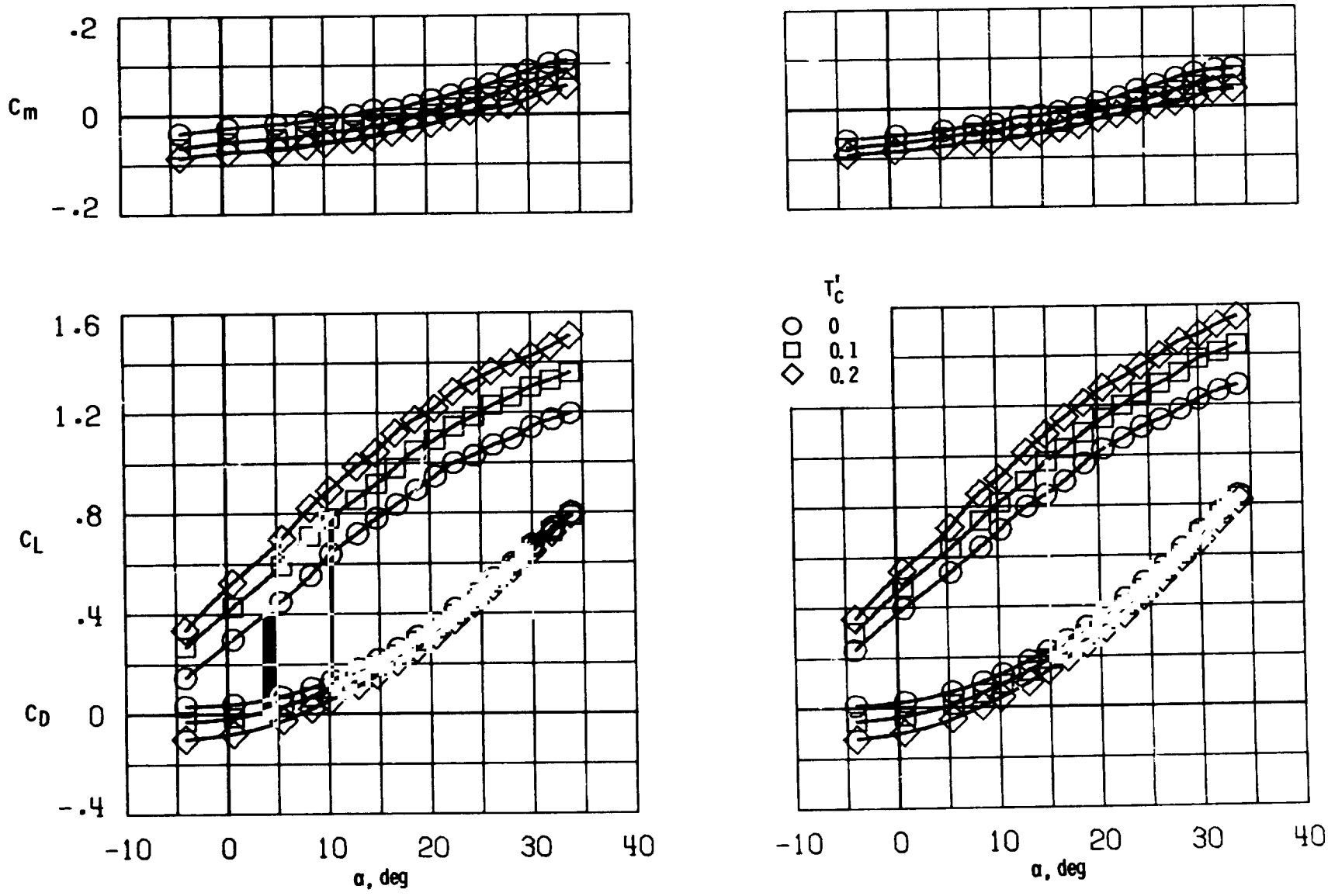

(a) $\delta_f = 20°$, $C_\mu = 0.$

(b) $\delta_f = 20°$, $C_\mu = 0.04$

Figure 19. - Effect of thrust on longitudinal aerodynamic characteristics. Wing - body combination with upper surface engines and 20° elbow exhaust nozzles.

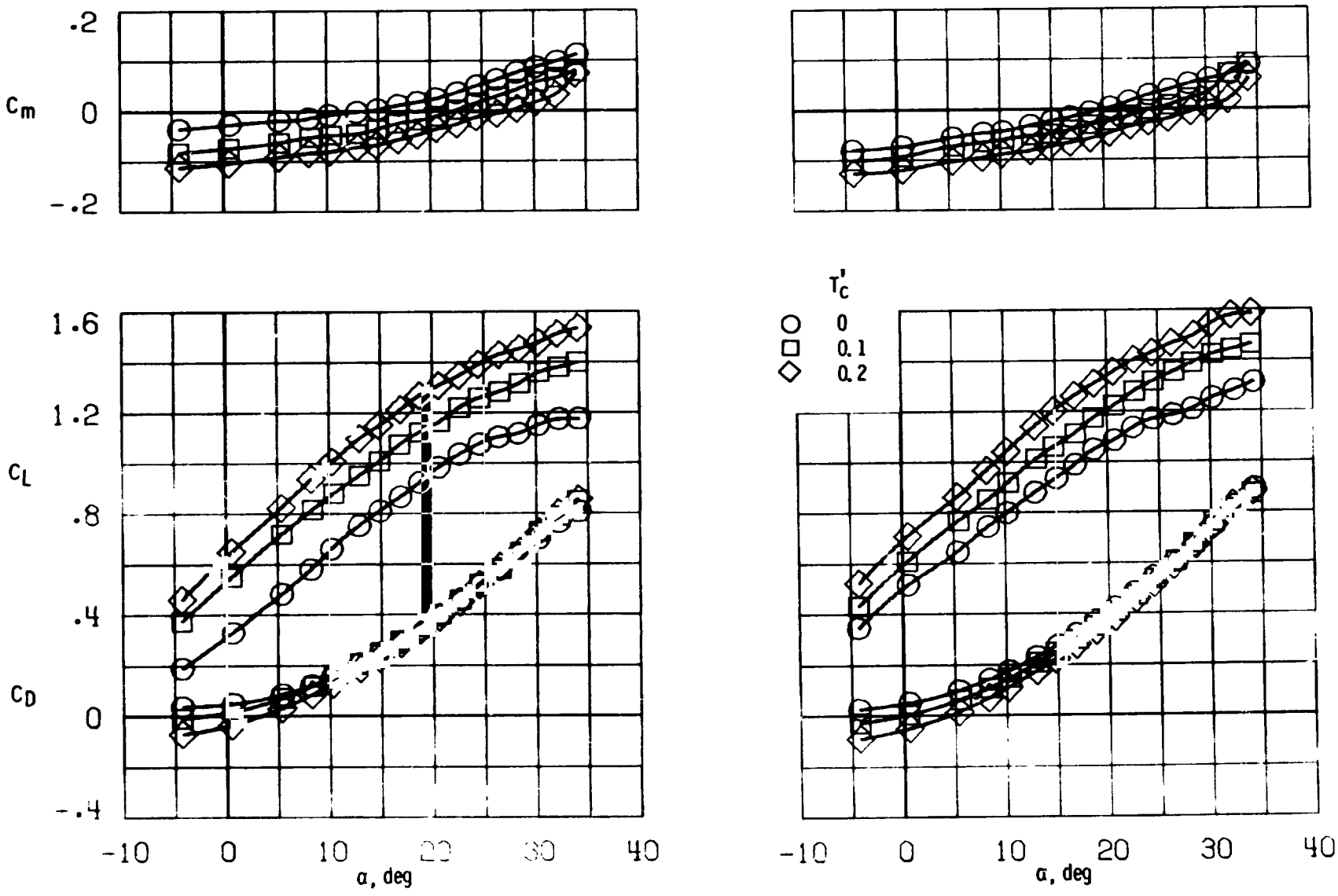

(c) $\delta_f = 30°, C_\mu = 0.$

(d) $\delta_f = 30°, C_\mu = 0.04.$

Figure 19. - Continued.

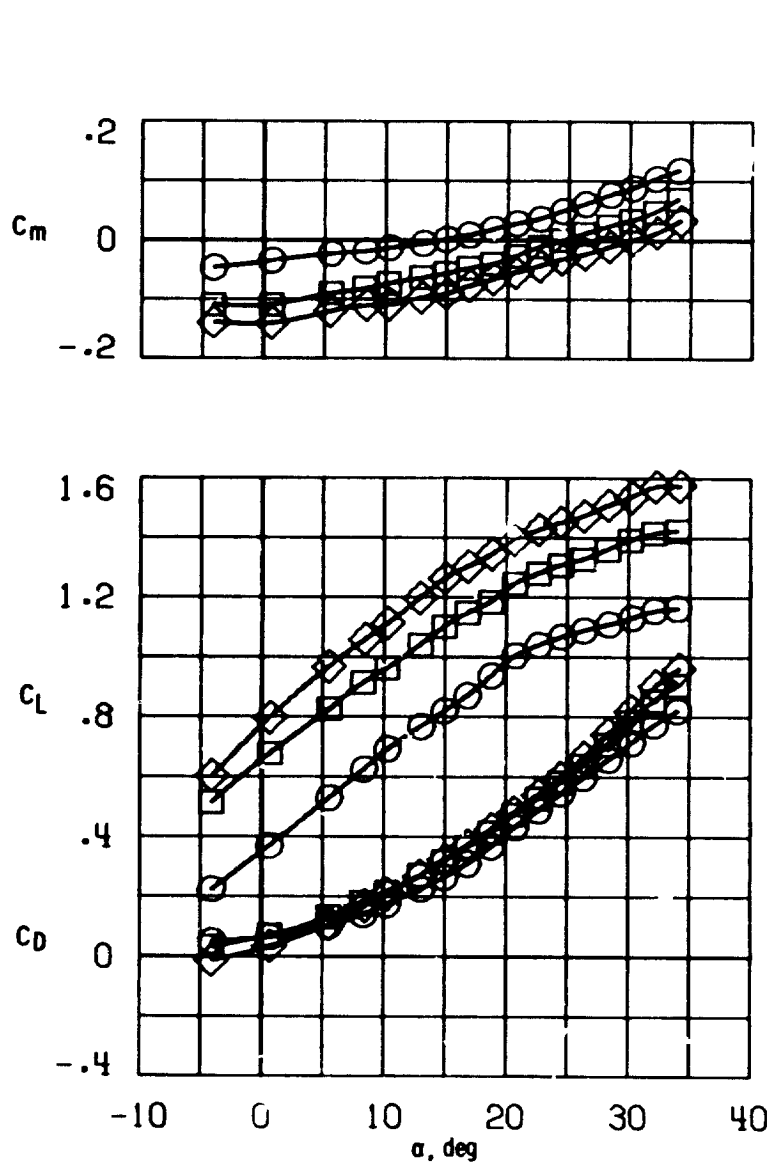

(e) $\delta_f = 40°$, $C_\mu = 0$.

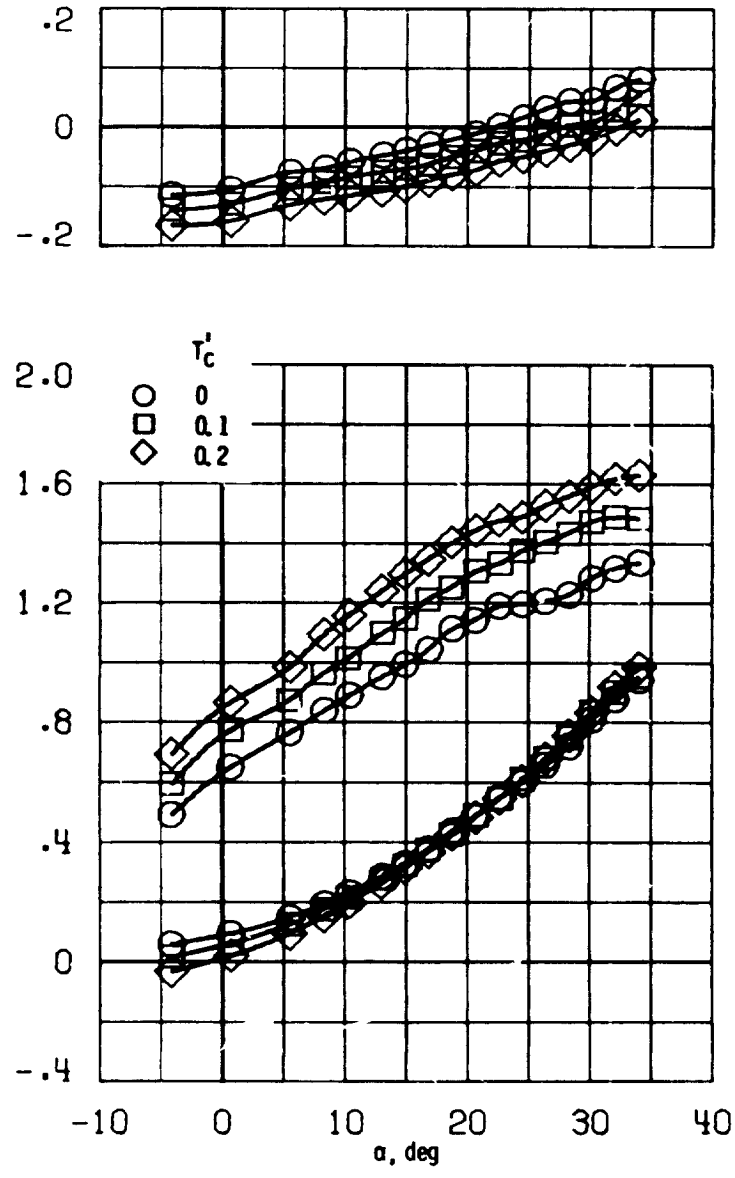

(f) $\delta_f = 40°$, $C_\mu = 0.04$.

Figure 19. - Concluded.

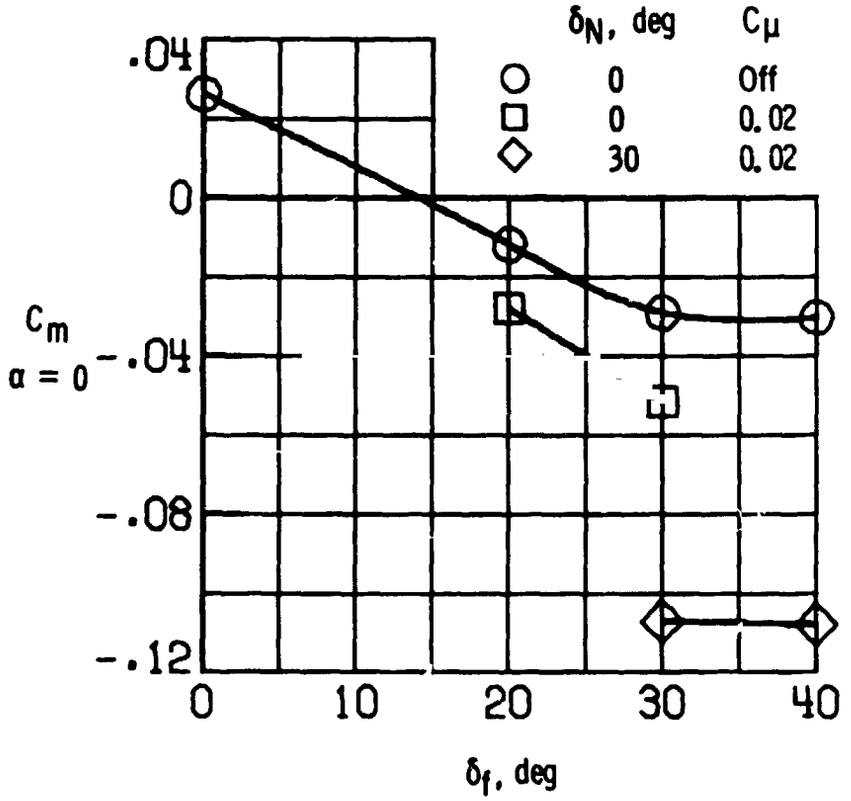

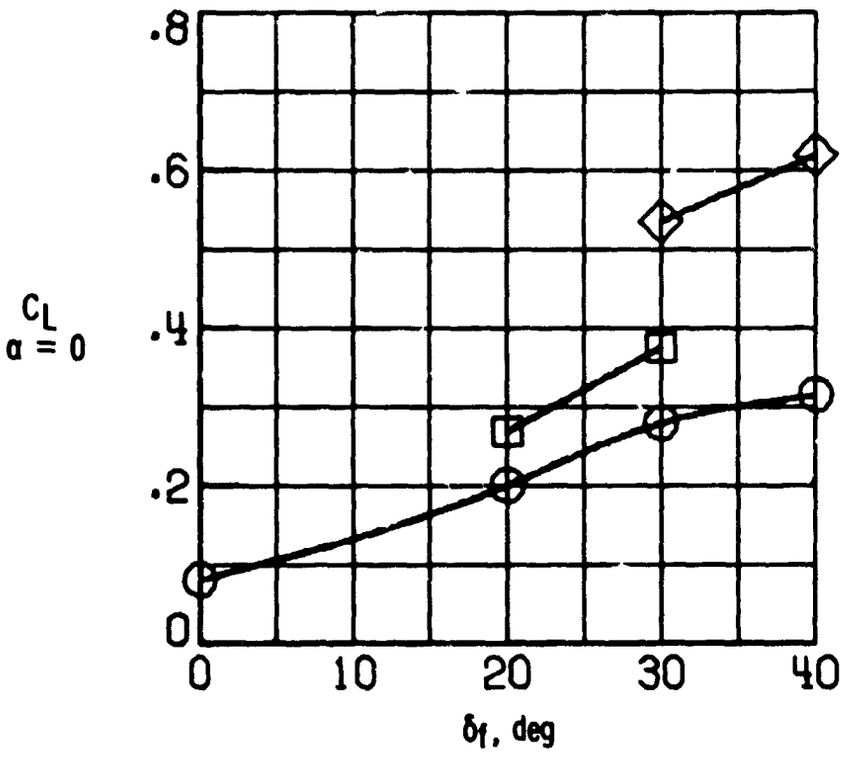

(a) Lower surface engines.

Figure 20. - Comparison of lift and pitching-moment coefficients as a function of flap deflection. $\alpha = 0°$, $T_c' = 0.2$.

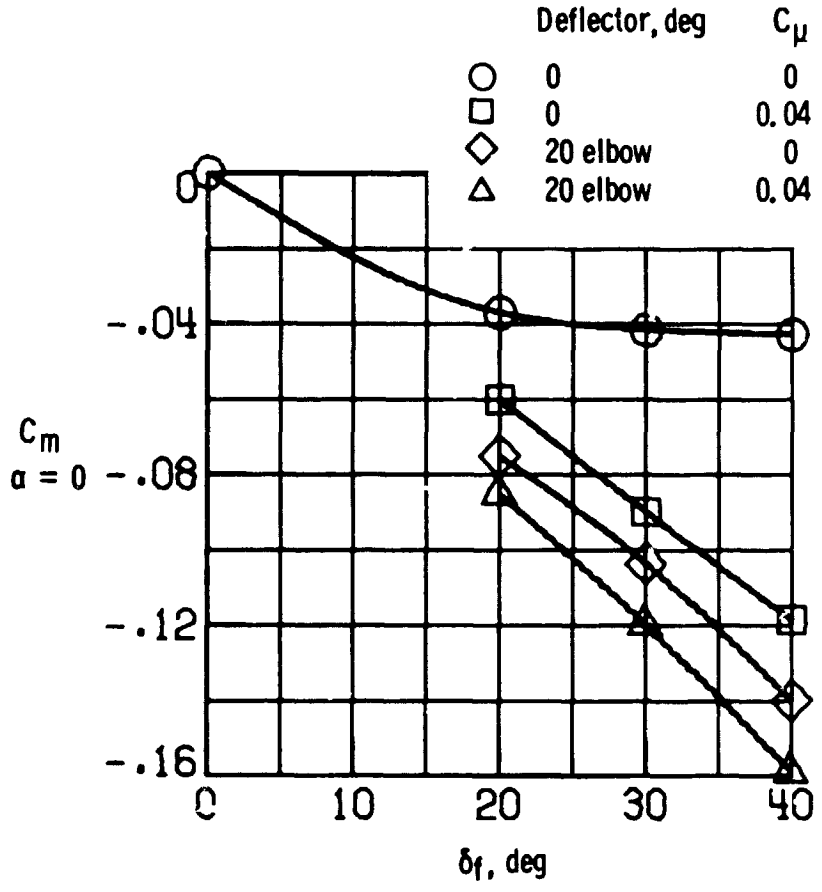

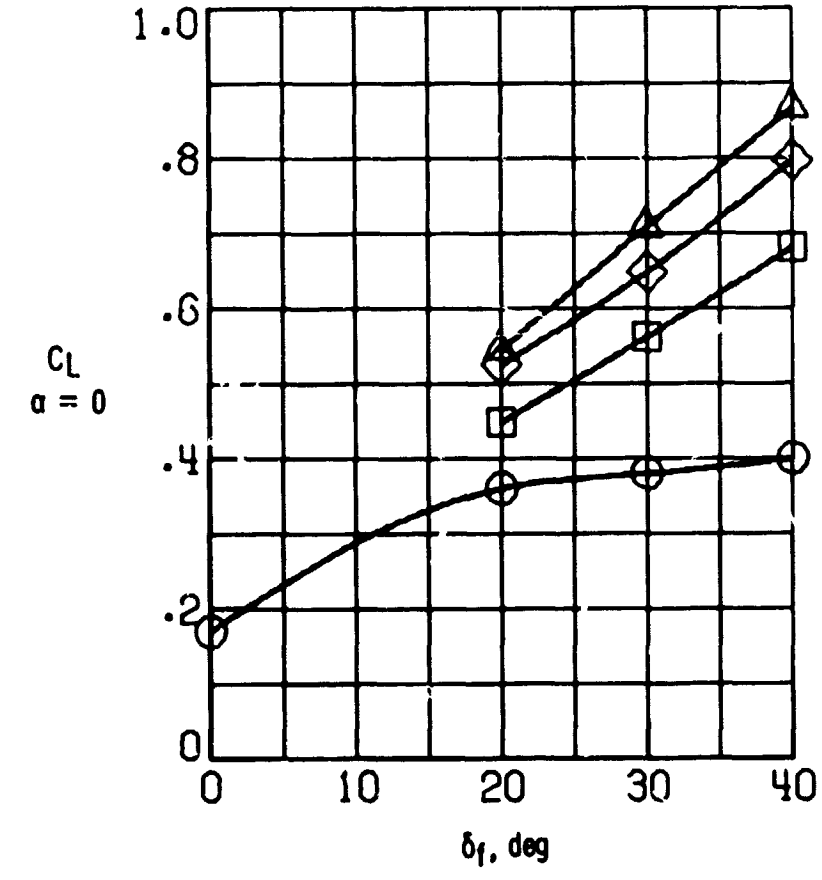

(b) Upper surface engines.

Figure 20. - Concluded.

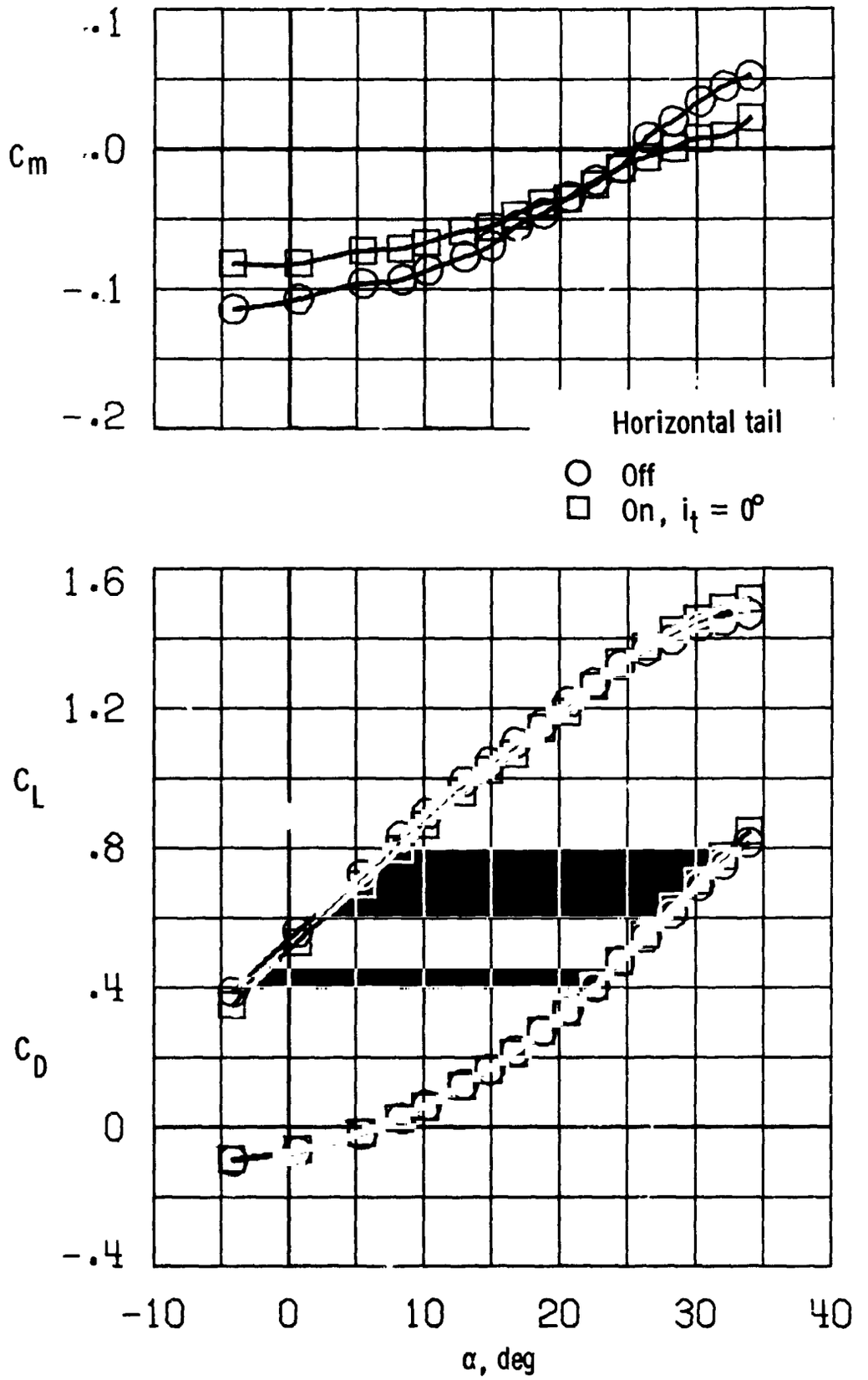

Figure 21. - Horizontal tail effectiveness. Lower surface engine configuration. $T_C' = 0.2$, $\delta_N = 30°$, $\delta_f = 40°/30°/20°$, $C_\mu = 0.02$.

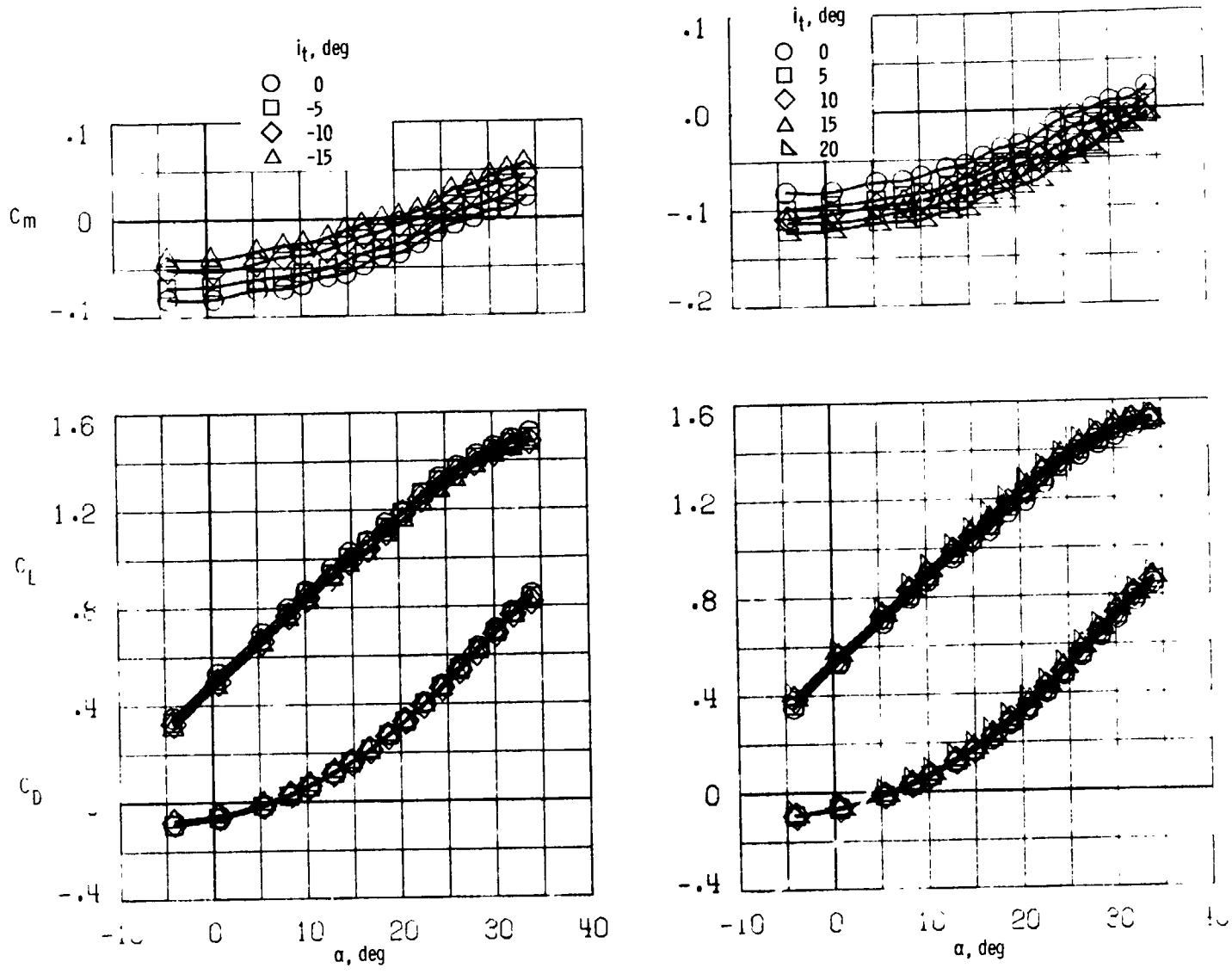

(a) Negative i_t.

(b) Positive i_t.

Figure 22. - Effect of horizontal tail incidence. Lower surface engine configuration.
$T_C' = 0.2$, $\delta_N = 30°$, $\delta_f = 40°/30°/20°$, $C_\mu = 0.02$.

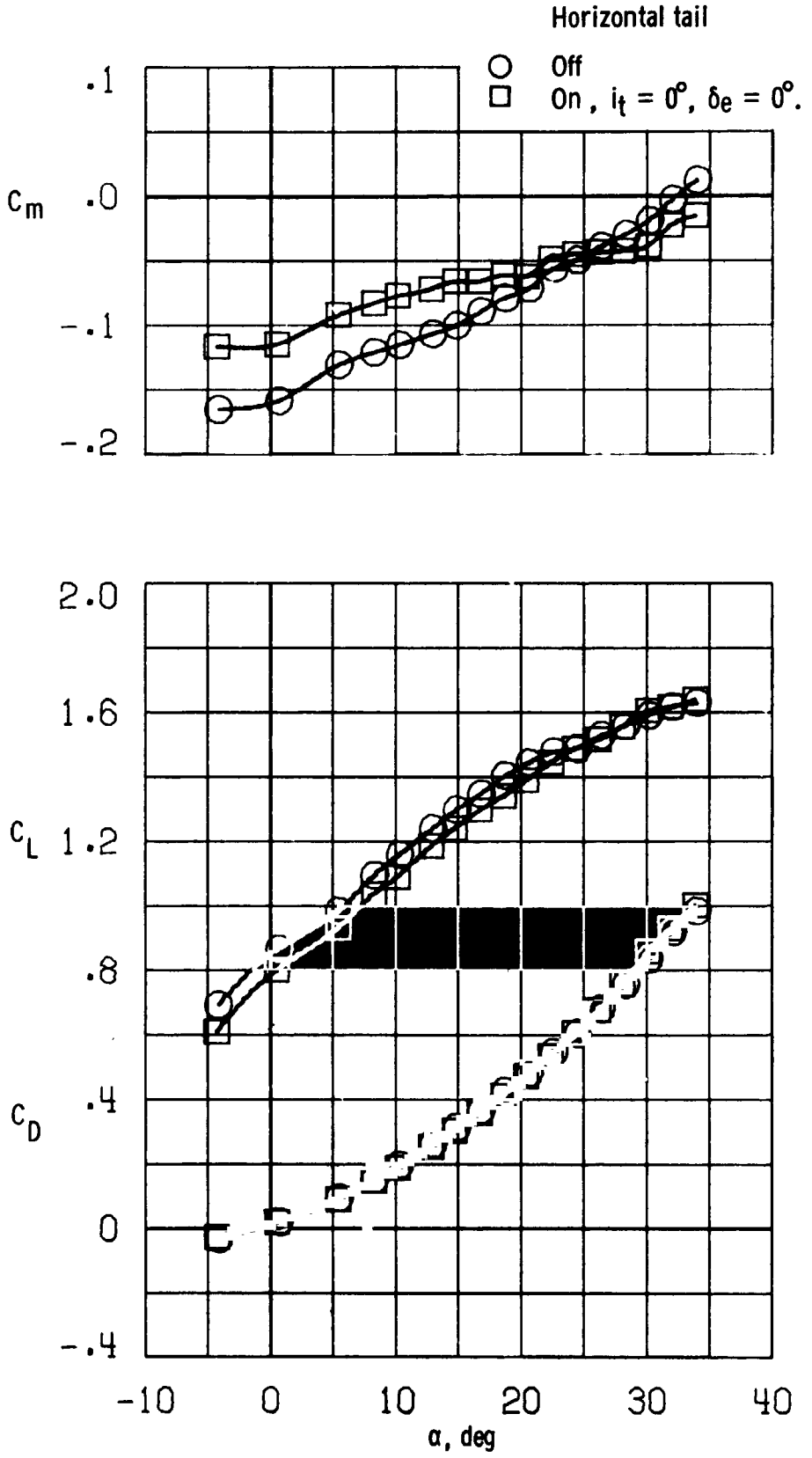

Figure 23. - Horizontal tail effectiveness. Upper surface engines with 20° elbow exhaust nozzles. $T_c' = 0.2$, $\delta_f = 40°$, $C_\mu = 0.04$.

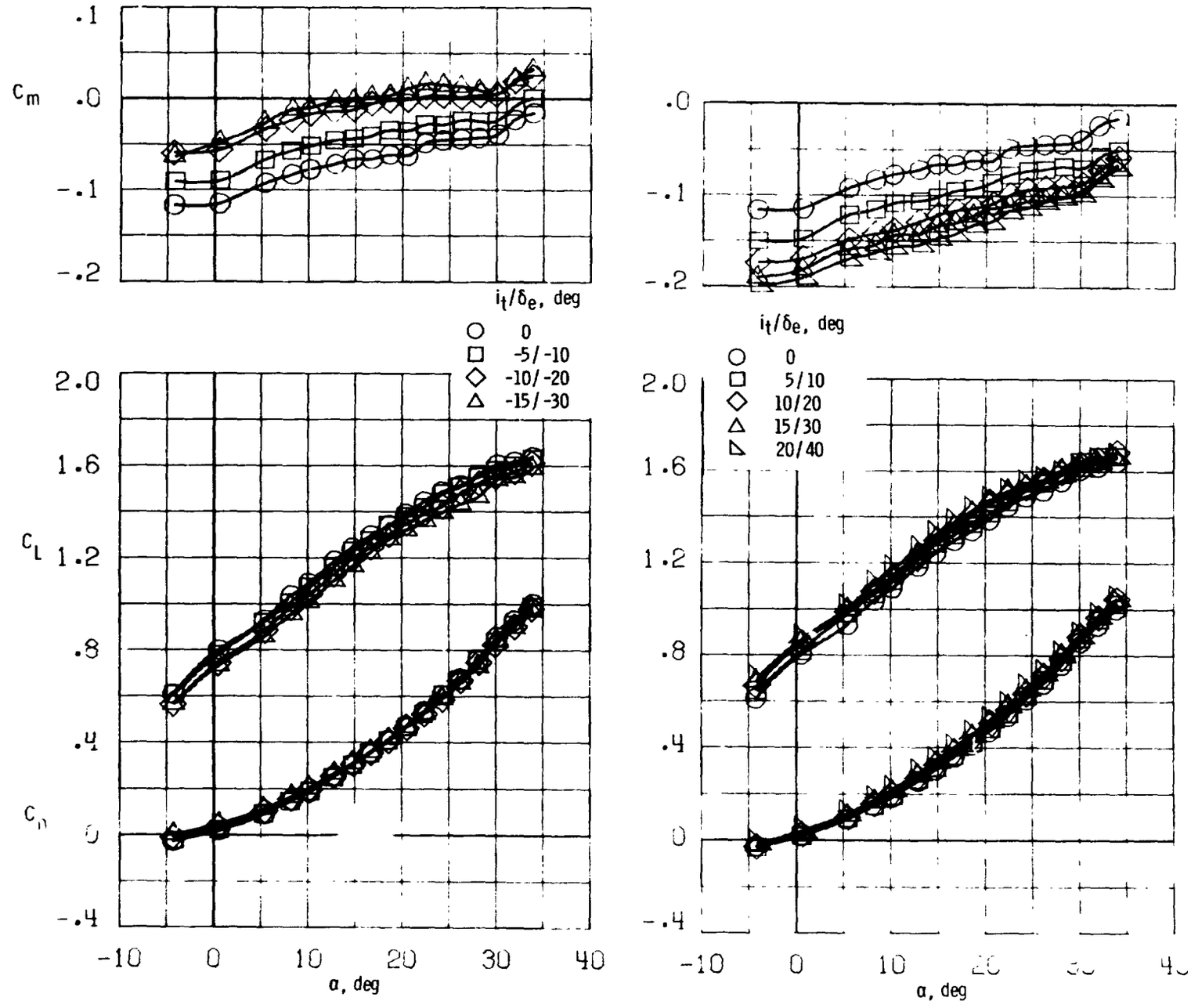

(a) Negative deflections

(b) Positive deflections

Figure 24. - Elevator effectiveness. Upper surface engines with 20° elbow exhaust nozzles. $T_c' = 0.2$, $\delta_f = 40°$, $C_\mu = 0.04$.

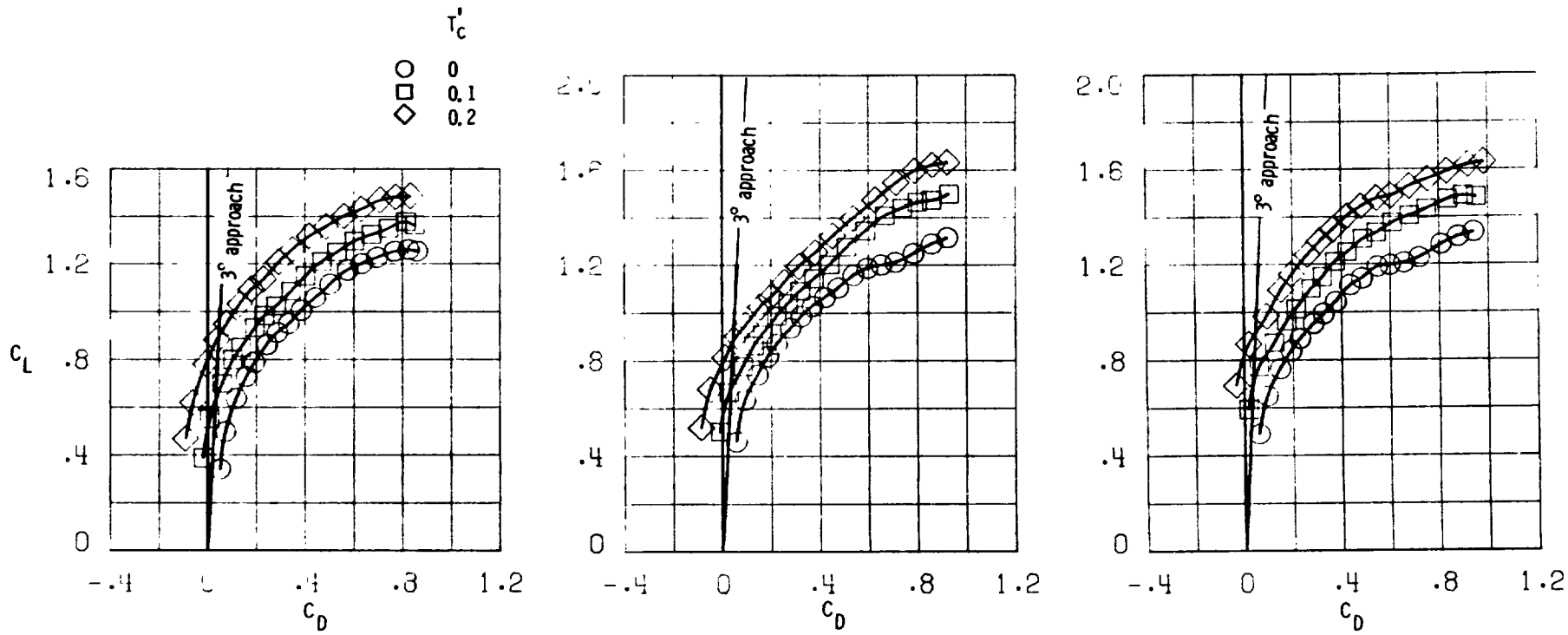

(a) Lower surface engines with 30° deflected nozzles.

(b) Upper surface engines with straight nozzles.

(c) Upper surface engines with 20° elbow exhaust nozzles.

Figure 25. - Lift-drag polars for the 3° approach condition. (δ_f = 40°, with BLC)

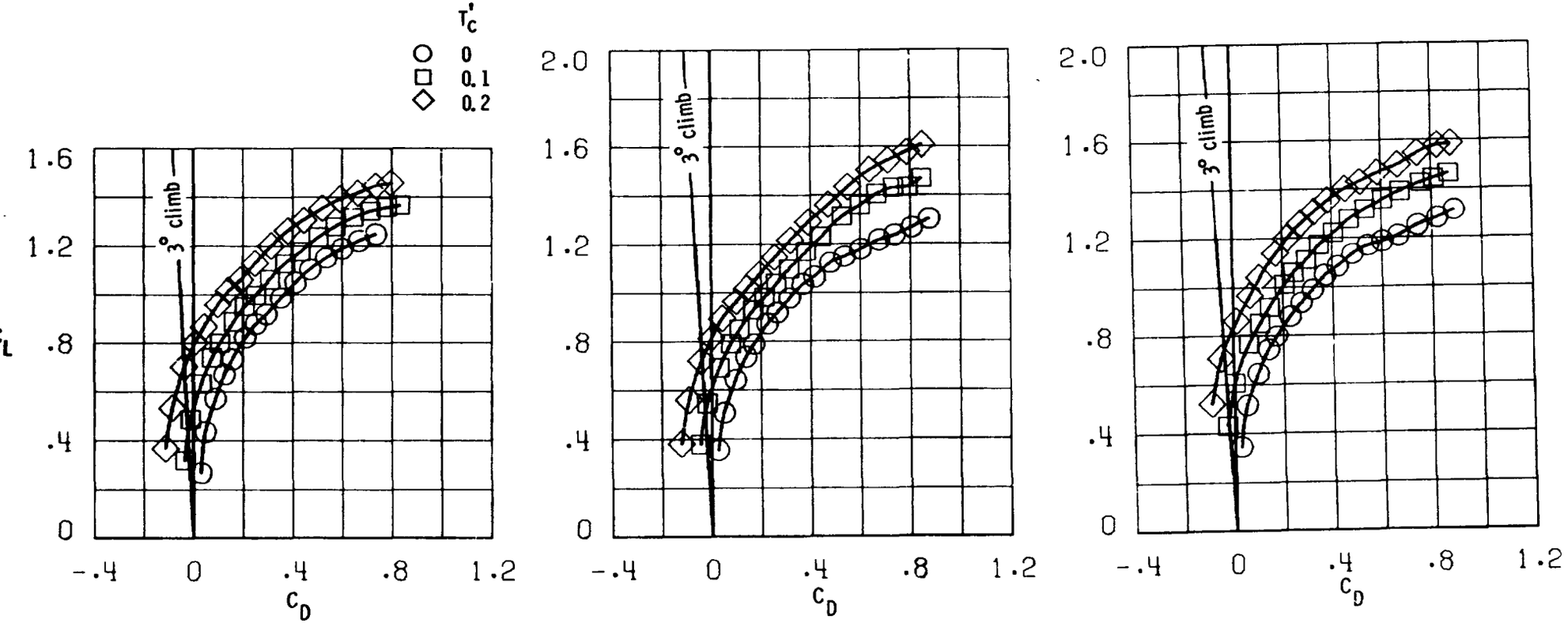

(a) Lower surface engines with 30° deflected nozzles.

(b) Upper surface engines with straight nozzles.

(c) Upper surface engines with 20° elbow exhaust nozzles.

Figure 26. - Lift-drag polars for the 3° climb condition. (δ_f = 30°, with 3LC)

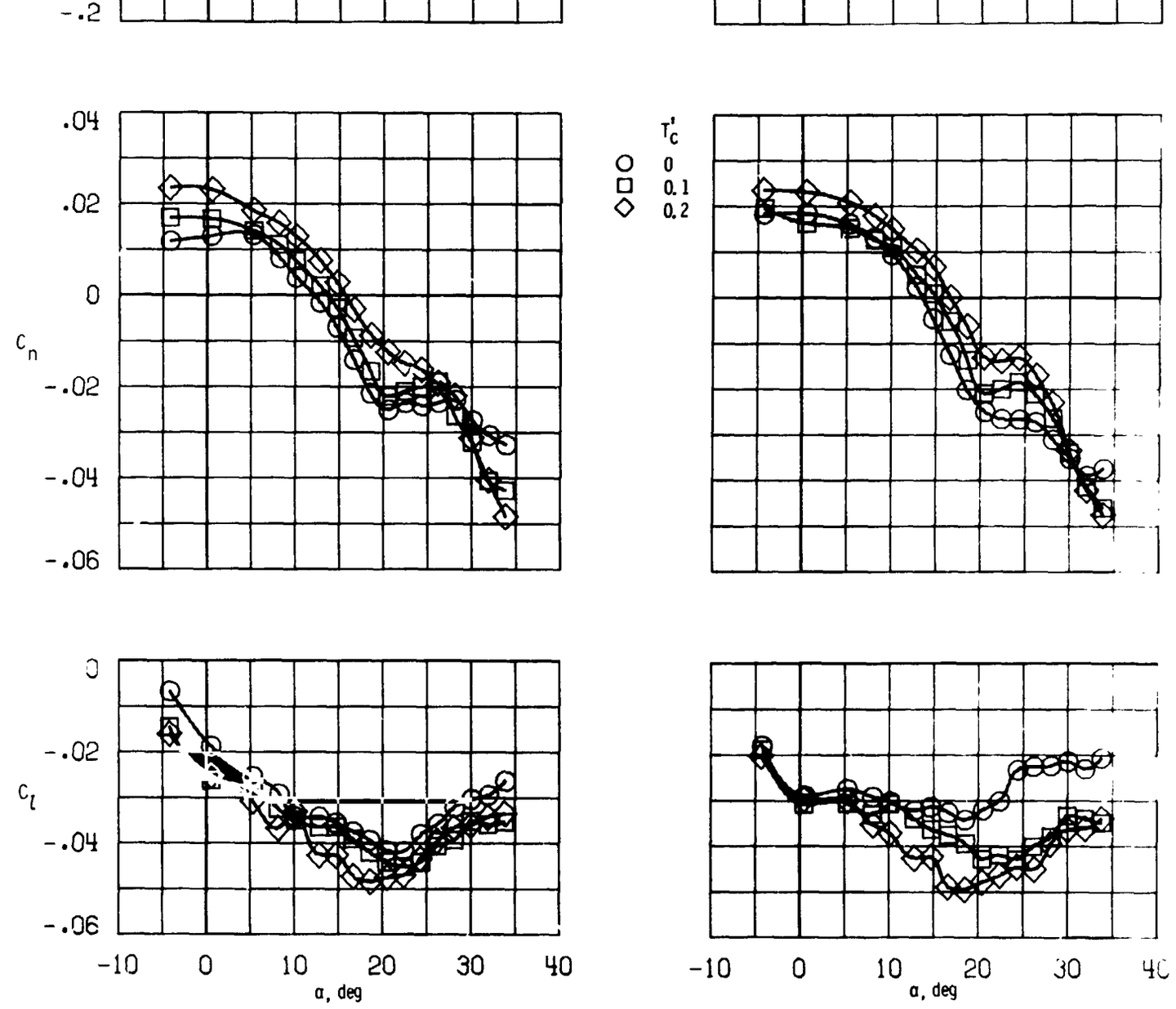

(a) $C_\mu = 0$

(b) $C_\mu = 0.04$

Figure 27. - Variation of static lateral-directional coefficients with angle of attack for the upper surface engine configuration with 20° elbow exhaust nozzles. $\delta_f = 40°$. $\beta = 10°$.

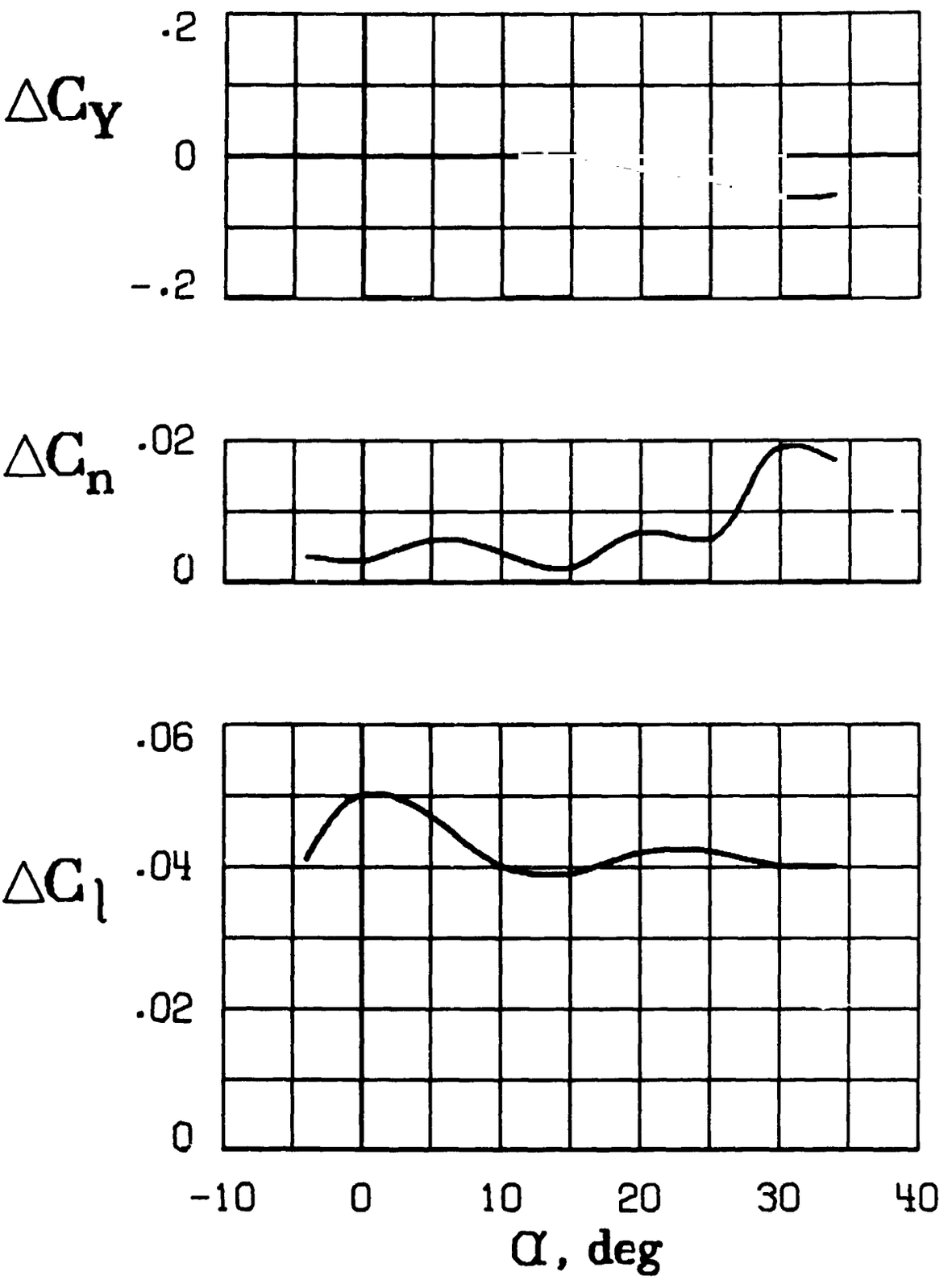

(a) Incremental lateral-directional characteristics obtained for $\delta_s = 70°$.

Figure 28. - Effect of right wing spoiler deflection for the upper surface engine configuration with 20° elbow exhaust nozzles. $T_c' = 0.2$, $\delta_f = 40°$, $C_\mu = 0.04$.

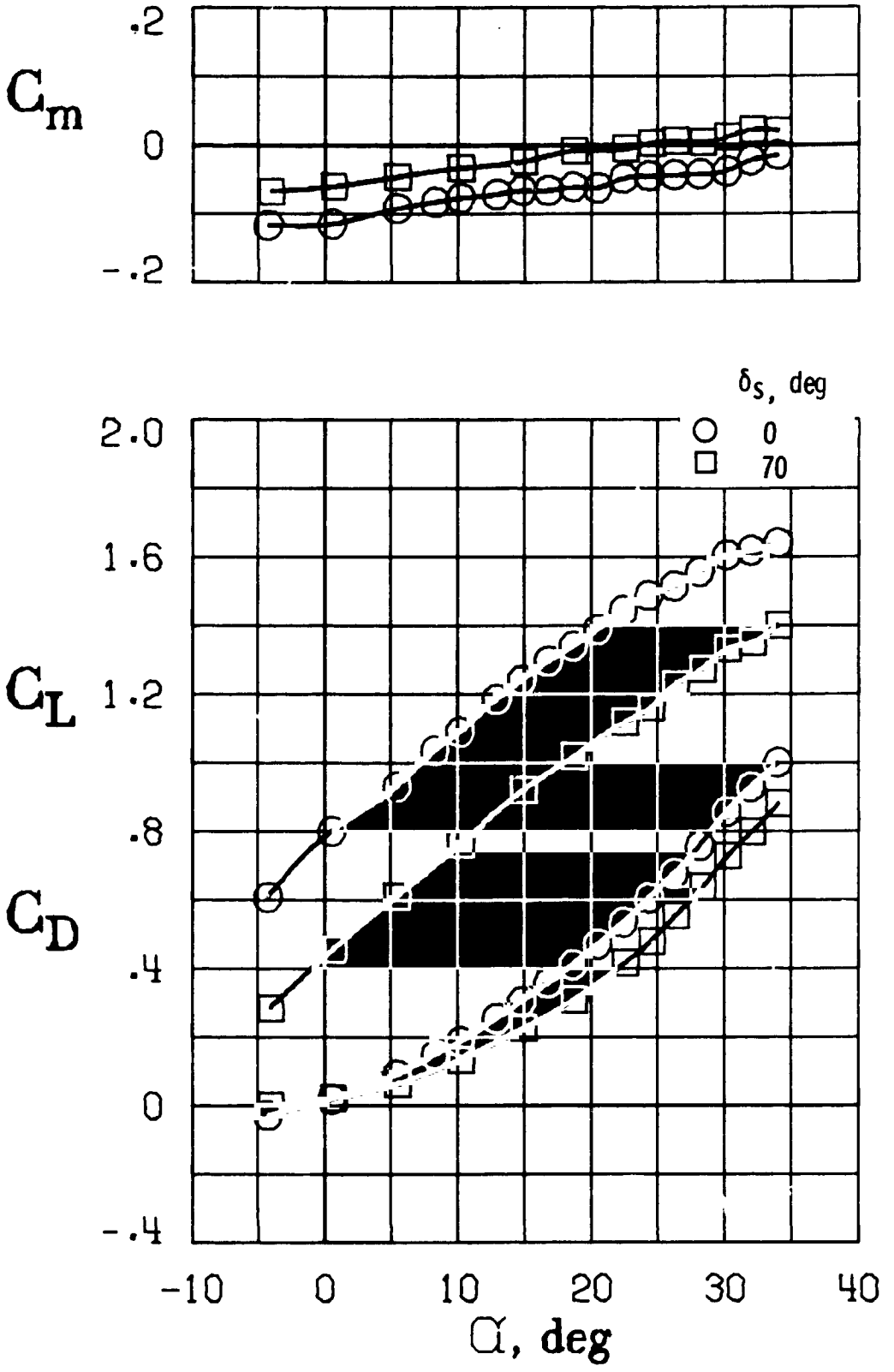

(b) Longitudinal characteristics.

Figure 28. - Concluded.

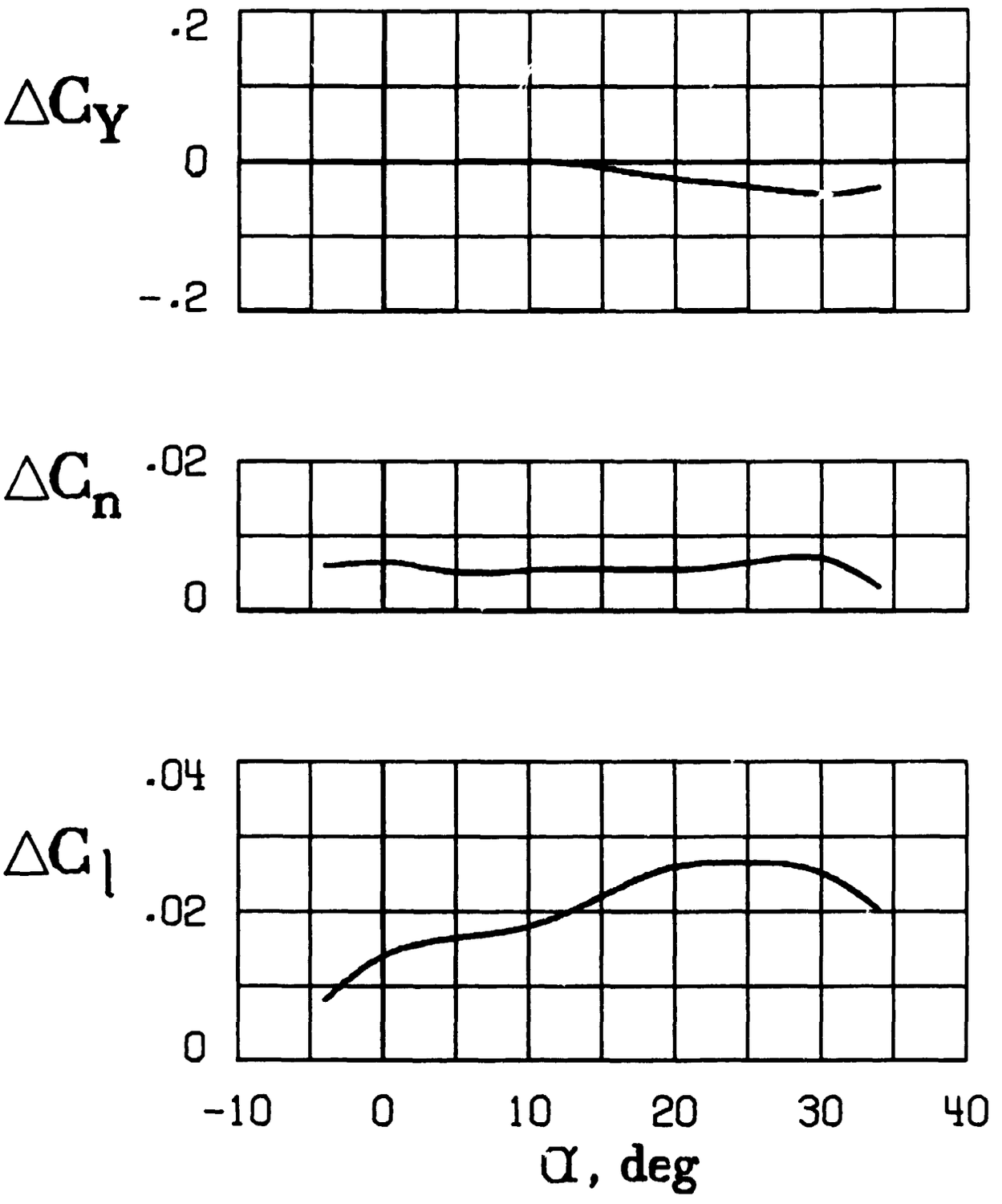

(a) Incremental lateral-directional characteristics.
$T'_{c,L} = 0.1$, $T'_{c,R} = 0$, $C_{\mu,L} = 0$, $C_{\mu,R} = 0.02$.

Figure 29. - Effect of inoperative right engine and asymmeteric boundary-layer control for the upper surface engine configuration with 20° elbow exhaust nozzles, $\delta_f = 40°$.

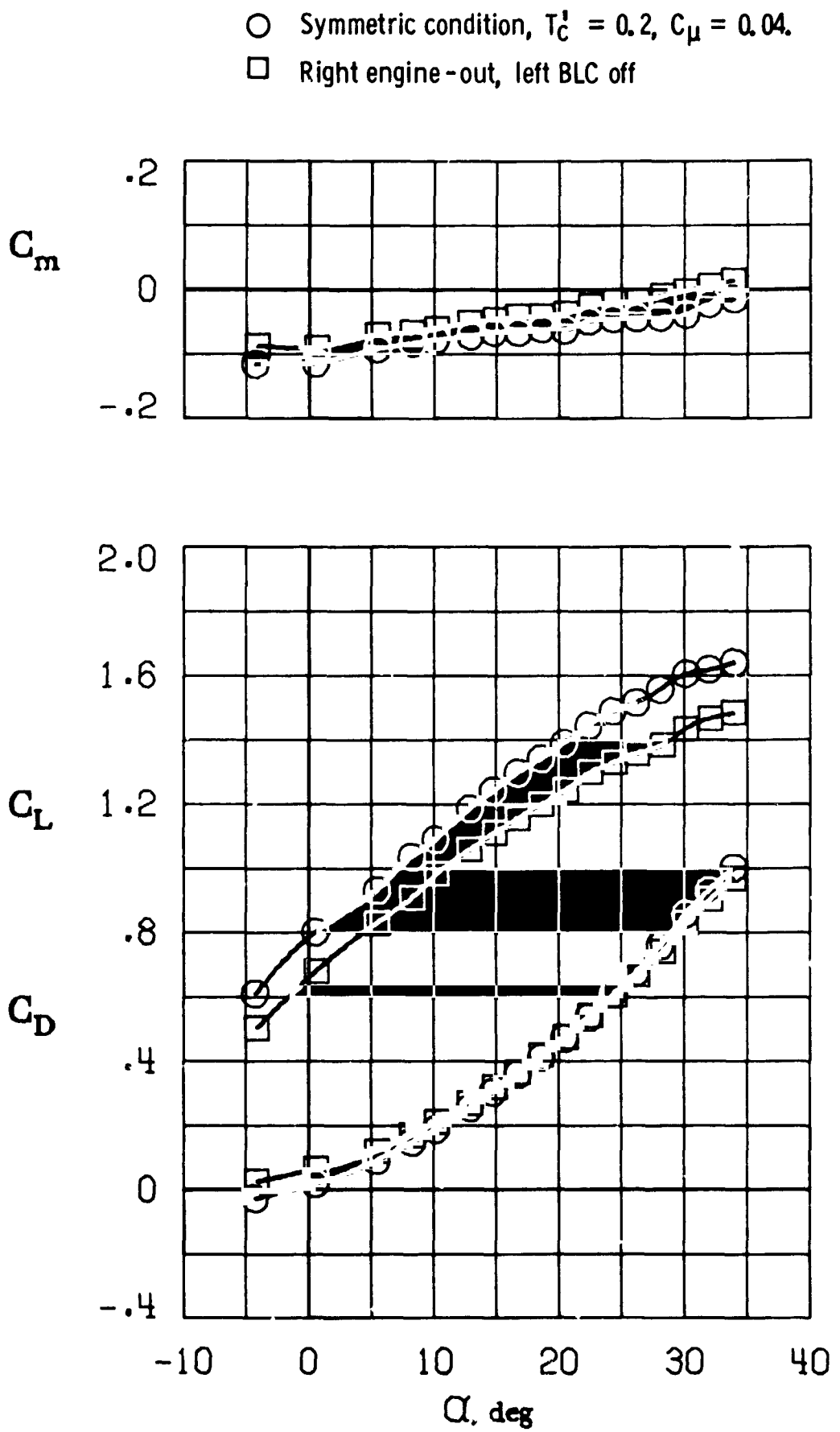

(b) Longitudinal characteristics.

Figure 29. - Concluded.

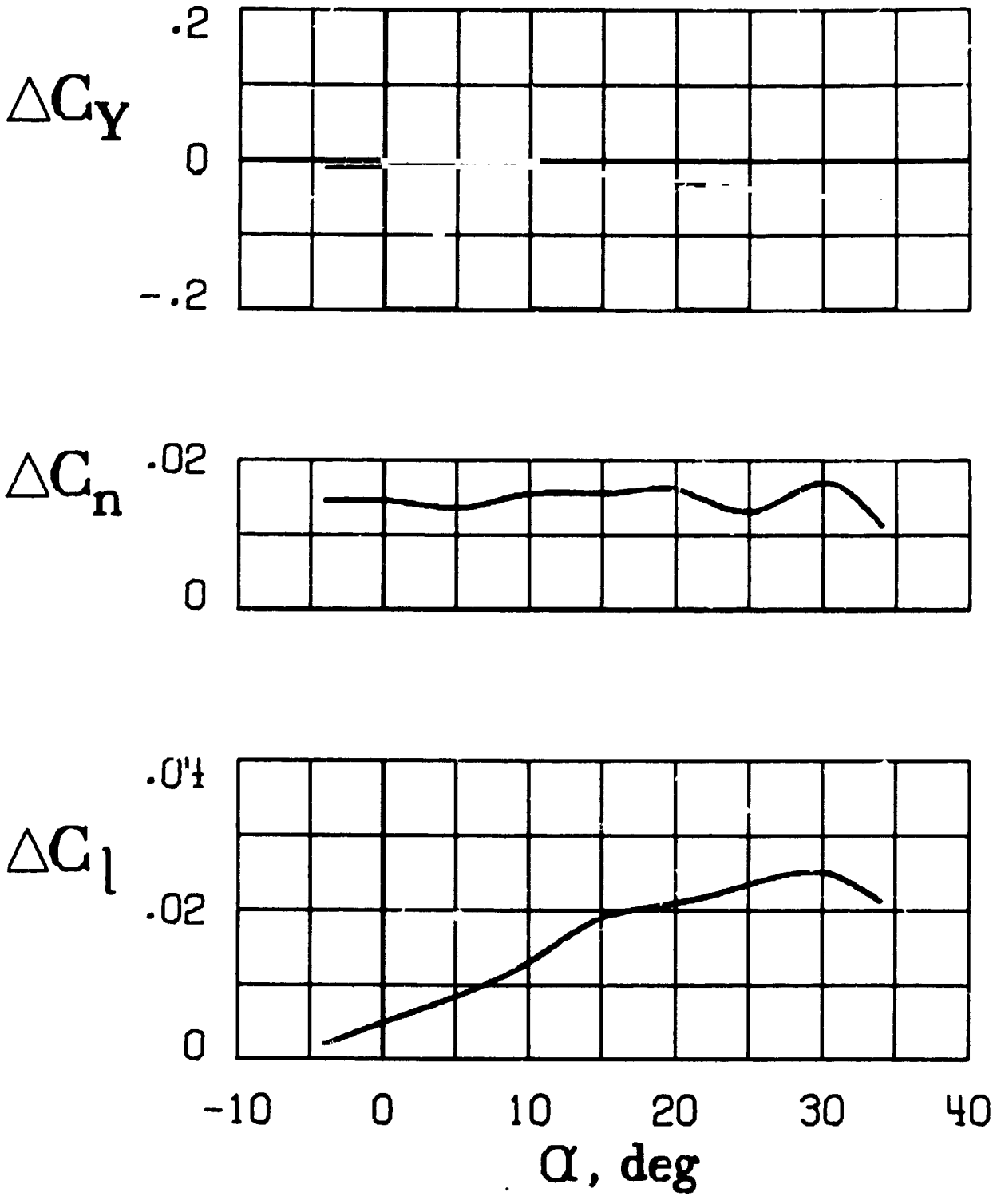

(a) Incremental lateral-directional characteristics $T_{c,L} = 0.1$, $T_{c,R} = 0$, $C_{\mu,L} = 0$, $C_{\mu,R} = 0.02$, $\delta_{f,L} = 30°$, $\delta_{f,R} = 40°$.

Figure 30. - Effect of inoperative right engine and differential flap deflection with asymmeteric boundary-layer control for the upper surface engine configuration with 20° elbow exhaust nozzles.

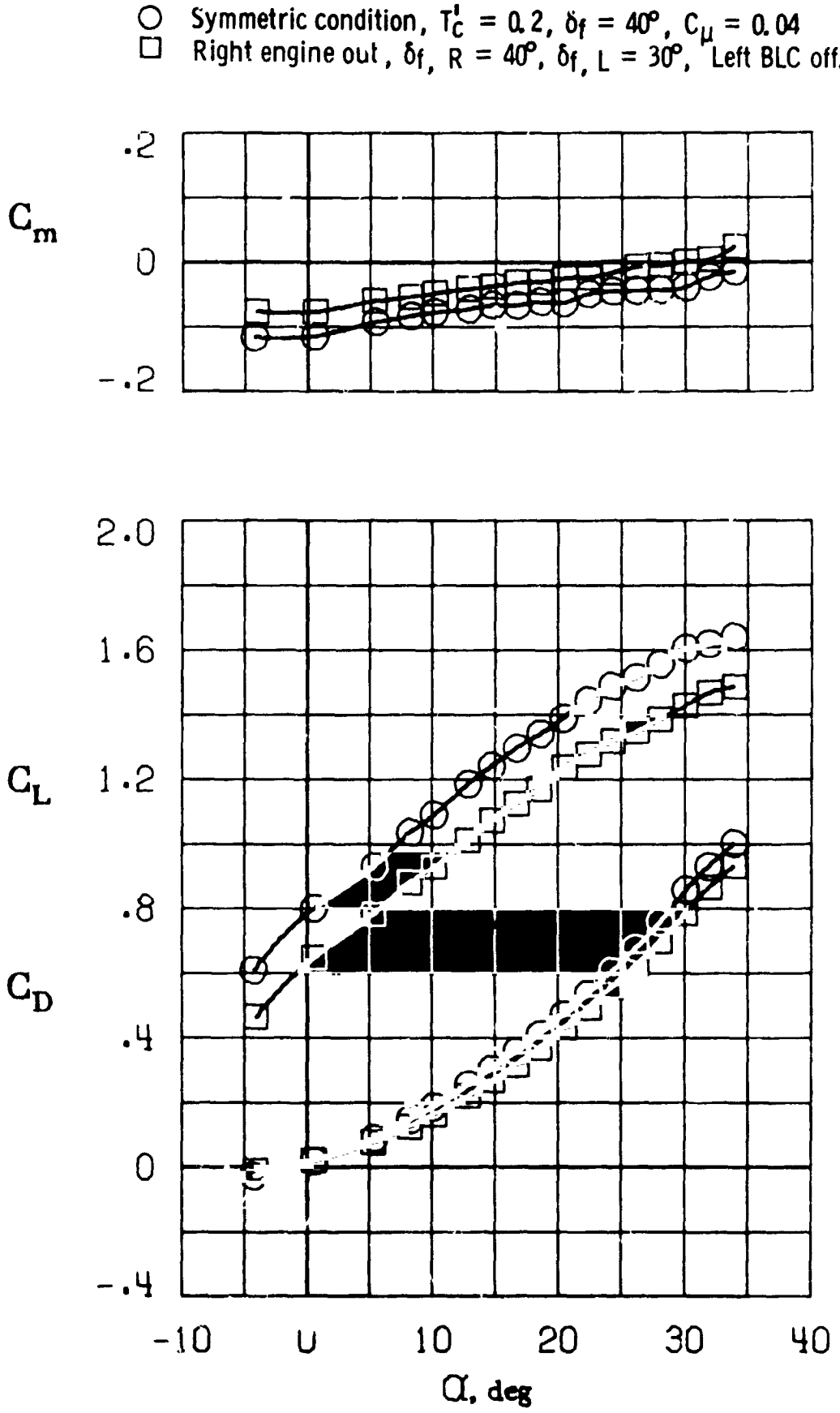

(b) Longitudinal characteristics.

Figure 30. - Concluded.